FLORIDA INTERNATIONAL UNIVERSITY

Miami, Florida

NEW CONNECTION DETAILS TO CONNECT PRECAST CAP BEAMS TO PRECAST COLUMNS USING ULTRA HIGH PERFORMANCE CONCRETE (UHPC) FOR SEISMIC AND NON-SEISMIC REGIONS

A dissertation submitted in partial fulfillment of

the requirements for the degree of

DOCTOR OF PHILOSOPHY

in

CIVIL ENGINEERING

by

Mohamadreza Shafieifar

2018

To: Dean John L. Volakis
College of Engineering and Computing

This dissertation, written by Mohamadreza Shafieifar, and entitled New Connection Details to Connect Precast Cap Beams to Precast Columns Using Ultra High Performance Concrete (UHPC) for Seismic and Non-seismic Regions, having been approved in respect to style and intellectual content, is referred to you for judgment.

We have read this dissertation and recommend that it be approved.

Ton-Lo Wang

Arindam Gan Chowdhury

Seung Jae Lee

David Garber

Wallied Orabi

Atorod Azizinamini, Major Professor

Date of Defense: October 17, 2018

The dissertation of Mohamadreza Shafieifar is approved.

Dean John L. Volakis
College of Engineering and Computing

Andrés G. Gil
Vice President for Research and Economic Development
and Dean of the University Graduate School

Florida International University, 2018

DEDICATION

I dedicate this dissertation to my beloved parents, and my caring sisters and brother for their unconditional love and endless support.

ACKNOWLEDGMENTS

First and foremost, I have to thank my dear family for their support throughout my life. Thank you for giving me the enthusiasm to stand even when circumstances seemed impossible.

I would like to thank Dr. Ton-Lo Wang, Dr. Arindam Gan Chowdhury, Dr. Seung Jae Lee, Dr. David Garber, Dr. Wallied Orabi and Dr. Atorod Azizinamini as my dissertation committee members. I would also like to thank Dr. Jawad Gull, Dr. Alireza Mohammadi, Dr. Ramin Ramin Taghinezhad and Dr. Huy Pham with whom I gained knowledge and research skills. I would also like to thank my friends and fellow graduate students, Dr. Somayeh Fakharian Qom, Alireza Valikhani, Mahsa Farzad, Azadeh Jaberi, Amir Sadeghnejad and Rozita Mazaheri for their friendship and exceptional help. The author is indebted to Sheharyar e Rehmat for his assistance with editing this report.

A special thank goes to Carlton Ng, Edgar Polo, Jessica Teran, Jose Velazques, Aileen Sanchez, and administrative staff at Florida International University for helping out with the departmental and university policies and procedures. Finally, I extend my thanks to all those unnamed individuals, whose encouragement and cooperation directly or indirectly contributed to the completion of this dissertation.

The research study, results of which reported in this dissertation were partially sponsored by Accelerated Bridge Construction University Transportation Center (ABC-UTC) at Florida International University. ABC-UTC is a Tier 1 UTC funded by U.S. DOT. I would like to acknowledge and thank the sponsors for their support. The author is also thankful to Ductal® by LafargeHolcim, for providing the UHPC material.

ABSTRACT OF THE DISSERTATION

NEW CONNECTION DETAILS TO CONNECT PRECAST CAP BEAMS TO PRECAST COLUMNS USING ULTRA HIGH PERFORMANCE CONCRETE (UHPC) FOR SEISMIC AND NON-SEISMIC REGIONS

by

Mohamadreza Shafieifar

Florida International University, 2018

Miami, Florida

Professor Atorod Azizinamini, Major Professor

Several connection details have been developed for the connection of precast cap beams to precast columns in Accelerated Bridge Construction (ABC) applications. Currently, the suggested details involve some form of either reinforcement or portion of the precast column to penetrate inside the cap beam. Such details present many challenges in the field, such as necessitating bundling of reinforcement in the cap beam or creating a congested reinforcement arrangement. Furthermore, closer inspection of some of the test data indicates that for currently used details, cap beams could sustain some damages during major seismic events, whereas they are designed to be capacity protected. Additionally, construction of such details demands precision.

To overcome these challenges, two new connection details are envisioned. Both details completely eliminate penetrating of column into the cap beam. In the first detail, the rebar of the cap beam and the column are spliced in the column and joined with a layer of Ultra High Performance Concrete (UHPC). The use of UHPC in the splice region allows the tension development of reinforcing bars over a short length. High workability of UHPC

and large tolerances inherent with the suggested details can facilitate and accelerate the on-site construction. In the second detail, to confine the plastic hinge with a limited length in the column, two layers of UHPC were employed. Confining the plastic hinge is achieved by sandwiching a desired length of the column, using normal strength concrete (plastic hinge region) in between two layers of UHPC. The most interesting aspect of this detail is the exact location and length of the plastic hinge.

The primary goal of this research is to provide a description of the newly developed details, verifying their structural performance and recommendation of a design guide. These goals are achieved through a diverse experimental and numerical program focused on the proposed connections. Results show that both details are equally applicable to seismic applications and able to achieve adequate levels of ductility. Lack of failure in splice region indicated that UHPC can provide a good confinement and shear capacity even when confining transverse reinforcement was not used.

TABLE OF CONTENTS

LIST OF TABLES

TABLE PAGE

LIST OF FIGURES

FIGURE PAGE

CHAPTER 1 INTRODUCTION

1.1 An Introduction to Accelerated Bridge Construction (ABC)

Accelerated Bridge Construction (ABC) offers a new solution for reducing onsite construction time while building bridges. Federal Highway Administration (FHWA) defines ABC as a bridge construction methodology employing innovative planning, design, materials, and construction techniques in a safe and cost-effective manner to reduce the on-site construction time [1]. The main reason to use ABC is to reduce traffic interactions and ensure safety of workers by reducing the onsite construction activities.

The main focus of this research is on innovative connections between precast columns and precast beams. In these systems, the precast elements are separately shipped and assembled at the field to form the bridge. As the precast elements are built off-site and under controlled environmental conditions, their quality and durability can be maintained. The use of precast elements, such as columns and cap beams can minimize the on-site construction time and its related activities [2].

1.2 Cap Beam to Column Joint

Traditionally, in bridge construction, columns are cast first with the longitudinal steel reinforcement extending beyond the column top and then the cap beam is formed. Next, the cap beam reinforcement is placed and then cast in-situ. In this case, as the column steel reinforcement extending into the cap is fully developed in the cap beam concrete, a rigid connection between the columns and cap beam is achieved.

Utilizing the precast elements requires joints but durability and structural behavior of theses joints may pose a challenge for designers [1,3] and can affect the service life of the bridge. One commonly used joint is the connection between precast cap beams and columns (Figure 1-1). Such connections play a critical role in the structural behavior of the bridge.

The primary advantage of using precast cap beams is to facilitate and accelerate the field construction, especially in ABC applications, and to increase the safety by reducing worker exposure in work zones. Also, to reduce the weight and facilitate the shipping, SHRP 2 proposed an alternate solution of using a number of smaller cap beams and joining them in the field to create a single cap beam [4].

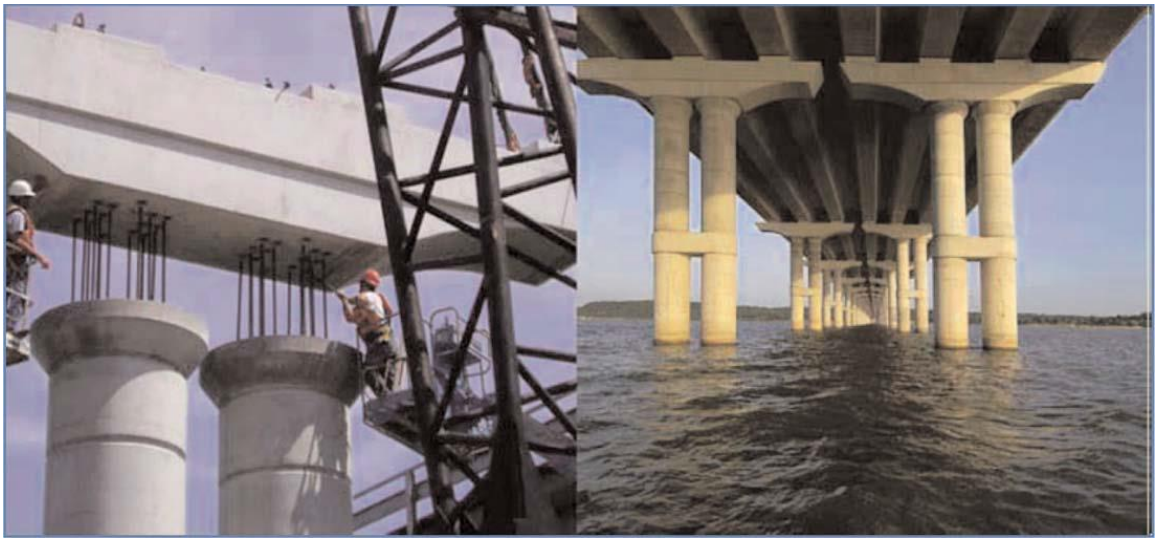

Figure 1-1 Precast concrete cap beam used in crossing state highway 36 over Lake Belton, Tx [5].

Generally, the connection between cap beams and columns are designed to transfer loads to the columns, for both axial and moments. Bridges should be designed so that the damage (i.e. plastic hinge) intentionally forms in columns so that it can be easily inspected

and repaired after an extreme event [6–9]. A plastic hinge is defined as a region of a bridge that yields in flexural and has plastic rotation while having enough flexural strength [9].

Texas Department of Transportation (TxDOT) provided a detailed literature review of designing cap beams and their connection to the columns to guide the development of a new precast connection suitable for cap beams [10]. In this report, design of cap beams and their connection to the columns were evaluated and some design recommendations based on the previous researches were suggested [10,11]. To investigate the structural behavior of cap beam and their connections, an experimental test program was also conducted. Six full-scale specimens were tested which included a control test, a pretensioned cap beam, and four additional specimens to investigate the effect of shear reinforcement spacing, the amount of prestressing, and connection detailing. This report concluded that application of AASHTO LRFD 2012 design procedures for cap beams leads to many designs that are controlled by the minimum area of steel and/or spacing requirements [11].

1.3 Current Approaches

Several details have been researched and suggested to connect precast columns to precast cap beams, but generally, none of these methods have entirely solved construction issues. An ideal connection detail should be easy to implement while satisfying the structural behavior criteria such as ductility and load-carrying capacity. Common connection details to connect precast columns to cap beams are bar coupler, grouted duct, pocket, socket, hybrid, and integral connection.

A summary of the state-of-the-art practice of connection details for prefabricated elements in ABC projects and the discussion on implementation of these connections is

provided by Culmo [12]. Details were categorized based on their performance and frequency of use. The report also provides information on performance rating, their durability, initial cost, and maintenance of the connections. Marsh et al. provided a summary of available connections between the cap beams and columns that have been tested or implemented [13]. In the following sections, a brief description of each different connections and their background is presented.

1.3.1 Bar Coupler

In this connection, a mechanical reinforcing bar coupler is used in the column to splice the rebars together. A bar coupler directly joins the longitudinal rebars and creates a continuity between them in the precast column and the cap beam (see Figure 1-2 (a)). Several types of the couplers including threaded sleeve, grouted sleeves (Figure 1-2 (b)) and external clamping screws are commercially available. This connection has been experimentally and numerically investigated for their performance by other researchers [14–16]. Although the connection provides ductile behavior, the use of bar coupler may have tighter construction tolerances and the construction detailing of this connection demands precision.

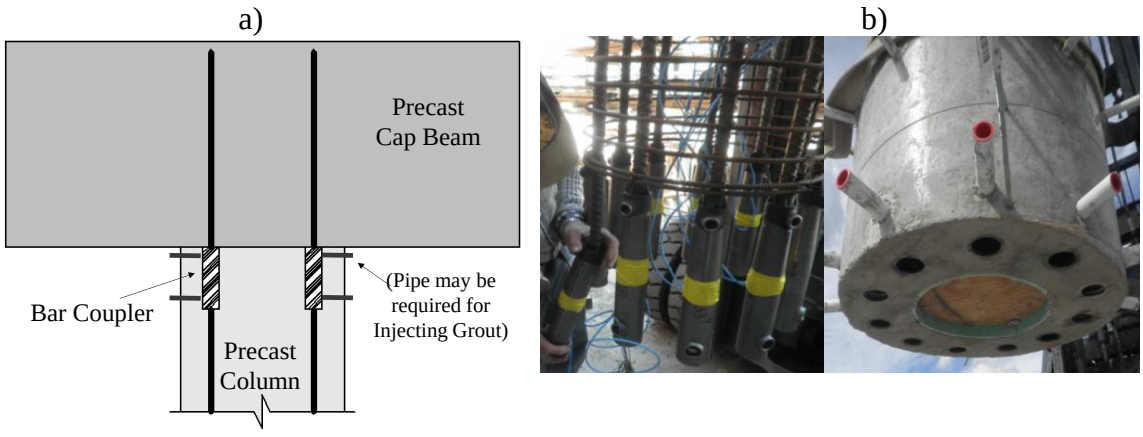

Figure 1-2 Bar coupler connection a) Schematic of the connection b) Installation [16].

Several studies have been conducted to evaluate the seismic behavior of this connection between columns and footings/cap beams. Haber et al. tested five specimen to evaluate the performance of grouted sleeve coupler connections between precast columns and Cast in place (CIP) footings [17]. The different parameters for connection included using different types of couplers, their location and using a pedestal above the connection. The connection was tested under cyclic loading. The results of the test showed that the behavior of specimen with couplers were similar to the traditional connection (CIP) up to 6 percent drift. Ductility of this connection was acceptable for moderate to high seismic zones.

In 2018, Hongay conducted quasi-static cyclic test for 1/3-scale specimens of different precast concrete columns [18]. The experiment was conducted on three specimens, one as a control specimen and two had the same column-footing connection (grouted splice sleeve coupler), but the column cap connections were grouted splice sleeve coupler and grouted corrugated duct connection. The cyclic test results showed corrugated duct connection had less energy dissipation when compared with grouted splice sleeve coupler.

1.3.2 Grouted Duct

In this connection, longitudinal bars of the column are individually inserted into the cap beam through a series of ducts. After placing the cap beam, ducts are filled with grout (see Figure 1-3 (a)). The ducts are usually corrugated to increase the bond between the bars and cap beam [14,19–22]. These connections face the similar challenge as bar coupler connections and may not provide large tolerances for the construction.

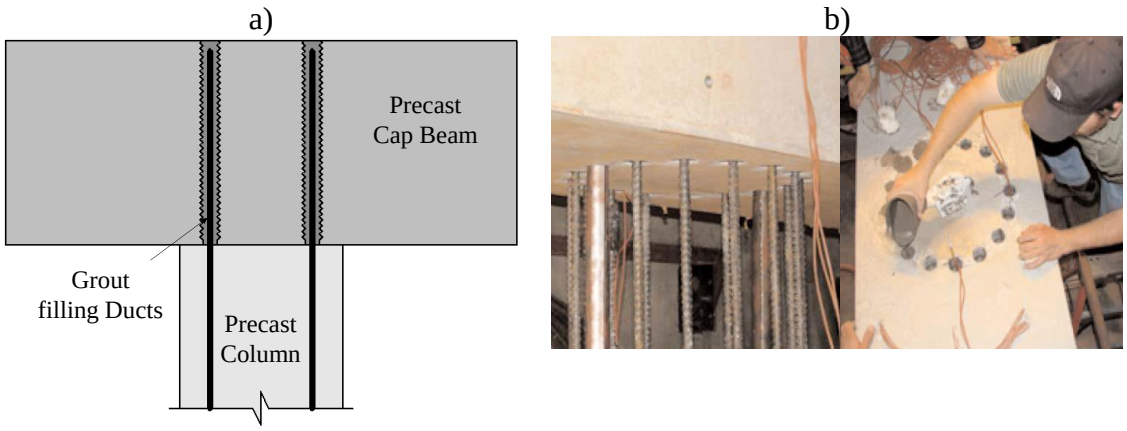

Figure 1-3 Grouted duct connection a) Schematic of the connection b) Cap placing and topping off ducts with grout [14].

Grouted duct connections have been used for both seismic and non-seismic regions. Lake Belton Bridge on SR 36 in Texas [23] and the SR 520/SR 202 bridge in Washington State [13], are an example for using grouted ducts were used to connect precast cap beams to columns. Washington State Department of Transportation (WSDOT) [24] investigated the performance of this connection for seismic regions.

Pang et al. built and tested scaled specimens to evaluate the grouted duct connections for joining precast columns to precast cap beams [22]. The precast specimens were compared with a conventional specimen that had approximately the same size and steel reinforcement details. The precast specimens were similar to the conventional connection in structural behavior and energy dissipation. All grouted connection had wide, stable hysteresis loops and failed by bar buckling followed by fracture. The plastic hinge formed outside the cap beam but some damages were also observed at cap beam interface. In general, it was concluded this type of connections is acceptable for joining precast cap beams to precast columns.

1.3.3 Pocket Connections

The pocket connection uses a single duct in the cap beam, and exposed longitudinal reinforcing bars from the precast column are inserted and anchored within the large duct. After placement of the elements, the duct (pocket) is filled with concrete or grout (Figure 1-4 (a)). Similar to the grouted duct, corrugated ducts can be used to increase the bond with adjoining concrete [14,25,26]. Generally, cap beams are heavily reinforced and placing a single duct may present many construction challenges.

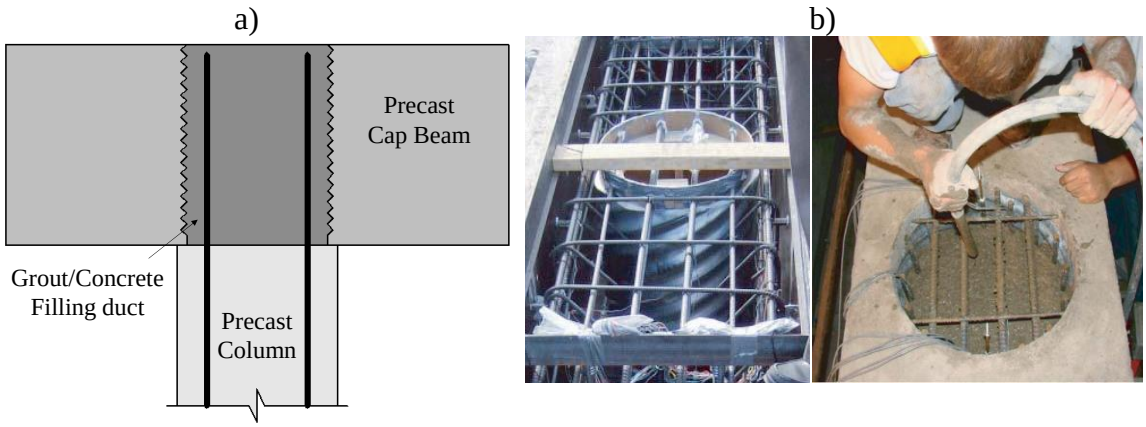

Figure 1-4 Pocket connection a) Schematic of the connection b) Concreting of cap pocket connection [14].

NCHRP (Report 681) focused on the performance of pocket connection and its implementation in high seismic regions [14]. In this report, the results of scaled specimens with an 18-in. nominal diameter corrugated metal pipe as pocket is presented. Two types of pocket connections were tested and examined: cap pocket full ductility (CPFD) designed for use in high seismic regions and cap pocket limited ductility (CPLD) for low to moderate seismic regions. The geometry of specimens was similar but different transverse and longitudinal reinforcement were provided along with pockets which were filled with concrete. Test results showed that the plastic hinge formed in the column and the connection had an acceptable performance. The CPLD, which was designed for moderate

seismic regions, showed more joint shear cracking and deformation in comparison to the CPFD. Both specimens had an acceptable structural behavior in comparison to CIP (control) connection. The mode of failure was buckling of the longitudinal reinforcement.

The pocket connection showed favorable results during the inelastic cyclic loading tests representing high seismic regions performed by Restrepo et al [14]. The main advantage of a pocket connection is large tolerances. Large construction tolerances can be achieved by using large pocket which can accept moderate misalignment of column reinforcement. Another advantage of pocket connection is the use of regular concrete. Generally, using grout results in increasing the cost and potential durability concerns due to the air voids during its casting.

1.3.4 Socket Connections

In this type of the connection, the entire column is inserted into the cap beam and the remaining gap is filled with grout. To increase the bond between the column and the cap beam, it is recommended to roughen the adjoining surfaces (see Figure 1-5). The difference between the socket and pocket connections is that in the pocket connection reinforcements are inserted into the cap beam, but in the socket connection, the entire column is inserted. In this connection, to accommodate construction tolerances, the opening is made larger which can widen the cap beam [13,27–29].

Figure 1-5 Socket connection a) Schematic of the connection b) Inserting the column to the connection [29].

Motaref et al. tested scaled specimens with a socket connection on a shake-table [30]. Precast columns had different materials including fiber-reinforced polymer (FRP) composites and engineered-cementitious composite (ECC). In both specimens, columns were embedded in to the pocket with a length of 1.5 column diameters. The experimental results showed that in both specimens plastic hinge formed in the columns and the displacement ductility was greater than 6.

Ziehl et al. studied on socket connections between cap beam and column [31]. The study was carried out on full-scale specimen. A pocket was created with a 3-ft diameter corrugated pipe and cardboard. The precast column were embedded 26-in. and the pocket was filled with low shrinkage concrete. They observed that the plastic hinging was formed in the column and ductility of the specimen was acceptable. No major cracks was observed in the cap beam and stresses at the connection were lower than allowable stresses. Regarding the construction tolerances, the main disadvantage was that the cap beam with socket connection were required to be wider than corresponding conventional cap beams.

1.3.5 Hybrid Connections (Self-Centric)

The hybrid connection has a "self-centric" behavior [32] and usually unbonded prestressed tendons are employed to join the precast column and the precast cap beam (Figure 1-6). The prestressed tendons are anchored in the cap beam/footing and provide a self-centering mechanism and remain elastic at all the times [14,33–37]. The main disadvantages of this type of the connection are difficulty in anchoring the tendons in the footing and higher construction and inspection cost [13].

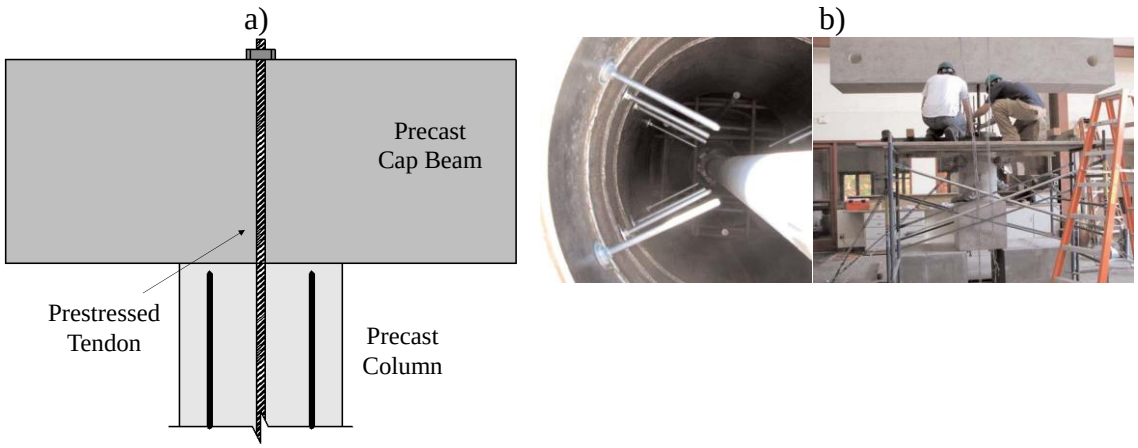

Figure 1-6 Hybrid Connection a) Schematic of the connection b) Unbonded tendon and sitting the cap beam the connection [14].

Hybrid connections in building industry was used before the bridge construction industry. Stone et al. tested hybrid connections for buildings in high seismic regions [38]. The results showed that the connection had large lateral drift capacity and the residual drift was significantly less than the corresponding conventional specimen. Based on their experimental tests, a guideline for hybrid connections for buildings was provided.

Cheok et al. studied the hybrid connections numerically. Regardless of the construction cost, their results indicated that performance of this connection is equivalent or better than conventional connections [39].

NCHRP (Report 681) evaluated hybrid connections for joining precast cap beams to the precast columns for seismic regions [14]. The experimental test showed that the hybrid connection has a better performance in comparison to conventional specimen in terms of ductility, damages, and residual drifts. As this type of connection are basically different from other mentioned connections, in this case, a special designing procedure should be used [36].

1.3.6 Integral Connections

In this connection, initially, a precast lower stage cap beam is constructed to support the girders. Then the precast column is connected to the cap beam in an integral connection within a joint. The lower stage of the cap beam, then filled with concrete to create an integral connection. The lower stage of the cap beam, as a "stay in place formwork", should be strong enough to carry the loads during the construction. This type of connection eliminates bridge deck joints enhancing the service life. However, the cap beam is generally of large dimension to accommodate additional stresses and thus requires large pours in the field which can affect the speed of construction [14,40,41].

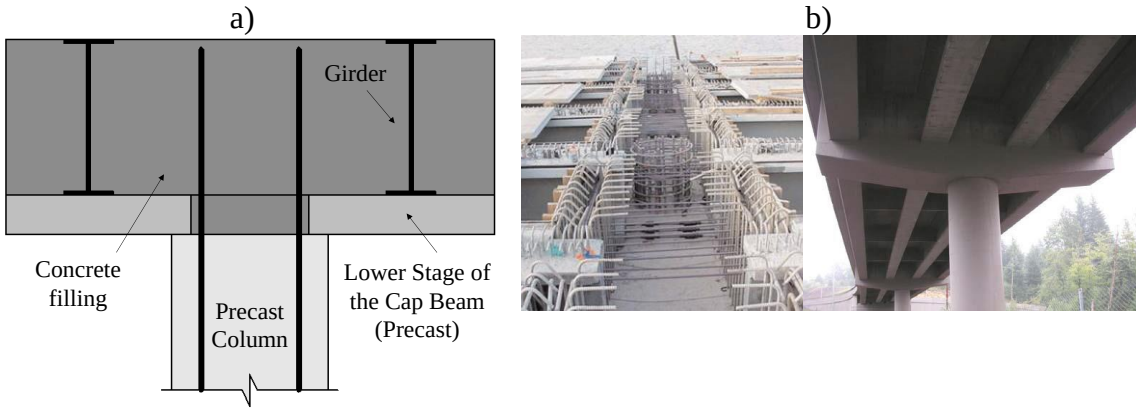

Figure 1-7 Integral connection a) Schematic of the connection b) San Mateo-Hayward Bridge widening Project [42] and two-stage cap beam [13].

There are advantages regarding each mentioned approach that can be taken so long as the precise design is provided. However the aforementioned construction issues can be challenging in the field. Therefore merging new details and advanced structural materials can be beneficial to accelerate the on-site construction.

1.4 Utilization of UHPC to Connect Prefabricated Elements

Using steel fiber reinforced concrete is an alternative for traditional reinforcing concrete and can improve the performance of the structures. Chalioris studied steel fiber reinforcement concrete (SFRC) beams under cyclic loading [43]. Several beam specimens with a shear span-to-depth ratio of 2 were tested. He tested plain concrete beams and SFRC with 5% and 0.75% of fibers. The steel fiber reinforced sections had a better performance in terms of shear capacity and residual drifts.

As the Federal Highway Administration (FHWA) reports, Ultra High Performance Concrete (UHPC) is a cementitious material formulated by mixing Portland cement, fine silica sand, silica fume, quartz flour, high-range water reducer, discontinuous internal steel or organic fibers, and less than 0.25 water-to-cement (W/C) ratio. UHPC offers more than 21.7 ksi compressive strength and greater than 0.72 ksi sustained post-cracking tensile strength [44].

The superior material properties of UHPC, such as rapid early age strength gain, durability, self-compacting, high flowability, and low long-term and life-cycle cost, promote the implementation of UHPC in ABC projects [45–47].

The concept of UHPC was first developed by Richard and Cheyrezy and was produced in the early 1990s at Bouygues Laboratory in France [48]. Afterward, the effect

of fiber addition on the improved ductile behavior of beams was investigated by Oh [49] and Ashour et al. [50]. Moreover, the increased bearing capacity and shear strength of fiber-reinforced beams were studied by Campione [51], and by Lim et al. [52], respectively.

The mechanical properties of UHPC and High-Performance Concrete (HPC) were studied by Dili and Santhanam [53]. 2-in. cubes which were wet cured at 90°C and tested to measure the compressive strength. The maximum compressive strength observed for UHPC was 29 ksi. Moreover, they investigated the flexural behavior of 1.6×1.6×6.4 in. prisms including both plain and fiber reinforced UHPC. In the research, the flexural strength of fiber reinforced UHPC and HPC prisms were reported to be greater than the flexural strength of the plain prisms. However, the flexural strength of UHPC prisms was observed considerably greater than that of HPC prisms.

Figure 1-8 UHPC premix, fibers, mixing and flowability test.

1.5 UHPC Background

As UHPC is a relatively new material, limited designing guidelines has been published to date. FHWA, French Association of Civil Engineering (AFGC), Swiss Standard (SIA 2052) published several reports to this regard. In this section a brief background of designing guideline available for UHPC is provided.

1.5.1 Setting Time and Flow

FHWA conducted an extensive experimental study on six different commercially-available materials being marketed as "UHPC-class" [54]. This report indicates that these materials had initial setting time between 4 and 9 hours, and the finial setting time was between 7 and 24 hours. The flowability of UHPC should be measured prior to casting using the flow table test. Static flow measurements of this material ranged between 4 and 10 in. Fine aggregate and water admixture contents, and fiber geometry can affect the followability.

1.5.2 Shrinkage of UHPC

Early-age shrinkage of UHPC can be divided into three parts: chemical shrinkage (due to the chemical reactions), autogenous shrinkage caused by self-drying (hydration), and drying shrinkage (evaporation) caused by external drying [55]. At low water/cement ratios (w/c), all the water is rapidly drawn into the hydration process and the need for more water creates very fine capillaries. The surface tension within the capillaries causes autogenous shrinkage which can lead to cracking. UHPC which has a very low water to cement ratio is more prone to develop autogenous shrinkage [54]. Additionally, UHPC materials are designed to have large contents of very fine and reactive cementitious

materials, which increase the chemical shrinkage of the system. On the other hand, the lower the w/c of a cementitious system, the smaller capillary pores will form in the cement matrix and lower drying shrinkage. This may explain why UHPC materials do not show considerable higher shrinkage with respect to their autogenous shrinkage. It is important to note that large amount of fiber reinforcement can prevent forming shrinkage cracking [54].

FHWA tested six different commercially UHPC material and reported that the shrinkage of different UHPC was varied form 294 microstrain to 1262 microstrain [54]. They indicated that UHPCs commonly exhibit proportionally more autogenous shrinkage than conventional concretes, particularly at early ages (before 24 hours). In total, UHPC tends to exhibit approximately 800 microstrain of shrinkage as measured from casting through 1 year [56].

1.5.3 Flexural Design

Flexural design of UHPC sections are extensively described in chapter 3.

1.5.4 Shear in UHPC

Use of UHPC increases the shear capacity and may lead to total or partial elimination of conventional transverse steel reinforcement. Parra-Montesinos recommended the use of deformed steel fibers as an alternate option to conventional minimum shear reinforcement [57].As UHPC has more strength than regular concrete, the available provisions cannot necessarily predict the shear behavior of UHPC sections.

The Association Française de Génie Civil (AFGC) Interim Recommendations for Ultra High Performance Fibre-Reinforced Concretes (2002) is a design guide that includes the contribution of fiber reinforcement to shear capacity [58]. In this provision, the ultimate

shear strength of the cross-section includes three parts, the concrete, fibers and transverse steel reinforcement.

The concrete contribution to the shear capacity, *Vc*, is defined by Equation (1-1). In this equation, γ_E and γ_b are safety factors. The compressive strength is f_c', b_0 is the web width, and *z* is the lever arm at the ultimate moment. The lever arm is assumed to equal the distance from the center of the compression block to the center of the tension reinforcement. Note that all measurements are in metric units.

$$V_c = \frac{0.24}{\gamma_E \gamma_b} \sqrt{f_c'} b_0 z \tag{1-1}$$

AFGC, suggested Equation (1-2) for the fiber portion (V_f,). In this equation, *S* is the area of the shear plane which is assumed to equal 90% of the web width multiplied by the depth to the centroid of the tension reinforcement. σ_p is the average tensile stress carried by the fibers which can be assumed as 1 ksi for UHPC with 2% of fiber [59]. The variable γ_{bf} is a factor of safety.

$$V_f = \frac{S\sigma_p}{\gamma_{bf} \tan 40} \tag{1-2}$$

Graybeal conducted several tests investigating the shear capacity of UHPC beams and validated the mentioned equations [59]. He tested several prestressed UHPC girders and focused on the shear capacity and found that even though this method of calculating the shear capacity of UHPC sections is more reliable than other suggested equations, the method still underestimates the shear capacity of UHPC sections.

1.5.5 Punching Shear

Harris and Roberts-Wollmann investigated the punching shear capacity of UHPC slabs by testing several slabs with different thicknesses [60]. Several slabs were tested to failure to determine punching shear capacity. Three slab thicknesses (2, 2.5 and 3 in.) were tested with varying loading plate areas. The results of the experimental test were then compared to several methods for calculating punching shear of UHPC slabs. They concluded that a thickness of 1 in. of a UHPC slab is needed to prevent the punching shear failure under wheel load (Load = 37.2 kips and size: 8×20 in.). To predict the punching shear of UHPC slabs, they suggested the following equation based on the work by Fuchs et al [61].

$$P_N = k_1 f_t \frac{(3h + c)^2 - c^2}{\sqrt{h}} \quad (1\text{-}3)$$

In this equation, f_t is the split cylinder tensile strength (ksi) and k_1 is empirical constant which can be assumed 0.38 for UHPC. *h* and *c* are representing the slab thickness and loading plate width in inches. This equation was compared to the test results and a curve fitting software was used to determine the value of the empirical constant k_1.

1.5.6 Development Length of Steel Reinforcement in UHPC

The bond between UHPC and reinforcement (rebar or strand) is critical in determining development and lap splice lengths. A comprehensive investigation on bond behavior and development length of reinforcing steel in UHPC were conducted in 2014 by Yuan and Graybeal [62]. They evaluated the effect of embedment length, concrete side cover, bar spacing, bar size, bar type and compressive strength of UHPC by testing more than 200 pullout specimens. Their study focused on a commercial available UHPC

containing 2% steel fiber (by volume) and different bar sizes. For UHPC with the strength of more than 13.5 ksi, they suggested $10d_b$ as the minimum embedment length (where d_b is the diameter of the bar) when the minimum side cover is more than $3d_b$.

In 2018, Zachary et al. evaluated the material properties of different commercially available UHPC and used them for connecting prefabricated bridge deck connections [17]. They tested two types of specimens, direct tension pullout and prefabricated bridge deck connections. Results showed that the lap-splice guidance presented by Graybeal [62] was applicable to the UHPC specimens and for the rebar size #5 and smaller, they suggests $10d_b$ as the embedment length of steel reinforcement ($f_y \geq 74$ ksi) in UHPC when the clear cover is between 1 in. and $3d_b$. They also concluded that the lap splices of straight lengths of deformed steel reinforcement shall be at least 0.75 times of the embedment length.

Ronanki et al, performed several tests including pull out tests and beam tests with lap splices to evaluate the bond behavior of steel reinforcing bar in UHPC [63]. A total of 16 pullout and 12 beam specimens were tested. They evaluated the bond between UHPC and different size of steel reinforcement (#4 to # 7). The embedment length and side cover for the pull out tests were varied from $6d_b$ to $8d_b$ and $1d_b$ to $3.5d_b$, respectively. Their results indicated that because of enhanced tensile mechanical properties of UHPC, the bond strength was higher and the development length is significantly shorter than regular concrete. The results showed that the development length required for rebar in UHPC is in the order of 20–30% of that in regular concrete.

1.5.7 UHPC to Concrete Bond Behavior

Previous studies indicated that the UHPC has a strong bond to regular concrete compared with other cementitious grout materials [64]. The same as other grout material, UHPC has a better bond to precast concrete elements when the substrate is wet and roughened [64,65].

Recently, FHWA conducted several test to understand the bond behavior between different commercial UHPC and regular concrete [54]. To evaluate the UHPC to concrete bond behavior, they tested specimens with the exposed aggregate and dry surface; thus, interface pre-wetting was not employed. The results showed that the interface failure (bond strength) occurred at approximately the same stress level as the substrate failure, indicating that the bond strength of these materials might be mainly controlled by the tensile strength of the concrete substrate. Peak tensile stress at failure was more than 0.5 ksi and 0.4 ksi from bend and direct tensile test, respectively.

1.6 Problem Statement

As discussed, several details for column to cap beam have been suggested. Currently, the suggested details require either some reinforcement or portion of the precast column to penetrate inside the cap beam. Generally, cap beams are heavily reinforced and such details present many construction challenges. As a consequence, it may be necessary to bundle the reinforcement in the cap beam or create a very congested reinforcement arrangement. Furthermore, closer inspection of some of the test data indicates that for currently used details, cap beams may experience cracking under cyclic loading [14], whereas they should be capacity protected and damage free [6]. The main purpose of this

research is to develop a new UHPC connection between cap beam and column for Accelerated Bridge Construction (ABC) for both seismic and non-seismic regions with desired plastic hinge location and structural behavior.

To overcome the challenges in existing joints, two new connection details are envisioned and tests were carried out to verify their feasibility. The development of the new connection detail includes conducting a combination of experimental and numerical investigations. The research provides a description of the newly developed details, designing procedure and their structural behavior.

1.7 Proposed Connection

Two details are proposed. Both details are equally applicable to seismic applications. The details completely eliminate penetrating into the cap beam and the connection is made outside the cap beam and within the precast column. In the first detail (Figure 1-9 (a)), the longitudinal reinforcement of the cap beam and the column are spliced in the column and simply joined with a layer of UHPC in the field. The use of UHPC in the splice region allows the tension development of reinforcing bars over a short length. Consequently, the length of the gap to be filled by UHPC in the field is relatively small. Moreover, the suggested detail provides contractors with large tolerances to work with.

In the second detail, to confine the plastic hinge with a limited length in the column, two layers of UHPC are employed. Confining the plastic hinge is achieved by sandwiching a desired length of the column, using normal strength concrete in between two layers of UHPC. For this detail, the system consists of two separately prefabricated parts and joined together in the field using UHPC, as described below. The first part of prefabricated

component consists of a cap beam, a layer of UHPC which is placed immediately adjacent to cap beam along with a desired length of plastic hinge using normal strength concrete. The second part is the precast column. Both parts are then joined together in the field using UHPC (Figure 1-9 (b)). The most interesting aspect of this detail is the exact location and length of the plastic hinge.

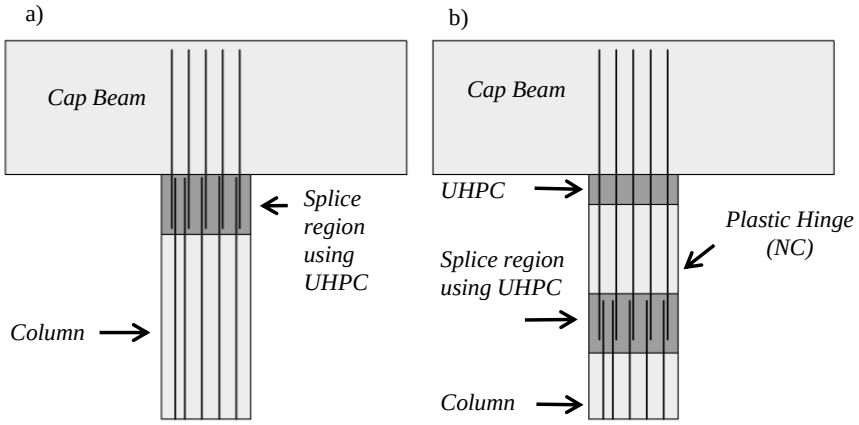

Figure 1-9 Details of the concept of the proposed connection a) Detail 1 b) Detail 2.

1.8 Organization of Dissertation

This dissertation is organized in nine chapters.

Chapter 2 evaluates the main characteristic of UHPC in comparison with Normal strength Concrete (NC) to make an apple-to-apple comparison. This chapter includes two parts, one experimental and one numerical. The experimental part focuses on determining the basic material properties from small-scale testing of UHPC and the numerical part provides a calibrated material model of UHPC based on the obtained experimental data.

Chapter 3 describes and evaluates the existing methods of calculating the moment capacity of reinforced UHPC sections through an experimental and numerical study.

Chapter 4 discusses an experimental investigation on a large scale specimen having Detail 2. In this chapter, the seismic performance of the proposed connection such as the forming plastic hinge, cracks developments, yielding bars were highlighted.

Chapter 5 summarizes an experimental program to evaluate the performance and structural behavior of both proposed connections with a circular sections. In this section, four specimens were subjected to a constant axial load and cyclic lateral loading to study the effect of the axial load and stirrup spacing in the plastic hinge and splice region.

Chapter 6 presents an experimental study on the performance and structural behavior of Detail one. The experimental program consisted of four specimens with Detail one and two control specimens with a circular sections. The connections were subjected to constant axial compressive loads and cyclic lateral loading to study the effect of lap splice length and rebar size.

Chapter 7 summarizes an extensive parametric study using calibrated nonlinear finite element model developed based on the results of the previous chapters and literature. The investigated parameters include axial load and splice length.

Chapter 8 provides a brief design guide recommended for the proposed connections.

Chapter 9 summarizes the conclusions, recommendations, and suggestions for future studies.

CHAPTER 2 MATERIAL PROPERTY CHARACTERIZATION OF UHPC

2.1 Introduction

Ultra-High Performance Concrete (UHPC) is an advanced technology in concrete industry with superior characteristics such as high strength in compression and tension, ductility, and durability. UHPC is a cementitious based material with fine aggregates, silica fume, fibers, superplasticizer, and low water/cement ratio.

Many bridges need rehabilitation and the use of UHPC can increase their durability [66–70]. The US Federal Highway Administration (FHWA) has been considering the use of UHPC in bridges since 2001. Currently, several bridges (more than 180) in which UHPC was used mostly to connect precast elements, are open to traffic in North America [71,72]. Also, using innovative and recycled materials in such advanced concrete can improve the sustainability characteristic of UHPC [73–75]. Considering exceptional properties of UHPC and extending the use of this material in buildings and bridge industry [76–78], in-depth knowledge is required to understand the approach which aids in calculating the moment capacity of UHPC sections.

This chapter determines the tensile and compressive behavior of UHPC and a comparison is made with Normal Strength Concrete (NC) for the development of a numerical model to simulate the behavior of UHPC using the Finite Element (FE). The basic mechanical properties of UHPC and Normal strength Concrete (NC) were obtained to make an apple-to-apple comparison. The experimental tests included cylinder and cube compressive test, flexural, briquette and splitting tension tests which were performed to evaluate the ultimate capacity of the material in compression and tension and its modulus

of elasticity. The numerical analysis provides the mechanical properties of UHPC that can be used in FE software using Concrete Damage Plasticity model (CDP) to define ductal UHPC in the absence of sufficient experimental data.

Ductal®, produced by Lafarge Inc. is a commercially available UHPC product which was used in this study and is composed of premix powder, water, superplasticizer, and metallic fibers (2% in volume).

This chapter includes two phases, one experimental and one numerical. The experimental phase focuses on determining the basic material properties from small-scale testing of UHPC and NC including the test of over 66 individual specimens (33 specimens UHPC and 33 specimens NC), with an emphasis toward determining the compressive and tensile behaviors. In this phase, the material characterization is completed according to ASTM standard procedures [79]. The test results from this study provide information to establish a prediction model for UHPC elements under various loading conditions for modeling proposed connections.

2.2 Experimental Study

2.2.1 Material Mixing

Among the advanced concrete technology [16] UHPC is receiving widespread attention. Three parts of the UHPC used in this study included: premix, fibers, and liquids. The premix (Ductal® JS1000) contains all of the cementitious, aggregate, and filler materials provided by Lafarge®. UHPC, when compared to conventional concrete, shows remarkably improved mechanical properties such as high compressive strength, high

tensile strength, and high workability. The premix was batched by the manufacturer and delivered to FIU's Structural Lab. Its composition is given in Table 2-1.

Table 2-1 Composition of Ductal®.

	Material	lb/ft^3	Percentage by Weight (%)
Premix	Portland Cement	44.4	28.5
	Fine Sand	63.7	40.8
	Silica Fume	17.4	9.3
	Ground Quartz	13.1	8.4
	Accelerator	1.9	1.2
	Total Premix	140.5	88.2
Superplasticizer		1.9	1.2
Steel Fiber (%2 by Volume)		9.7	6.2
Water		6.8	4.4

The liquids mixed with the UHPC included water, in the form of ice (for of hot weather) and Superplasticizer as a high-range water-reducing admixture (HRWA). The W/C ratio of all batches was 0.20 and straight steel fibers having circular cross-sections with a diameter of 0.008 in. (0.2 mm) and length of 0.5 in. (13 mm). The tensile strength of these fibers was specified with a minimum of 377 ksi by the manufacturer. The concentration of 2% by volume of fibers were used in the mix.

To obtain a consistent performance, a strict mixing procedure was followed, in which materials were weighed and placed in a mortar mixer. The premix was initially dry mixed for nearly 4 minutes. Then half of the superplasticizer and water (ice) were added to the mix and mixed for an additional 15 min. The remaining superplasticizer was then added, and the materials were mixed until the dry powder mix transformed into a wet paste concrete (approximately 2 min). Steel fibers were slowly added to the wet concrete paste in the mixer. Since fiber addition has a strong impact on the fiber distribution, this process was carried out carefully to ensure uniform distribution. The concrete was mixed for

another 6 minutes to ensure proper distribution of fibers, and then UHPC was ready to be cast.

As soon as mixing was completed, the casting was started. The casting of all UHPC specimens was completed within 15 minutes after completion of mixing. UHPC was scooped into the molds and was not rodded due to the presence of the fibers. The exposed surfaces of each specimen were then covered in plastic to prevent moisture loss.

Figure 2-1 UHPC specimens after demolding.

The NC used in the study was provided by a local supplier as a ready-mix with a nominal strength of 5000 psi, and a slump of 4 in. The compacting procedure for NC specimens was done according to ASTM specification (ASTM C31-69) [15].

The specimens were demolded approximately 24 hours after casting. The wet curing treatment was applied to all specimens for 27 days starting from the time of demolding day. After completion of curing period, the specimens were tested.

2.3 Test Procedures and Results

A universal testing machine (UTM) with a maximum capacity of 500 Kips and a 50-kip capacity MTS testing machine was used to apply the loads. Also, for all specimens, two potentiometers were placed to measure displacements. The collection of the data for all tests was completed using a data acquisition system set to record data at 10 Hz. The time, load, deflection values were all recorded. Density of UHPC and NC were 155 lb/ft^3 and 150 lb/ft^3 respectively.

2.3.1 Compression Testing

One of the most commonly specified and measured properties of concrete is compression strength. The modulus of elasticity, which is similarly measured through standardized compression test methods, is also an important parameter in the design of structures. All the compression tests discussed in this section were all completed according to the ASTM C39 [15] standard test method for cylinders and the ASTM C109 [79] standard test method for cubes.

2.3.1.1 Cylinder Tests

Uniaxial compression tests were performed on a total of 5 UHPC and 5 NC cylindrical specimens of 3 in.- diameter and 6 in.- high cast in a plastic mold using ASTM C39 guideline [79].

Prior to each test, all the cylinder specimens were grinded to minimize uneven surfaces at each end. The cylinders were measured to determine length, diameter, and density. Loading was applied at the rate of 440 lb/s; however, based on a study done by Graybeal [46] an increase in the load rate on compression testing results, would not be

detrimental. Figure 2-2 shows a picture of typical UHPC and NC cylinders after testing. In this figure, it is noticeable that in the presence of fiber the UHPC cylinder remains fairly intact after failure load.

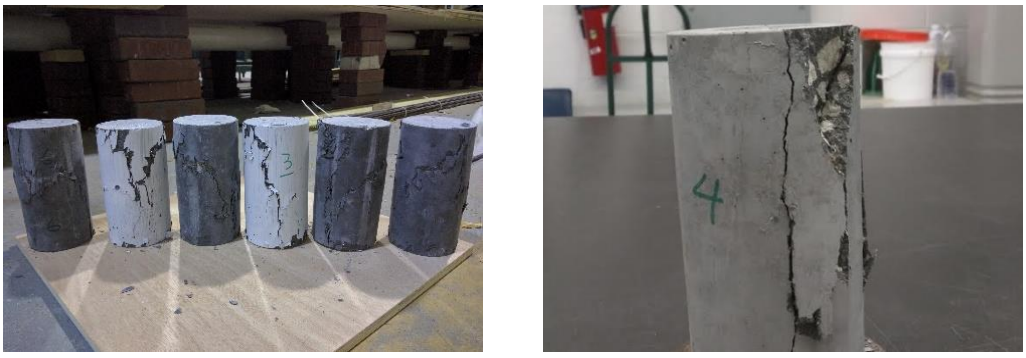

a) b)

Figure 2-2 Example of cylinder specimens after compression test: a) UHPC cylinders, and b) NC cylinders.

The stress-strain curve of UHPC and NC, which is shown in Figure 2-3, was obtained based on the load-displacement relationship, and the compressive strength and elastic modulus were calculated. FHWA [46] suggests calculating the elastic modulus by using values that correspond to 10% and 30% of the ultimate compressive strength. The average result of the test is listed in Table 2-2.

Table 2-2 Compressive cylinder test results.

Test	UHPC	NC
Compressive cylinder test	20.1 ksi	5.86 ksi
Modulus of elasticity	8700 ksi	3200 ksi

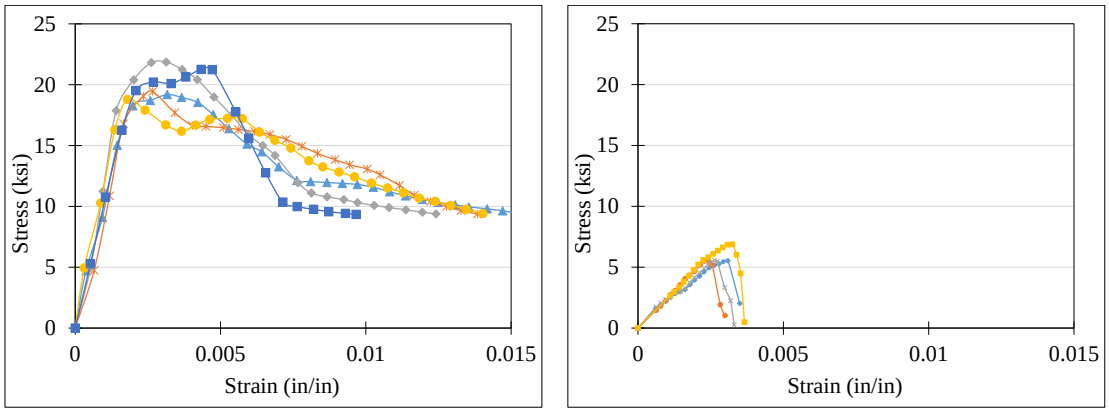

Figure 2-3 Stress-strain curve based on cylinder test of the specimens: a) UHPC, and b) NC.

The NC specimens behave elastically up to the peak strength followed by a rapid strain softening. After the formation of the first crack, when lateral deformation surpassed its tensile capacity, the NC specimens lost their total strength and failed in a sudden explosive manner (see Figure 2-3(b)). In contrast, UHPC specimens behave elastically until approximately 50% of their compressive strength, followed by strain hardening behavior up to peak strength. The interaction between the fibers and the matrix resulted in ductile compressive failure where the concrete surface remains intact even at total strength loss; see Figure 2-3(a). As illustrated in the results, no descending branch in the case of NC is observed which indicates the brittle behavior of the material, while in UHPC descending branch of the stress-strain curve is observed.

2.3.1.2 Cube Tests

At the same time as the cylinder tests, 2 and 3-in. cube specimens were also tested to measure the compressive strength according to ASTM C109 [79] standard test method. Generally, the cylinder compressive strength is lower than its cube strength for the same concrete. This is due to the confining effect of the testing machine plates and the aspect

ratio of the specimen. A strength reduction factor used to convert the cube strengths to cylinder strengths is usually in the vicinity of 0.82 for normal concrete and increases to 1.0 as the concrete strength increases [50].

The load rate for 2-in. and 3-in. cube compression tests were set at 200 lb/s and 675 lb/s respectively. In order to keep the test results consistent, uneven loading surfaces were minimized by applying the load on the vertical molded faces. The average result of the test is listed in Table 2-3.

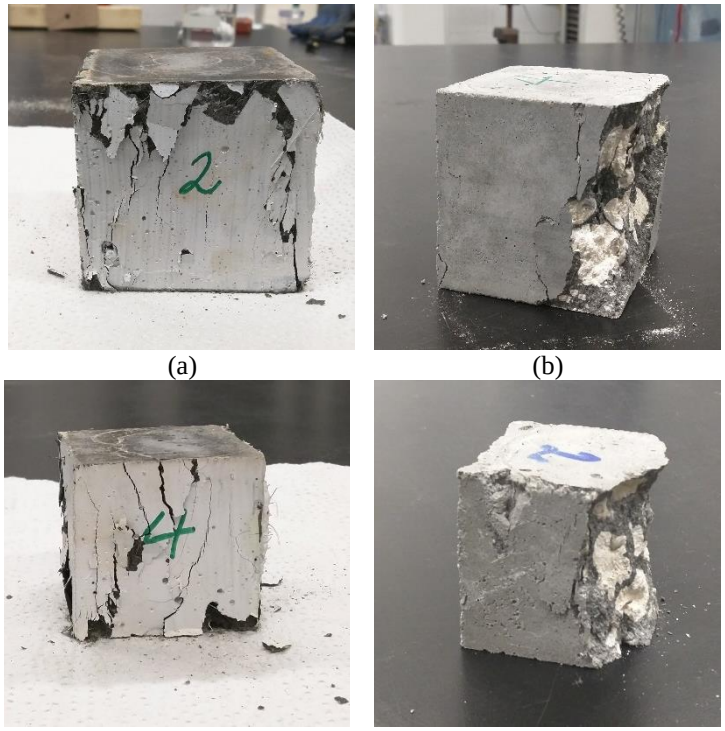

Figure 2-4 Example of cube specimens after compression test a) 3-in. UHPC cube, b) 3-in. NC cube, c) 2-in. UHPC cube, and d) 2-in. NC.

Table 2-3 Compressive cube test results

Test	UHPC	NC
Compressive 2-in. cube test	24.8 ksi	7.62 ksi
Modulus of elasticity of 2-in. cube test	7850 ksi	3417 ksi
Compressive 3-in. cube test	19.4 ksi	9.4 ksi
Modulus of elasticity 3-in. cube test	7400 ksi	3461 ksi

The compressive stress-strain curve for both materials obtained from cubic tests is shown in Figure 2-5.

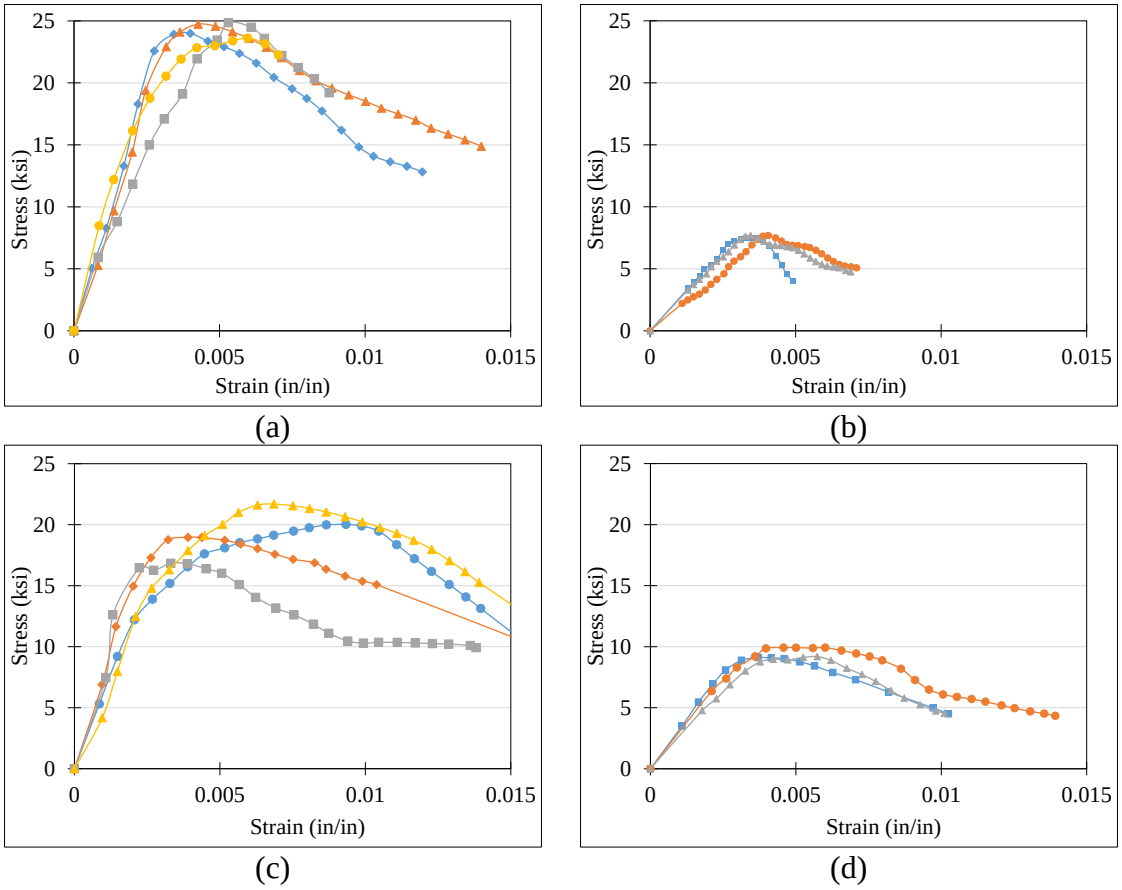

Figure 2-5 Stress-strain curve based on cubic test of the specimens: a) UHPC 2 in. , b) NC 2 in., c) UHPC 3 in., and d) NC 3 in.

2.3.2 Tensile Behavior

Even though concrete is not typically designed to resist direct tension, and tensile strength is almost ignored, it is used to estimate the load under which cracking will happen. In contrast, the tensile strength of UHPC is much higher than that of NC, meaning that it can sustain tensile strength after the occurrence of the first crack. Consequently, determination of tensile strength of UHPC plays a major role in design.

In this investigation, three test methods were used to determine the tensile strength of concrete including flexural test, direct tensile test, and splitting tension.

2.3.2.1 Flexural Test

The ASTM C1018 [79] Standard test method for flexural toughness was one test used to determine the tensile properties of UHPC and NC. Prisms of 20×6×6 in. with a span of 18 in. were used for this test (see Figure 2-6). The prisms were placed on the roller supports with the vertical molded faces located at the compression and tension faces. To ensure low horizontal forces due to support friction, the specimens were supported by steel rollers. The load was then applied via the hydraulically controlled constant load rate (29 lb/s) at the middle length through failure.

a) b) c)

Figure 2-6 Example of prism specimens after flexural test a) UHPC prisms before test, b) UHPC prisms after test, and c) NC prisms after test.

This method of testing is based on simple beam bending theory and linear elastic stress-strain behavior up to failure. Due to the nonlinear behavior of concrete, the assumption of a linear stress distribution is not valid; therefore, results obtained using this method are always greater than the direct tensile strength. Figure 2-6 also shows pictures of typical UHPC and NC beams before and after testing. Notice that in the case of UHPC, the beam remains intact due to the presence of the fibers, while NC prisms failed in brittle

behavior. The average result of the tensile strength from the flexural test of UHPC and normal concrete were 3.17 ksi and 0.7 ksi respectively. The load-displacement curve for both materials obtained from flexural tests is shown in Figure 2-7.

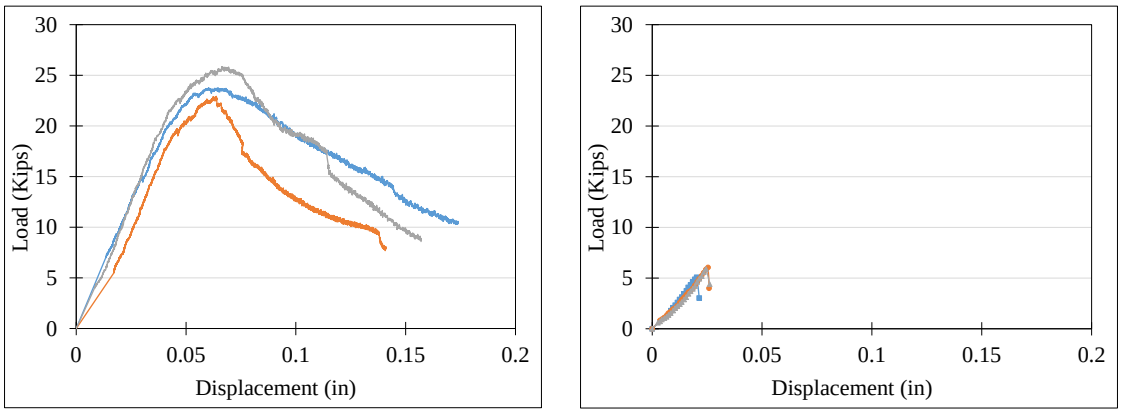

Figure 2-7 Load-displacement curve for beam test of the specimens: a) UHPC, and b) NC.

As shown, the UHPC prism's deflection increased linearly until the initiation of initial crack and was proportional to the load. After the first crack, deflection increased nonlinearly until the ultimate capacity was reached. UHPC showed 4.5 times higher flexural strength compared to NC. The ductile behavior of UHPC compared to NC also can be seen in the curves.

2.3.2.2 Direct Tensile Test

The direct tensile test is a uniaxial test in which the tensile strength of a mortar is determined by pulling the specimen apart. AASHTO T132 [80], describes a test method called briquette tension test method, involving a direct tension testing of a small cement mortar briquette. The dog-bone shaped briquette has a 3-in. length, 1-in. thickness, with a 1-in^2 cross section at mid-length. Since this method is recommended for cement mortar specimens, it cannot be a reliable method for the normal concrete with coarse aggregates.

However, due to a comparison of materials behavior in this study, the direct tensile test was done for NC as well. In addition, in the case of UHPC as the composition shows the aggregate size of UHPC will not be an issue; however, due to the small cross-section of the briquette, fibers will not be randomly distributed as is preferred.

In AASHTO T132 [80], the loading rate is recommended at 600 lb/min. This portion of the test method was modified, and the tests were conducted at a displacement rate of 0.001 in./s suggested by Graybeal [46].

Figure 2-8 shows typical UHPC and NC briquettes before and after testing. As shown, the steel fibers bridge the crack at the middle. As the fibers pull out of the matrix across the crack, the load capacity decreases until the total strength loss, while NC briquettes took apart suddenly after reaching the peak load. The average results of the tensile strength from briquettes for UHPC and regular concrete were 1.3 ksi and 0.51 ksi, respectively.

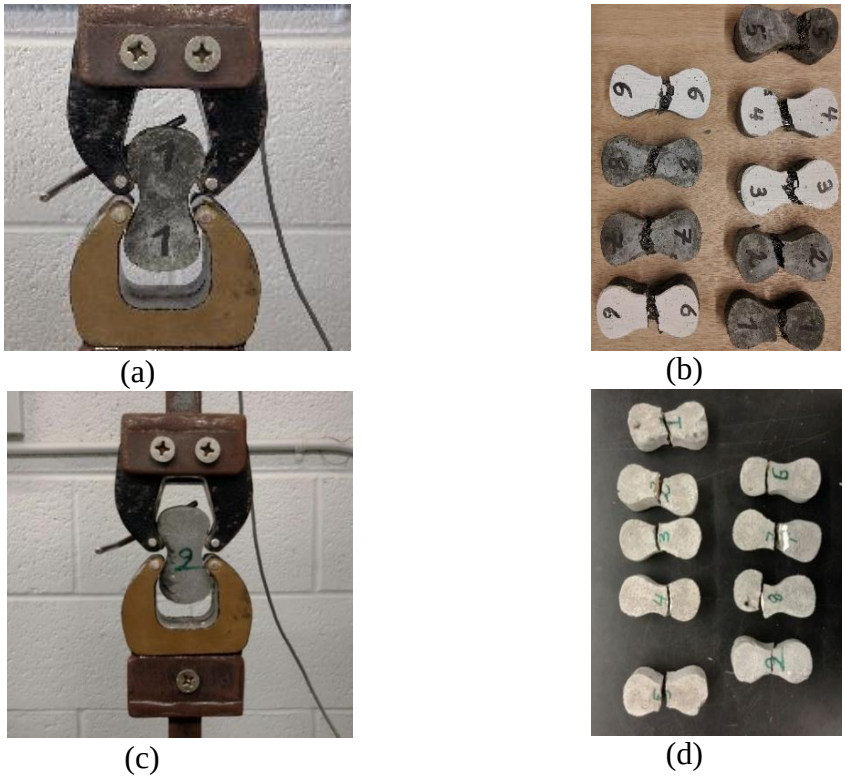

Figure 2-8 Example of briquette specimens a) UHPC briquette before test, b) UHPC briquettes after test, c) NC briquette before test, and d) NC briquettes after test.

Figure 2-9 presents the load-displacement that resulted for each concrete type. The results indicate that UHPC behaved linear-elastically up to first cracking, followed by a significant amount of post-cracking load-carrying capacity. This is explained by the presence of the composite action of the fibers that bridges across the cracks. On the contrary, the NC briquettes failed briskly owning with the localization of the maximum strain in a single crack.

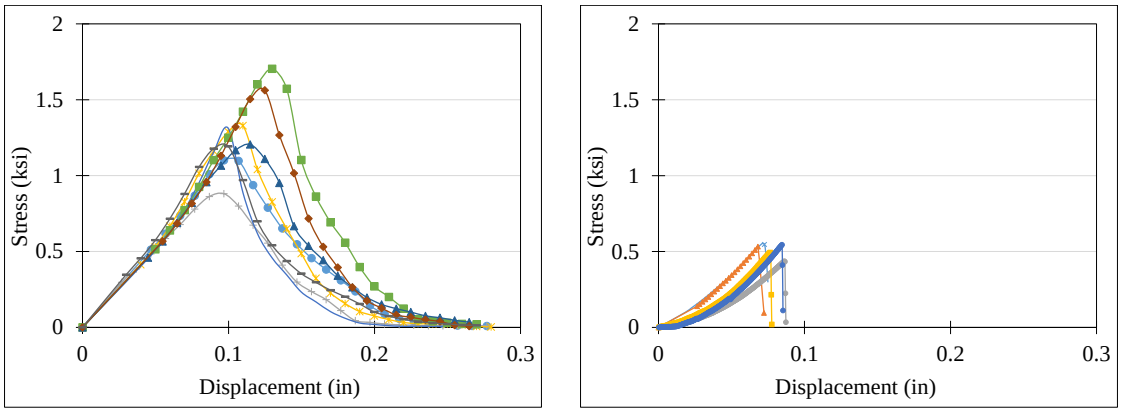

Figure 2-9 Stress-displacement curves of the briquette specimens: a) UHPC, and b) NC.

2.3.2.3 Splitting Tensile Strength

In the splitting tensile strength test method, a cylindrical or cubical test specimen is located on its side under compression loading until it splits into two pieces lengthwise when its tensile strength is reached. Therefore, the peak load carried by the specimen is used to determine the splitting tensile strength. This test is increasingly popular as it can be more easily run. It was commonly known as the "Brazilian Method" in the 1970's and is currently cited by ASTM C 496, "Splitting Tensile Strength of Cylindrical Concrete Specimens" [79].

This test used 3-in. diameter cylinders. The load rate for these tests was set at 210 lb/s. Although this method is commonly completed on brittle concrete where a complete failure occurs with a single crack, again in order to compare the material behavior of NC and UHPC it has been done for both NC and UHPC. The reason that this method is not reliable for fiber-reinforced concrete can be explained due to the different behavior of ductile materials, particularly UHPC. In these concretes, fibers enable the specimen to carry the load after the failure that has already taken place.

In the case of UHPC, the results show significant compressive crushing arises at the platens of the testing machine owning with the steel fiber content. It is also noticeable that the UHPC cylinders did not split into two pieces, and that is due to the presence of fibers. The average result of the tensile strength from the splitting test for UHPC and regular concrete were 3 ksi and 0.48 ksi.

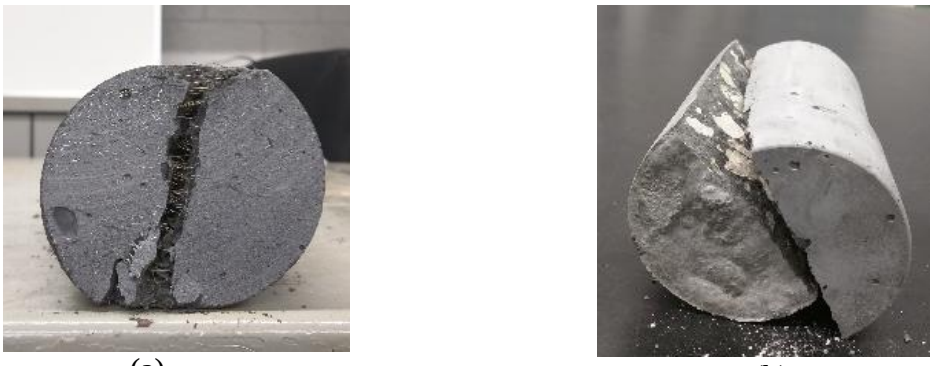

(a) (b)

Figure 2-10 Example of cylinder specimens after splitting tensile test a) UHPC splitting cylinder after test, and b) NC splitting cylinder after test.

In this study, the splitting tensile strength of UHPC was determined as the first point in which the load carrying instability take place by crack initiation, and further load carried by the specimen after crack initiation was recognized more related to toughness than the actual increase in tensile strength of the material. The results of the splitting test are illustrated in Figure 2-11.

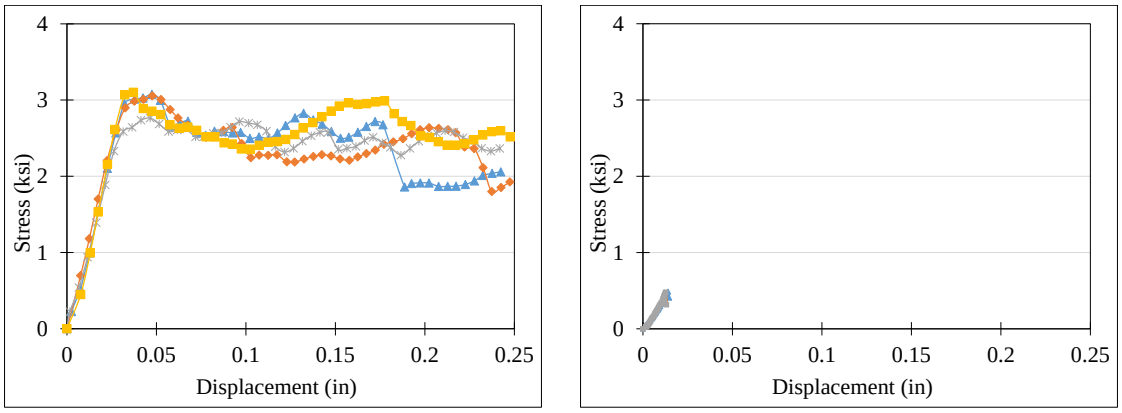

Figure 2-11 Stress-displacement curve: a) UHPC, and b) NC.

Frequently, the tensile strength of concrete is defined as a percent of the compressive strength. The results from flexural prisms, briquette, and splitting tensile tests have been normalized by the 28-day compressive strength of cylinders.

2.4 Experimental Result Discussion

Experimental results show that among the two considered material, UHPC had a significantly improved performance compared to normal strength concrete. In general, the compressive and tensile strength, ductility and modulus of elasticity of UHPC were notably higher than normal strength concrete. The mode of failure and behavior of UHPC test specimens after peak load exhibit the influence of fibers For UHPC, the compressive strength was similar for the cube (3 in) and cylinder specimens (3×6 in.) while the cube (2 in.) specimen exhibited higher ultimate strength. Figure 2-12 displays the average compression and tensile strength of tested UHPC compared with normal concrete.

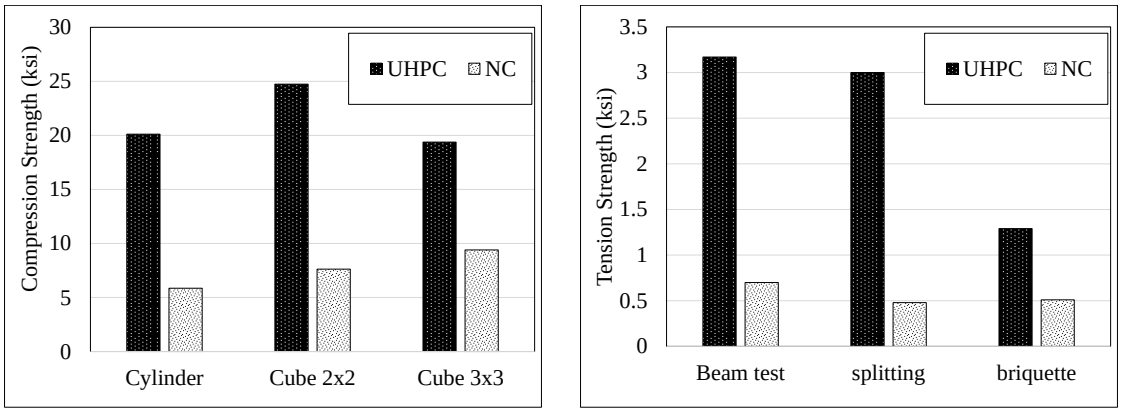

a) b)

Figure 2-12 Average compression and tensile strength of tested UHPC compared with normal concrete a) Compression strength and b) Tension strength.

2.5 Numerical Study

This section presents the numerical study of UHPC behavior and failure. The simulation of UHPC material through commercial FE software allows for the study of the structures including UHPC. A three-dimensional FEM simulation is used to model the failure process of the experimentally tested compression cylinders and cubes along with flexural prisms. The commercial software Abaqus is commonly utilized in the research, and the concrete plasticity damage (CDP) model in this software can predict the behavior of the concrete with reasonable accuracy. This model has been employed by researchers to model conventional concrete [81]. In this study, the CDP model was used to simulate UHPC, and the mechanical behavior obtained through experiment is transferred to the numerical model.

The concrete material parameters used in this study are the modulus of elasticity (E), Poisson's ratio (v), and the CDP parameters. In the CDP, for cracked concrete, a constant value for Poisson's ratio is considered. The primary values of the CDP parameters include dilation angle (ψ), shape factor (K_c), stress ratio σ_{b0}/σ_{c0}, eccentricity, and viscosity

parameter. In the current study, the value of all parameters and modeling technique were based on previous studies done by other researchers [82–84], then calibrated with the experimental results obtained through tests. Table 2-4 presents all the parameters for CDP modeling.

The influence of mesh size on the accuracy of the numerical simulation has been investigated with three different sizes of mesh including 0.5 in., 1 in., and 1.5 in. Due to the uncertainty in boundary condition, such as grip slippage in briquette tensile test and different behavior of fiber reinforced concrete in splitting tensile test, these tests have not been included in the FEM. The friction of boundary condition has not been considered in simulation, and the loading of all models was displacement control.

Table 2-4 The employed material parameters for the FE computation.

Elastic Parameter					
Young's Modulus	7500 ksi		Poisson's Ratio	0.18	
Concrete Damage Plasticity (CDP) Parameters					
Plasticity		Compressive Behavior		Tensile Behavior	
Dilation Angle	56	Yield Stress	Inelastic Strain	Yield Stress	Cracking Strain
Eccentricity	0.1	18 ksi	0	0.1 ksi	0
fb0/fc0	1.1	20 ksi	0.001	1.4 ksi	0.0035
k	0.66	11 ksi	0.009	0.3 ksi	0.05
Viscosity Parameter	0				
Mesh Type: C3D20R (A 20-node Quadratic brick, reduced integration)					

Figures 2-13 shows the Abaqus FE predictions with different mesh size for each group of specimens compared with the results of laboratory experiments, which closely follow the test data.

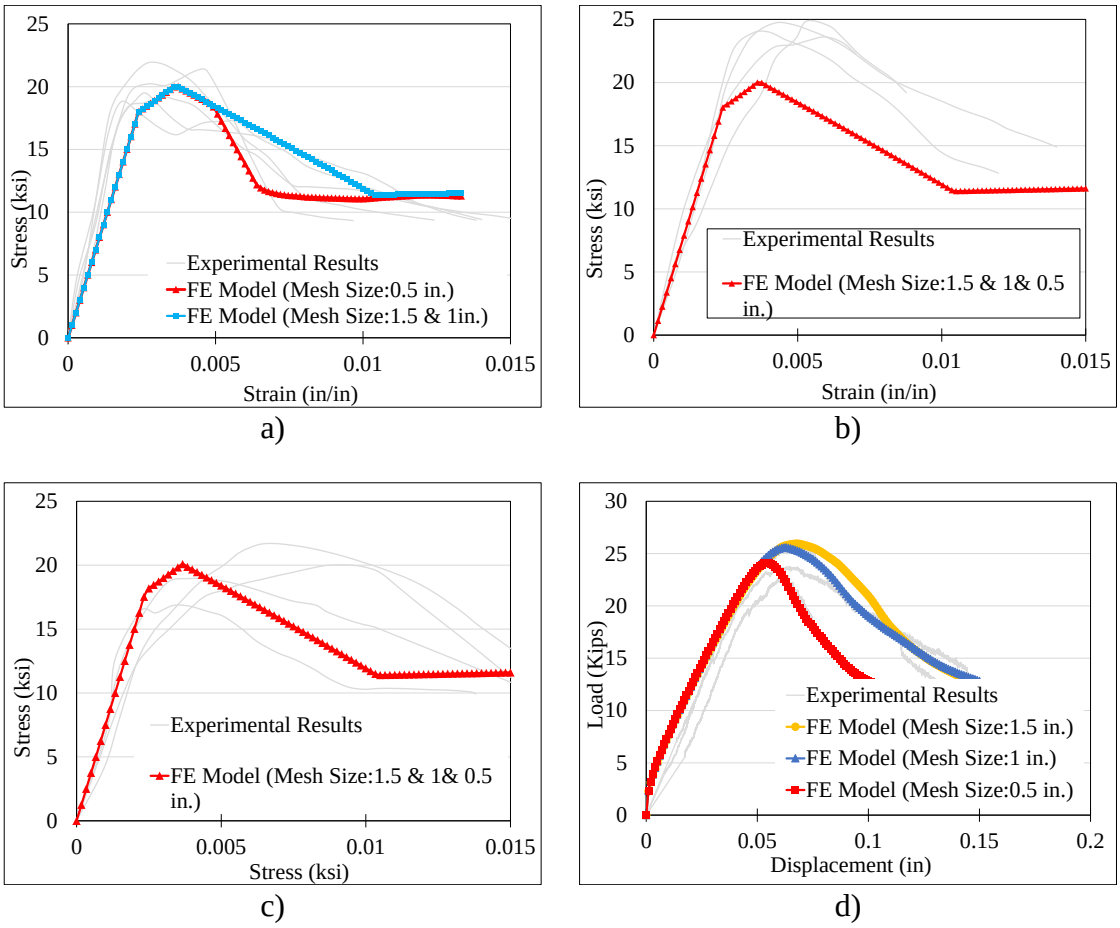

Figure 2-13 Comparison between numerical and experimental UHPC test a) compression cylinder b) 2 in. cubic compression test c) 3 in. cubic compression test d) flexural strength test.

Although there is good agreement between the laboratory tests and numerical models, the slight difference in performance can be explained by the difference in boundary condition of the experimental specimen and the FE model, for example, the amount of friction between the loading plates and the specimens are not considered in FE modeling. Most importantly, in modeling, the effort was to define one single material to have good agreement with the experimental data for all test specimens. Therefore, it was not possible to fit all results completely. It is worth to mention that there are many parameters that can affect the results of the test results including the amount of fibers, the age of the concrete, etc. The influence of each parameter can be considered for future studies.

2.6 Conclusion

To determine the basic behaviors of UHPC and NC, experimental tests have been done on the materials including cylinder, and cube compressive strength (2x2- and 3x3-in.) tests, as well as three-point flexural strength, briquette tensile, and splitting tension test.

Results obtained from the experimental phase of the study indicate that the compressive strength of commercial UHPC, used in this study, was three to four times greater than normal strength concrete. Moreover, higher modulus of elasticity (approximately two times) of UHPC specimens was obtained when compared with the NC. The strong mechanical interlocking force between steel fibers and concrete matrix cylinders and cubes remained intact even after failure loading, whereas the control sample of normal strength concrete split into large concrete pieces after failure. Consequently, UHPC can foster high compressive strength without sacrificing the ductility.

Furthermore, in the case of UHPC specimens, a higher tensile strength and ductility of the material was observed when compared to regular concrete (two to four times greater). This is a result from a strong interlocking force between fibers and concrete matrix after the ultimate tensile capacity. Briefly, the results demonstrate the superior material properties of UHPC, particularly compared to regular concrete in both compression and tension. As shown in the result, employed material parameters for the FE model can provide the researchers a reliable prediction, which can be used for the next step of this research.

CHAPTER 3 MOMENT CAPACITY OF UHPC SECTIONS

3.1 Introduction

Many researchers have performed experimental studies on the structural behavior of UHPC sections to establish a reliable analytical method to calculate the flexural capacity of the section. However, most of these studies were performed through a limited number of specimens due to the high cost of UHPC. To design the proposed connection as it will be discussed in chapter 8, the moment capacity of the UHPC section is needed. The objective of this chapter is introducing the concept of the stress distribution of well-known existing methods and comparing their accuracy to calculate the moment capacity of a reinforced UHPC section through a parametric study. To that aim, several small-scale beams were constructed and tested to evaluate the flexural behavior and ultimate moment capacity of the reinforced UHPC sections. The performance of the tested specimens is discussed regarding the moment capacity, load-deflection curves, crack development and the modes of failure.

By using the information from the previous chapter, the obtained results through the experiments were, then, used to validate the Finite Element (FE) model. Comparing the numerical and experimental results indicates that generally, the numerical method can predict the structural behavior of UHPC beams reasonably. Hence, the validated FE model was employed as a reference point to evaluate the existing analytical approaches to calculate moment capacity of UHPC beams. A series of large-scale beams with different geometries and reinforcing details were numerically simulated, and the results were compared with the results obtained through the analytical methods. The results showed that

some of the existing methods can predict the ultimate moment capacity of the UHPC beam with an acceptable accuracy.

Notation	
a: depth of a rectangular stress block;	f_c: compression strength of UHPC;
A_s: area of steel rebar in tension;	f_t: the tensile stress of UHPC;
b: width of the beam;	f_y: yield strength of steel rebar;
c: depth to the neutral axis;	h: height of the beam;
d: depth from extreme compressive fiber to centroid of rebar steel;	l_f: length of fibers;
	ρ_s : rebar percentage;
d_f: diameter of the fibers;	σ_{fy}: fiber yielding stress;
Ef_s: modulus of elasticity of fibers;	τ_f : fiber-concrete bond strength;
E_{UHPC}: modulus of elasticity of UHPC;	β_1: stress block parameter.

The moment, shear and compression capacity of a normal strength reinforced concrete is well understood based on which the codes have developed procedures to obtain the moment capacity. Although several experimental and numerical tests have been performed on the flexural behavior of the reinforced UHPC beams, and are documented as a technical report, there is no general design guideline for the material in the US standards.

The ductility and tensile strength resulting from the fibers is a characteristic material behavior of UHPC that cannot be ignored. These characteristics change the behavior of the UHPC beams compared to normal strength reinforced concrete ones. Accordingly, the procedures developed in codes for normal strength concrete beams cannot be straightforwardly used for UHPC sections without modifications.

Due to the complicated character of developing a Finite Element (FE) model, a simplified analytical procedure can facilitate the design process [85–89]. The developed analytical procedure should provide basic assumptions to calculate the moment capacity of the UHPC beams.

The objective of this chapter is to evaluate the existing methods to calculate the ultimate moment capacity and understand the flexural behavior of a reinforced UHPC beam section. To do so, several small-scale UHPC beams with different percentage of longitudinal reinforcement and effective depth were tested. The results of these experimental tests were used to validate the FE models. The material properties of UHPC adopted in this model were based on the material properties used in the previous chapter and its published paper [90]. The FE model was able to predict the behavior of the tested beams including load-deflection curves, ultimate capacity, and mode of failure with a good agreement. This model was able to predict the behavior of UHPC specimens with different geometries, and loading conditions, and reinforcing details with a reasonable accuracy, and was considered as a reference point. Then it was used as a benchmark for a parametric study on large-scale beams to evaluate the existing analytical method.

3.2 Experimental Program

Twelve small-scale UHPC beams were fabricated and tested under three-point loading. Construction of the specimens was undertaken in several stages. In the first stage, the forms were oiled and the steel bars were placed in their positions in the forms. Plywood blocks with holes drilled in them were used to support the steel bars. As the casting direction may affect the fiber orientation [91–95], all specimens were cast horizontally and trowel finished. After casting, the specimens were covered with polythene sheets for 72 hr. and then de-molded. The specimens were kept moist for one week after casting to control the rate of moisture loss and hence prevent premature shrinkage cracking. Then they were

cured in an air-dry condition until the test. Prior to the test, the beams were painted in white to facilitate tracing of the cracks.

All specimens designated as Sh×b- ρ_s –d/h (D) where: h and b specify the height and the width of the beam in inch, respectively. ρ_s shows the percentage of rebar in tension and d/h presents the ratio of effective depth to the height of the section (see Figure 3-1). As some specimens had the same geometry and rebar percentage and were cast as alternate specimens, (D) at the end of the specimen's names shows the duplicate specimen results. For example, S6×6-1.7-0.85 shows the specimen with the width and height of 6 in., 1.7% of rebar ratio and d/h=0.85 (d= 5.1 in.). Also, Specimen S6×6-0-0 and S6×6-0-0D show the specimens without rebar reinforcement. Based on previous studies [96], the development length in UHPC is much less than regular concrete and there was no need for the mechanical anchorage.

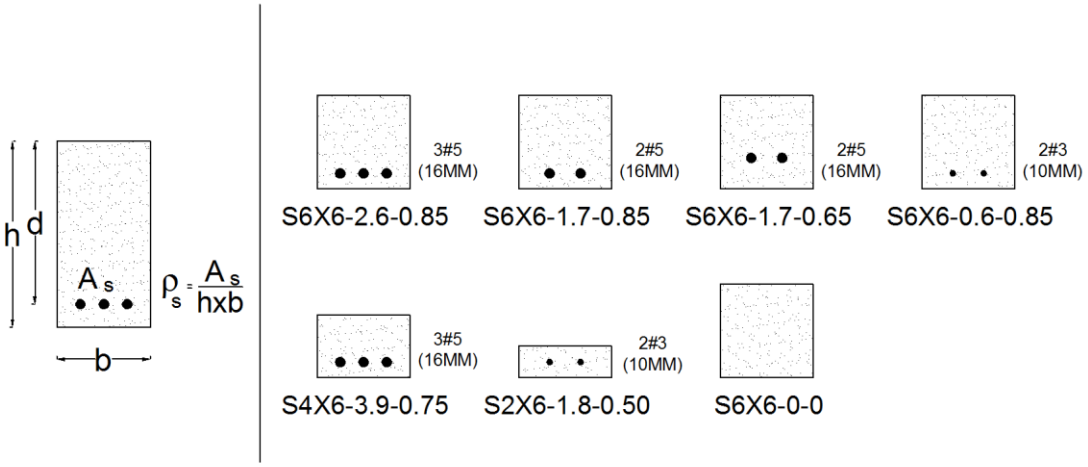

Figure 3-1 Designation of the beam (Sh×b- ρ_s - d/h) (units: in.).

The total length and load span of the beams were 20 in. and 18 in., respectively. To compare the results, all tested specimens had similar material and width and longitudinal reinforcement provided reinforcement ratios of 0% to 2.6%. The specimens were designed

to show flexure and shear behavior under center-point bending test loading approach for tensile based on AFGC [58].

3.2.1 Materials

The UHPC used in this study was composed of a blended premix powder, water, superplasticizer, and 2% steel fibers by volume which is the most common ratio suggested by commercial UHPC companies in North America. The premix powder included cement, silica fume, ground quartz, and sand. The fibers were 0.5 in. (13 mm) long with a diameter of 0.2 mm respectively, with a tensile strength of 400 ksi. Flow table test was performed according to ASTM C1437 [97], to obtain the rheology of the UHPC. Static and dynamic flowability of UHPC was measured 8 in., and 10 in., respectively.

The compressive and tensile strength of UHPC were obtained through testing cylinder specimens (3×6 in.) and dog-bone test, respectively. The mean compressive (f_c) and tensile (f_t) strength of the tested beams were 21 ksi and 1.4 ksi respectively.

All steel reinforcements were from one heat in manufacturing. Tension tests performed on three representative specimens resulted in an average yield strength of 68 ksi and ultimate strength of 113 ksi.

3.2.2 Testing Procedure and Loading

The test was conducted at the age of 150 days after casting. The load was applied constantly in the middle of the beam. Figure 3-2 illustrates the loading setup. Load cells and pressure transducers were used to measure the load at each level of loading. The deflection was measured by the potentiometers installed at the mid-span of the beams. The applied load, deflection, and crack tracing were recorded after each load increment. To

observe the post-peak behavior of the specimens, the loading was continued up to either the failure of the beam or 1-inch deflection.

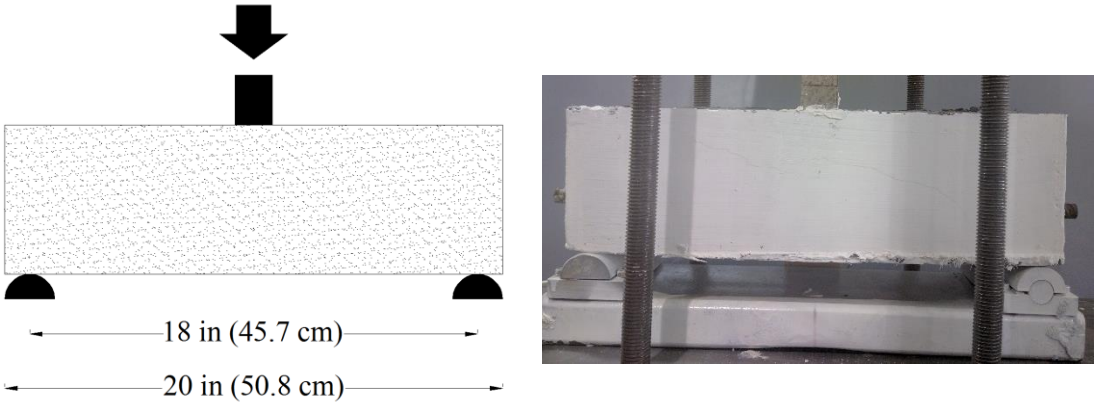

Figure 3-2 Load setup.

3.2.3 Analysis and Discussion of Experimental Results

The behavior of the specimens including crack patterns, mode of failure, load-deflection relation, and ductility are discussed in the following sections.

3.2.3.1 Cracking and Modes of Failure

The failure patterns of the tested beams are shown in Figure 3-3. Varying reinforcement ratio and effective height of the section changed the ultimate load capacity and initial stiffness of the beams. No significant cracks were observed in the early stages of loading. Different mode of failure including flexure, shear-flexure, and shear failure were observed for the specimens. The flexure cracks propagated at the middle of the beams and were followed by shear cracks near the supports in the shear zone. In general, failure of the UHPC beams started when the fiber began to pull out of the concrete matrix.

Specimen S6×6-0.6-0.85 having 0.85% rebar percentage failed by fracture of the rebars before reaching high ductility. This can be attributed to the short length of the plastic hinge due to the high bonding of UHPC and the stress concentration in the rebar.

S6×6-2.6-0.85

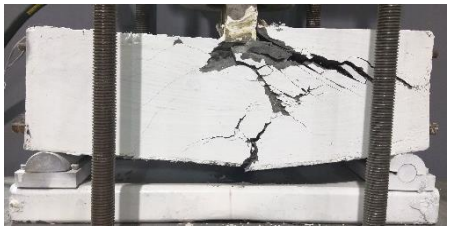

S6×6-2.6-0.85D

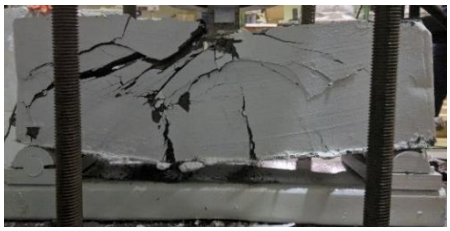

S6×6-1.7-0.85

S6×6-1.7-0.85D

S6×6-1.7-0.65

S6×6-1.7-0.65D

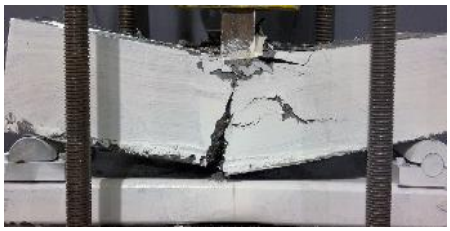

S4×6-3.9-0.75

S4×6-3.9-0.75D

S2×6-1.8-0.50

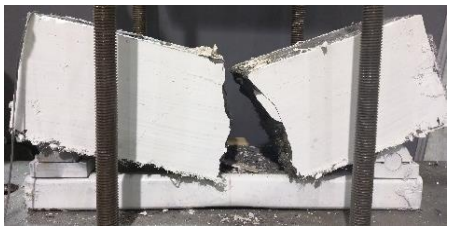

S6×6-0.6-0.85

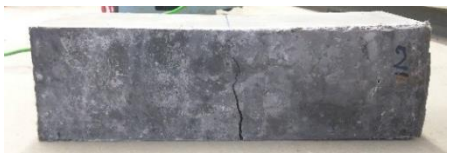

S6×6-0-0

S6×6-0-0D

Figure 3-3 Failure crack patterns of the specimens after the end of the test.

3.2.3.2 Load – Displacement Curve of the Tested Beams

The mid-span deflection curves throughout the loading of the tested beams are presented in Figure 3-4. Generally, using fibers minimizes the cracking and increases the ductility of the beams. The ductility ratio was defined as $(\frac{\Delta_y}{\Delta_u})$ where Δ_y was the ideal yielding displacement and Δ_u was the displacement associated to 0.85 of the ultimate capacity after the peak load. For example, the ductility ratio of specimen S6×6-2.6-0.85 and S6×6-1.7-0.85 were more than 6 and 5, respectively. The average ductility of specimens having no rebar (S6×6-0-0) was 3.7. Table 3-3 reports the corresponding load to the ultimate flexural capacity of the tested beams.

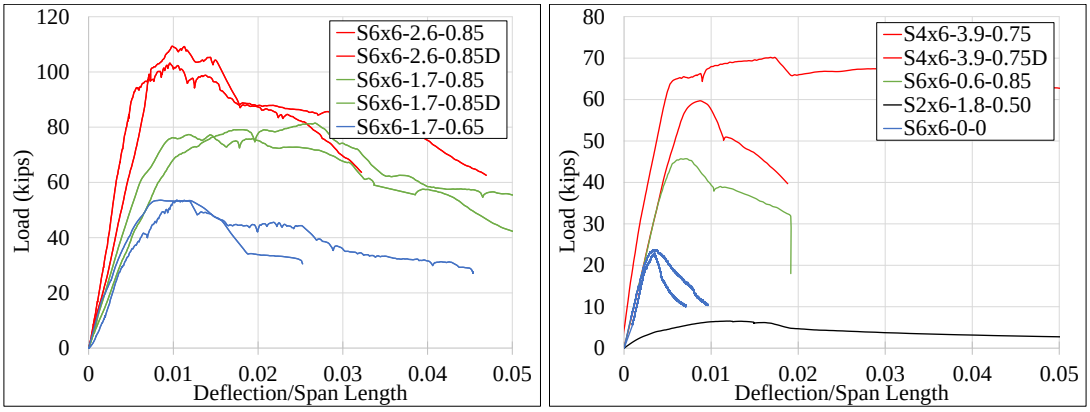

Figure 3-4 Normalized deflection (Δ/L) of the tested beams (L=18 in.).

3.3 Analytical Equations

There are some analytical solutions to calculate the flexural capacity of UHPC beams [56,58,98–100]. These analyses use internal stresses based on the stress-strain distribution to estimate the moment capacity.

An approach to calculate the moment capacity of a UHPC section can be the same as normal strength concrete considering its compressive strength and ignoring its tensile strength. In this approach, UHPC stresses in compression can be represented by an

equivalent rectangular stress block which is proposed for high strength concrete. This approach may cause conservative result for designing flexural elements. This procedure can be adopted from equations related to moment capacity of normal concrete beams suggested by ACI 318 [101]. This code provides minimum requirements for the material, analysis, design, and detailing of normal concrete.

$$M_n = A_s f_y \left(d - \frac{a}{2}\right) \quad (3\text{-}1)$$

Another approach can be adopted from ACI 544 [102] which is an available standard of fiber reinforced concrete. According to this code, the flexural capacity of a Steel Fiber Reinforced Concrete (SFRC) section with a rectangular h×b cross-section is calculated by the following equation:

$$M_n = A_s f_y \left(d - \frac{a}{2}\right) + f_t b(h-e)\left(\frac{h+e-a}{2}\right) \quad (3\text{-}2)$$

$$c = \frac{A_s f_y + f_t h}{f_t \frac{\varepsilon_f + 0.003}{0.003} + 0.85\beta_1 f_c} \quad (3\text{-}3)$$

$$e = \frac{\varepsilon_f + 0.003}{0.003} c \quad (3\text{-}4)$$

$$a = \beta_1 c \quad (3\text{-}5)$$

$$\sigma_{fs} = 2\tau_f \left(\frac{l_f}{d_f}\right) \leq \sigma_{fy} \quad (3\text{-}6)$$

$$\varepsilon_f = \frac{\sigma_{fs}}{E_{fs}} \quad (3\text{-}7)$$

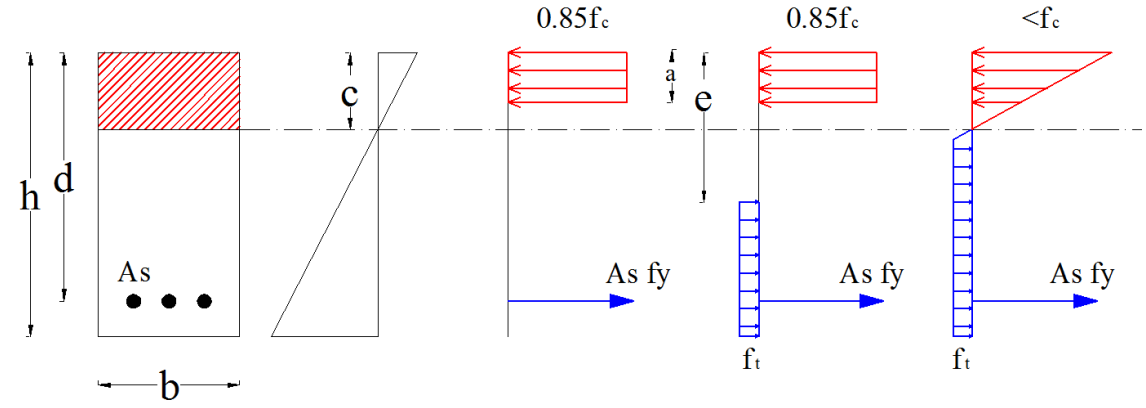

Strain distribution b) ACI 318[101] c) ACI 544 [102] d) FHWA [56]

Figure 3-5 Stress distribution assumption of previously suggested methods.

In this method, the tensile stress of concrete assumed to be uniformly distributed over an area with a height of (h−e). The distance from the extreme compression line to the top of the uniform tensile block (e) is calculated by the equations (Eq.3-2 to Eq.3-7). The depth of the neutral axis (c) is calculated by equilibrium equation of the section. The coefficient β_1 is equal to 0.65 for concrete strengths more than 8 ksi. Based on the literature, τ_f can be taken as 0.6 ksi [103–105] for fiber-reinforcement concrete.

Another method of calculating the flexural capacity of rectangular UHPC beams is based on one of the Federal Highway Administration (FHWA) reports [56]. In this model, using the equilibrium equation and strain compatibility, the moment capacity of a UHPC beam is estimated when either the extreme compression or tension strain reaches its limiting value. In this method, when the tension limit state controls, the following equation can be used for estimating the moment capacity of the section.

$$M_n = A_s f_y \left(d - \frac{c}{3}\right) + f_t b(h-c)\left(\frac{3h-c}{6}\right) \quad (3\text{-}8)$$

$$c = \left(\frac{\rho_s f_y + f_t}{f_t + 0.0035\, E_{UHPC}\left(\frac{c}{h-c}\right)}\right) \quad (3\text{-}9)$$

Note that estimating the neutral axis depth can be done by solving a quadratic equation or an iterative process. To estimate the modulus of elasticity of UHPC some other equations are provided by previous studies [46,58,106].

$$E_{UHPC} = 50000\sqrt{f_c}\ (psi) = 4200\sqrt{f_c}\ (MPa) \quad \text{(Sritharan)} \quad (3\text{-}10)$$

$$E_{UHPC} = 46200\sqrt{f_c}(psi) = 3840\sqrt{f_c}(MPa) \quad \text{(Graybeal)} \quad (3\text{-}11)$$

$$E_{UHPC} = 260000\sqrt[3]{f_c}(psi) = 9500\sqrt[3]{f_c}(MPa) \quad \text{(AFGC 2013)} \quad (3\text{-}12)$$

3.4 Finite Element Modeling

One option to predict the behavior of UHPC sections is using FE models. The FE software, Abaqus, has several models for concrete. For the present study, Concrete Damage Plasticity (CDP) was used for modeling the beams. The validation of UHPC material properties used in FE model for pure compression and tension was done in the previous chapter. UHPC behavior in tension and compression was assumed as multi-linear stress-strain and the effect of the fibers was assumed to be uniformly distributed. Table 3-1 shows all the parameters for CDP modeling used in the research. Also, a multi-linear stress-strain curve was used for modeling the steel reinforcing bars as shown in Table 3-2.

A three-dimensional FE simulation was used to model the failure process of the experimentally tested beams. Three steel loading plates were used as supports. The mesh size of the tested beams was assumed around 0.5 in. in height and length, and 1 in. in width of all the specimens. The beams were analyzed using 20 node brick elements (C3D20R) to model the UHPC. The rebar reinforcements were modeled using a 2-node linear 3-D truss element (T3D2) and embedded in the UHPC with a perfect bond. The supports and loading

plate were idealized as square prisms which were modeled with an 8 node brick element (C3D8) taking material properties of steel [32,84,107–109].

To observe the crack propagation, the damage parameter in tension can be also assumed to activate when the peak tensile strength is achieved. This parameter can be calculated through the equation 3-13, recommended by Mahmud et al. [110].

$$d_t = 1 - \frac{\sigma}{f_t} \tag{3-13}$$

Table 3-1 The employed material parameters of UHPC [90].

Elastic Parameter					
Young's Modulus	7500 ksi		Poisson's Ratio	0.18	
Concrete Damage Plasticity (CDP) Parameters					
Plasticity		Compressive Behavior		Tensile Behavior	
Dilation Angle	56	Yield Stress	Inelastic Strain	Yield Stress	Cracking Strain
Eccentricity	0.1	18 ksi	0	0.1 ksi	0
fb0/fc0	1.1	20 ksi	0.001	1.4 ksi	0.0035
k	0.66	11 ksi	0.009	0.3 ksi	0.05
Viscosity Parameter	0				
Mesh Type: C3D20R (A 20-node Quadratic brick, reduced integration)					

Table 3-2 The employed material parameters of steel reinforcement.

Elastic Parameter	
Young's Modulus	29000 ksi
Poisson's Ratio	0.30
Plastic Parameters	
Yield Stress	Plastic Strain
68 ksi	0
68 ksi	0.0127
113 ksi	0.0877
113ksi	0.1177
Mesh Type: T3D2 (3D truss elements)	

3.5 Numerical and Analytical Results of the Tested Specimens

3.5.1 Numerical Results

The load-displacement curves of both numerical and experimental tests are plotted in Figure 3-7. The model was able to predict the initial stiffness, peak load and

corresponding displacement of the tested beams as well as mode of failure with an acceptable accuracy. Figure 3-6 shows the stress distribution of the specimen (S6x6-2.6-0.85) at the peak load as an example.

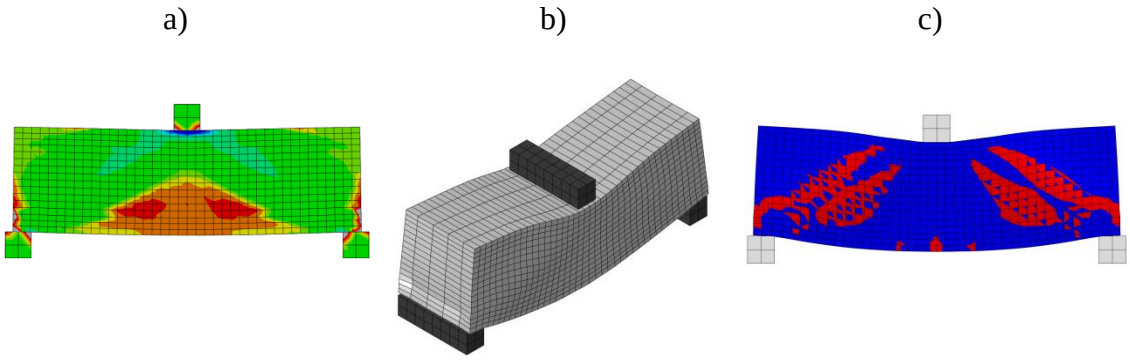

Figure 3-6 c a) Stress distribution b) exaggerated deformed model c) tensile damage representing cracks from FE model for specimen S6×6-2.6-0.85.

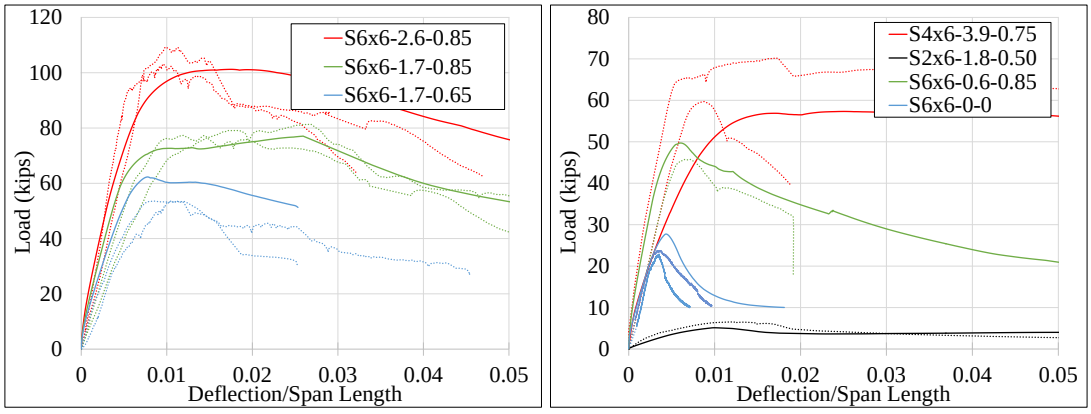

Figure 3-7 Load - normalized deflection (Δ/L) curve of the tested beams (doted) and FE model predictions (solid).

3.5.2 Comparison between the Models

Experimental results have been employed to validate results of the analytical and finite element methods. Maximum loads measured from the experiments, FE results, and existing analytical methods are compared as illustrated in Table 3-3. In these methods, the length and the diameter of the fibers were 0.5 in. (13 mm) and 0.2 mm, respectively. The nominal fiber's yield strength (σ_{fy}) was assumed 400 ksi. Therefore, based on ACI544

[102] analytical model (Equation 3-6), σ_{fs} was calculated 78 ksi. The tension strength (f_t), compression strength (f_c), modulus of elasticity of the UHPC and steel properties were assumed the same as the numerical model mentioned in Table 3-1 and Table 3-2.

To measure the accuracy of each method, Mean Absolute Percentage Error (MAPE) with the following equation was used.

$$MAPE = \frac{100}{n}\sum_{i=1}^{n}\left|\frac{E_i - P_i}{E_i}\right| \quad (3\text{-}14)$$

Where E_i is the experimental result and Pi is the predicted value.

Table 3-3 Results of the maximum load capacity of the tested beams compared with different approaches.

Specimen	S6×6-2.6-0.85 kips	S6×6-1.7-0.85 kips	S6×6-1.7-0.65 kips	S4×6-3.9-0.75 kips	S2×6-1.8-0.50 kips	S6×6-0.6-0.85 kips	S6×6-0-0 kips	Mean Absolute Percentage Error (MAPE)
Experimental	109.2	84.45	53.57	65.17	6.54	45.7	23.76	-
FE	101.20	82.75	61.07	57.31	5.13	49.70	27.73	11.8%
FHWA [56]	87.74	67.03	55.94	46.44	5.42	41.37	27.19	16.3%
ACI318 [101]	67.72	45.28	34.18	38.02	3.03	16.41	-	46.7%
ACI544 [102]	89.78	70.59	59.49	45.72	5.80	45.67	31.40	16.9%

Comparing the numerical and experimental results show that FE models reasonably predicted the responses of the ultimate moment capacity of UHPC beams for which the MAPE was 11.8%. The mean percentage error of initial stiffness of numerical model was reported 9.5% as well. As shown in Table 3-3, FHWA [56] and ACI544 [102] could calculate the ultimate moment capacity with a reasonable accuracy, while the ACI 318 [101] gives way less value than the experimental results. This is attributed to ignoring of the tensile capacity of the concrete in this approach. It should be noted that although some of the tested beams failed in shear/shear-flexural manner, still the experimental results may show higher capacity than the one calculated through the existing equations for flexural

capacity. This might be attributed to the conservative nature of analytical methods. Moreover, based on the results, the outcome of the suggested CDP finite element model is fairly reliable to calculate the ultimate moment capacity of the reinforced UHPC beams as it was for UHPC samples behavior in pure compression and tension. Therefore, this numerical model can be used as a benchmark for existing analytical models, making it possible to do more parametric study on UHPC beams. Using this, a parametric study has been done on UHPC beams to consider the effect of different variables on the accuracy of the existing analytical method. These variables include height, longitudinal reinforcement ratio, and cover to total height ratio. The details and results of this study are discussed in the following section.

3.6 Parametric Study

Considering the cost of the UHPC material, constructing and testing large scale beams is not economically possible; therefore a series of large-scale beams with different height, rebar percentage and cover to total height ratio was numerically modeled and compared with the analytical results obtained through existing analytical methods. The bar ratio and the height of the beam can considerably affect the beam capacity. The cover can affect the cracking pattern and consequently the capacity of the beam as well as the effective height of the beams. The designation of the specimens was the same as illustrated in Fig. 3-1 the length of the spans of the specimens were considered 12h and the width of the beams (b) were taken 0.5h, where h is the height of the beam. Although the moment capacity of the sections is usually calculated with a four-point loading test, to be in consistent with the calibrated model, three-point loading was used for the parametric study.

As an example, Figure 3-8 shows the crack formation of beams S24×12-3-0.9, S12×6-3-0.9 and S8×4-3-0.9. This figure shows the mesh sizes, crack formation, deformed shape of the specimens and supports conditions.

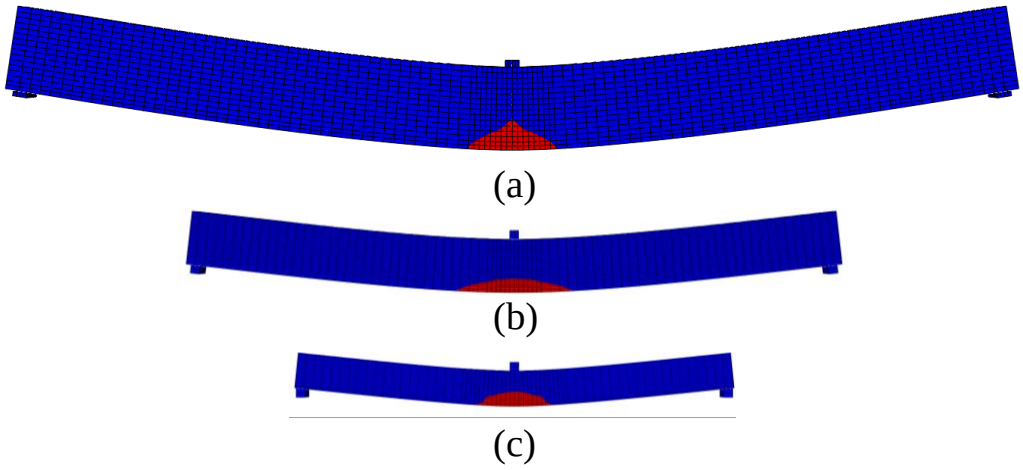

Figure 3-8 Crack formation of the simulated beams a) S24×12-3-0.9, b) S12×6-3-0.9 and c) S8×4-3-0.9.

Table 3-4 Load capacity of the beams with different approaches (h=24 in., b=12 in. and L =288 in.).

Specimen	S24×12-1-0.9 kips	S24×12-3-0.9 kips	S24×12-5-0.9 kips	S24×12-7-0.9 kips	S24×12-1-0.95 kips	S24×12-3-0.95 kips	S24×12-5-0.95 kips	S24×12-7-0.95 kips	Mean Absolute Percentage Error (MAPE)
FE	118.2	221.1	309.5	382.3	122.0	231.6	327.2	408.4	-
FHWA [56]	101.8	200.8	297.5	392.4	105	210.6	313.9	415.2	14.6%
ACI318 [101]	57.45	164.5	261.1	347.3	60.7	174.3	277.4	370.1	50.9%
ACI544 [102]	109.9	203.4	286.2	358.3	113.2	213.2	302.5	381.2	19.1%

Table 3-5 Load capacity of the beams with different approaches (h=12 in., b=6 in. and L =144 in.).

Specimen	S12×6 - 1-0.9 kips	S12×6 -3-0.9 kips	S12×6 -5-0.9 kips	S12×6 - 7-0.9 kips	S12×6 -1-0.8 kips	S12×6 -3-0.8 kips	S12×6 - 5-0.8 kips	S12×6 - 7-0.8 kips	Mean Absolute Percentage Error (MAPE)
FE	26.8	53.7	73.5	88.2	24.2	46.6	62.2	74.9	-
FHWA [56]	26.2	50.9	75.0	98.7	24.6	46.0	66.8	87.2	6.0%
ACI318 [101]	14.4	41.1	65.3	86.8	12.7	36.2	57.1	75.4	20.1%
ACI544 [102]	28.3	51.4	71.9	89.8	26.6	46.5	63.8	78.3	3.9%

Table 3-6 Load Capacity of the beams with different approaches (h=8 in., b=4 in. and L=96 in.).

Specimen	S8×4 - 1-0.9 kips	S8×4 - 3-0.9 kips	S8×4 -5-0.9 kips	S8×4 - 7-0.9 kips	S8×4 - 1-0.8 kips	S8×4 - 3-0.8 kips	S8×4 - 5-0.8 kips	S8×4 - 7-0.8 kips	Mean Absolute Percentage Error (MAPE)
FE	12.2	22.7	29.3	35.4	11.0	19.2	25.2	29.2	-
FHWA [56]	11.6	22.6	33.3	43.9	10.9	20.4	29.7	38.8	12.5%
ACI318 [101]	6.4	18.3	29.0	38.6	5.7	16.1	25.4	33.5	19.6%
ACI544 [102]	12.6	22.9	32.0	39.9	11.8	20.7	28.3	34.8	9.1%

Table 3-4, 3-5 and 3-6 show the results of the FE analysis compared to the analytical results obtained through the existing methods. In the first table, the ultimate moment capacity of the modeled beams with 24 in. height is tabulated while the second and third one show the similar results regarding the beams with 12 in. and 8 in. height respectively.

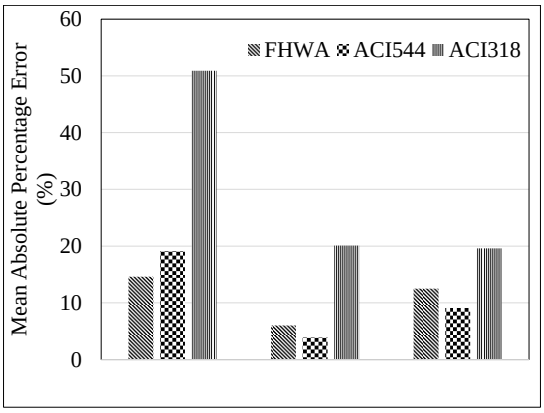

Figure 3-9 Mean absolute percentage error of load capacity of the beams with suggested method compared with calibrated FE results.

Figure 3-9 shows the summary of the results compared to FE model. The results indicate that both ACI544 [102] and FHWA [56] method can be used to calculate the ultimate moment capacity of the UHPC beams with a reasonable accuracy. Furthermore, large-scale experiments may be required to verify the accuracy of the listed methods. It is also worth to mention that designing UHPC beams based on ACI318 [101], which is suggested for normal strength concrete, leads to conservative design results and underestimation of the moment capacity of UHPC elements, especially for large beams.

3.7 Summary and Conclusions

This chapter aimed at calculating the ultimate moment capacity of the Ultra High Performance Concrete (UHPC) beams. Several small-scale beams were tested experimentally and the results were used to validate the numerical model. The UHPC material properties for Concrete Damage Plasticity (CDP) were previously used to predict the behavior of the material in pure tension and compression. Comparison of numerical and experimental results of the test demonstrated that the numerical model can fairly predict the behavior of the UHPC beams including load capacity, initial stiffness,

deflection at the peak, and post-peak behavior. The results show that the calibrated Finite Element (FE) model with a maximum error of 12% can be used to predict the behavior of the UHPC reinforced beams as well as beams without reinforcement when the actual material properties are not available.

Considering the accuracy of the FE model to predict the behavior of the tested beams, this model was used as a reference point to evaluate the existing analytical models. Comparing the results of these methods showed that ACI544 [102] and FHWA [56] methods can predict the ultimate moment capacity of UHPC beams with a maximum error of 12%. Furthermore, using ACI318 [101], suggested for normal strength concrete, lead to overdesign results.

CHAPTER 4 PRELIMINARY DEVELOPMENT OF CONNECTION DETAILS

4.1 Introduction

As discussed in the first chapter, various methods for joining column-to-cap beam have been developed, but none of these methods have entirely solved construction issues. These connections have been set in a way to transfer lateral seismic forces from the superstructure to the column. Among the methods are bar couplers, grouted ducts, pocket connections, member socket connections, hybrid connections, and integral connections. In addition, some of these connections were explored in an actual bridge in the United States for connecting precast elements [24]. In seismic regions, the design of a column should eventually lead to forming plastic hinges and dissipating seismic forces. The ends of a typical column where it connects to the footing and pier caps are the most critical parts [7].

Several studies have been conducted on the methods of connection between column and cap beam, which are commonly used in practice. In 2011, a comprehensive experimental research was performed under NCHRP project [14] on several precast bent cap details including cast-in-place, grouted duct, cap pocket, and hybrid connections. Design flowcharts were recommended based on the results for seven cap beam specimens [14]. Another research study evaluated seven cap beam-column connections for seismic and non-seismic areas. The study characterized precast or prefabricated elements in bridges in seismic areas into two categories, energy-dissipating and capacity-protected, and concluded that there is a significant gap in the knowledge about energy-dissipating connections [13]. In another study, Tazarv and Saiidi experimentally investigated a new column-to-footing connection using UHPC. Their results suggested the UHPC-filled duct

connection could be a suitable connection for high seismic regions and the plastic hinge will form in the column without any damage in that connection [19].

Based on AASHTO, bridges should be designed with one of the four Seismic Design Categories (SDCs), A through D. Except for the bridges classified as category A, seismic design and earthquake resistant systems are required. The bridge specifications are aimed to achieve minor damage to the bridges during moderate seismic event and prevent collapse during rare earthquakes.

Based on AASHTO, bridges should be designed so that damages (plastic hinge) intentionally forms and restricted in the columns/pier walls so that it can be easily inspected and repaired after an earthquake [6–9]. Figure 4-1 shows the recommended and not recommended Earthquake-Resisting Systems and the location of the plastic hinge. The "Plastic Hinge" is the region of an element that yields in flexural and has plastic rotation while having enough flexural strength. Also the cap beams, as a capacity protected element, should remain essentially elastic and damage free for the maximum capacity (overstrength plastic moment) of the column.

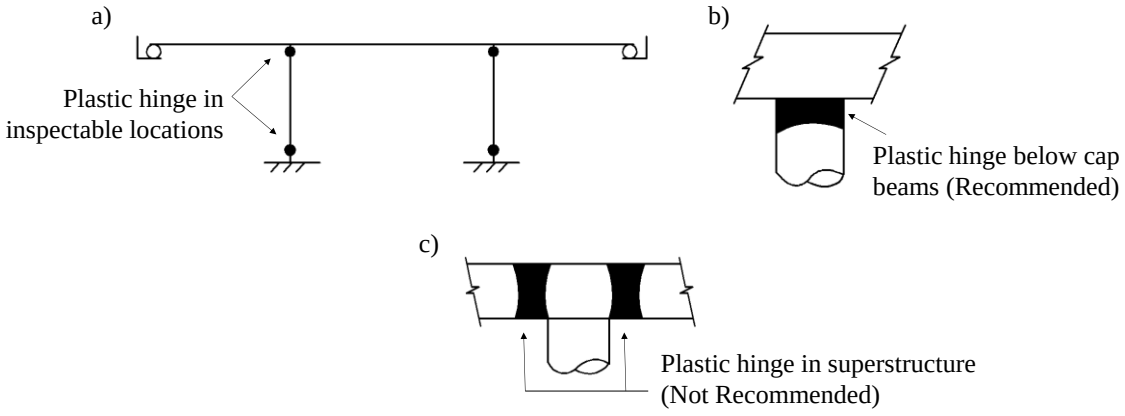

Figure 4-1 Earthquake-Resisting Systems a) Permissible Earthquake-Resisting Systems (ERSs) b) Permissible Earthquake-Resisting Element (EREs) c) Earthquake-Resisting Elements that is Not Recommended by AASHTO for new bridges [6].

The structural behavior of a member or connection beyond the elastic portion can be characterized by either ductile or brittle. Because of the sudden loss of load capacity after elastic limit, the brittle behavior is not recommended. Ductile behavior is characterized by significant inelastic deformations before any loss of load-carrying capacity occurs. Members with ductile behavior dissipate energy and warn of the failure by large deformations. The ductility of a member or connection can be provided by test or analytical approach.

The main material of the proposed connection in this research is UHPC, which can transfer forces between bars over a short splice length. Bond behavior and development length in UHPC has been investigated in several studies confirming that the development length in UHPC is much shorter than in regular concrete [19,62,111–113].

This chapter focuses on connection between a precast column and cap beam (Detail 2), which can potentially satisfy constructability requirements and expected seismic performance. The main characteristics of the proposed connection are desired plastic hinge location with limited length and large construction tolerances. An experimental test on a large scale specimen was performed to evaluate the seismic performance of the proposed connection.

4.2 Description of the Proposed ABC Connections

In the proposed connection, UHPC is used to join the precast elements in the field. Two details are proposed. In Detail 2, two layers of UHPC are employed. As shown in Figure 4-1 (b), in the absence of the top layer of UHPC, it was anticipated that the major damage will occur near the cap beam. Therefore, to prevent spreading of the damage to the

cap beam another layer of UHPC was used as a column capital. The use of UHPC in two layers guaranteed the formation of the plastic hinge at the desired location of the column. The use of UHPC in the splice region allows the development of reinforcing bars over a short length. Therefore, the length of the gap to be filled by UHPC in the field is relatively small. For the first detail (Figure 4-1 (a)), the cap beam and the column are simply joined with a layer of UHPC.

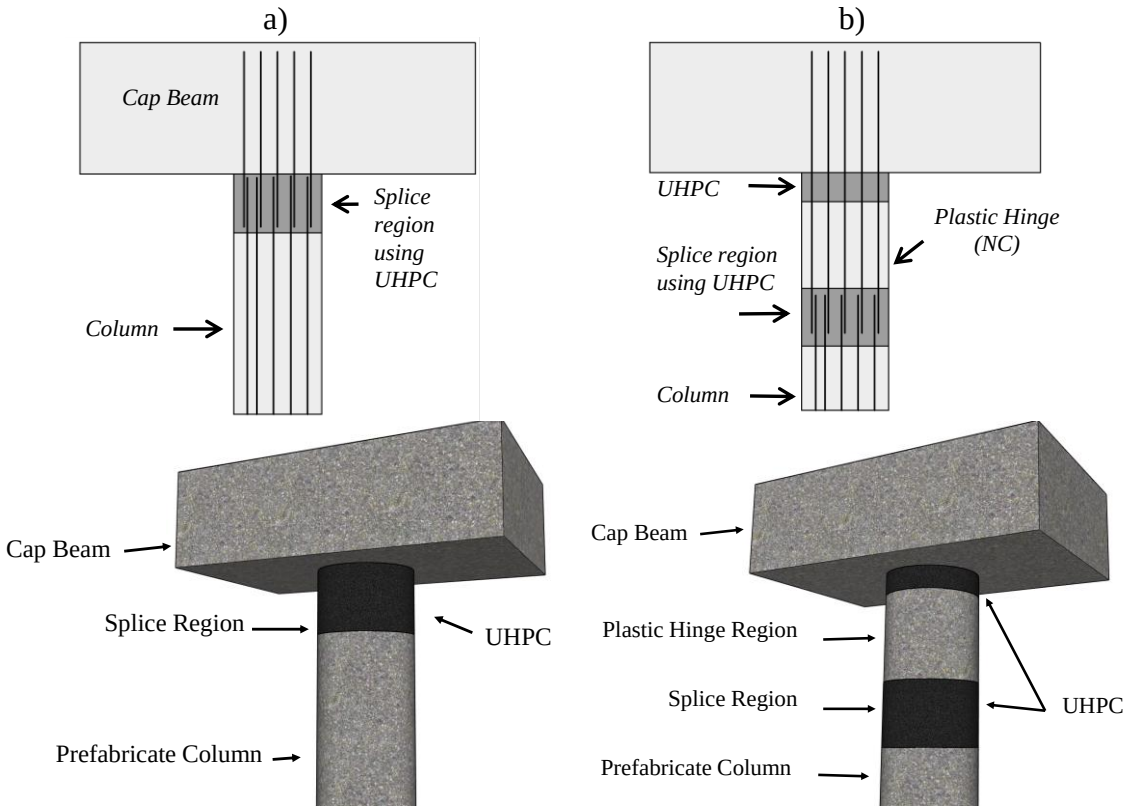

Figure 4-2 Details of the concept of the proposed connection a) Detail one b) Detail 2.

For Detail 2, the system consists of two parts. First part includes the cap beam, UHPC column capital and a part of column where the plastic hinge forms while the second part is the NC column. These two parts will be connected in the field using UHPC. The connection is proposed for precast column to cap beam or footing connections located in high seismic zones. Gaining the strength of UHPC over a short time and large tolerances

for construction of the proposed details, can provide a rapid method of bridge construction. The merits of the proposed connection system are large construction tolerance, confinement of damage within plastic hinge, and prevention of rebar yield in the cap beam in the case of a large seismic event. In order to investigate the structural behavior of this connection, a set of experiments were conducted.

This connection is proposed as a suitable precast column-to-cap beam or footing connections for high seismic zones. Formation of plastic hinge in the column without any damage in cap beam or UHPC connection is guaranteed in the proposed method. Among the merits of the proposed system are suitable tolerance, precise location of the plastic hinge, prevention of rebar yielding in the cap beam, and acceleration of field construction.

Based on AASHTO [6] the analytical length of the plastic hinge in the reinforced concrete columns (L_p), can be obtained by the following equation:

$$L_p = 0.08L + 0.15f_{ye}d_{bl} \geq 0.3f_{ye}d_{bl} \quad (4\text{-}1)$$

where:

L is the length of column from point of maximum moment to the point of moment contraflexure (in.)

f_{ye} is the expected yield strength of longitudinal steel bars (ksi)

d_b is the nominal diameter of longitudinal steel bars (in.)

4.3 Experimental Program

4.3.1 Description of the Test Specimen

A large-scaled connection between a precast column and cap beam was constructed and tested under combined axial compression and reversed cyclic loading to form the

plastic hinge and failure. The column was designed similar to a conventional cast-in-place column based on the AASHTO LRFD Bridge Design Specifications [7] and the Caltrans Seismic Design Criteria [8]. Figure 4-3 shows the specimen dimensions in detail. The column length from the footing surface to the center of the loading point was 10.5 ft with a cross section of 20×20 in. In order to limit potential localized failure and to spread yielding and crushing to the cap beam, the section height at the top of the column increased to 28 in. The column was reinforced longitudinally with 16-No. 6 bars and transversely with No. 4 stirrups at a 3-in. spacing. Clear cover of the rebars considered was 3 in. Longitudinal and transverse reinforcement ratios were 1.95% and 1.00%, respectively. The axial load of the column considered 200 kips which resulted in approximately 10% of the pure axial load capacity of the column section. The minimum lap splice length of rebar in UHPC was 9 in.

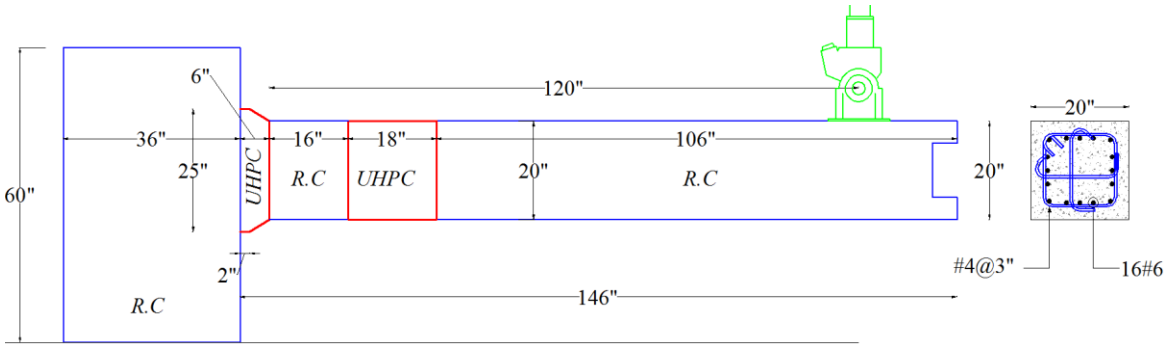

Figure 4-3 Specimen dimensions, unit: in.

4.3.2 Construction of the Test Specimen

The first step of the construction procedure was casting cap beam. Casting top layer of UHPC and the plastic hinge was cast one day later. Joining column and cap beam part with UHPC was carried out 28 days later. In order to avoid having cold joint effect between the normal concrete and UHPC, the substrate surfaces of the normal concrete were

intentionally prepared with a rough surface. Moreover, 1 in. of the top layer of UHPC was embedded in the support to prevent any local damage at the concrete support.

Figure 4-4 Specimen construction procedures.

4.3.3 Test Setup and Loading Procedure

To apply lateral loads to the column, a 240-kip hydraulic actuator was used in a cantilever configuration test setup. Note that based on test setup configuration, the column was placed horizontally. An axial load of 200 kips was applied to the column using two hydraulic rams. Slow cyclic displacement-control loading was applied to the column.

Figure 4-5 Loading setup and support conditions.

In order to estimate the idealized yield displacement of the column (Δ_y), few cycles were applied to the specimen. The displacement rate was initially set to 0.5 in./min and gradually increased to 2 in./min.

The idealized bi-linear load-displacement relationship is illustrated in Figure 4-6. The elastic portion was a straight line with the slope equal to the initial stiffness of the specimen observed in the first loading cycle. The plastic portion was approximated by a straight line that had the best fit to the peak loads. The yielding displacement of the column was determined as the intersection between these two lines. After obtaining Δ_y, which is considered 1.8 in., the column was subjected to three cycles of $2\Delta_y$, $3\Delta_y$, $4\Delta_y$ and $5\Delta_y$ displacement. At the end of each cycle, the loading was paused to inspect damages and map the cracks. To monitor the behavior of the connection, the specimen was instrumented with 8 strain gauges, 3 string pots, 16 potentiometers, 2 pressure transducers and 2 load cells. Potentiometers were utilized to evaluate column curvature at four levels in plastic hinge area. The maximum support movement during cyclic loading was 0.03 in. (0.8 mm). The compressive strength of conventional concrete for the column and plastic hinge was 7.1 ksi and 6.4 ksi respectively. The compressive strength of UHPC was 21.7 ksi. The

measured yield and ultimate strength of the longitudinal reinforcement used were 68.1 ksi and 112.2 ksi, respectively.

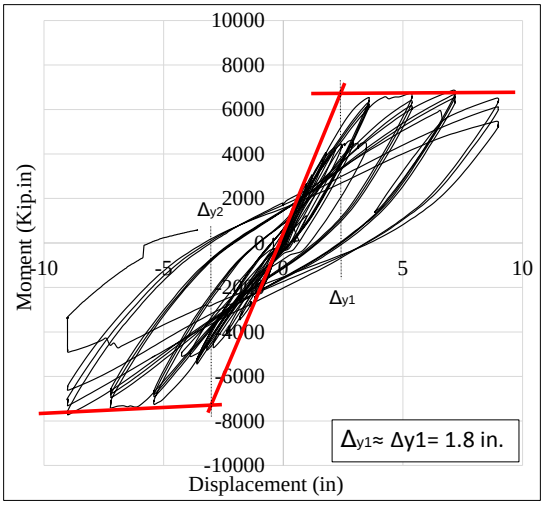

Figure 4-6 Experimental definition of yield displacement.

4.3.4 Experimental Results

The following sections describe the test results.

4.3.4.1 Observed Damage

The formation of the plastic hinge in the column is shown in Figure 4-7 at different displacement levels. First cracks formed in plastic hinge area followed by developing cracks in the column and then in the cap beam face. The spalling of the cover concrete was first observed at $3\Delta_y$ displacement level. A small portion of the cap beam around the column failed, which can be attributed to cold joint effect. The damage was limited to the plastic hinge zone, which consisted of normal strength concrete. No major crack or spalling was observed in UHPC portions. The concrete spalling was observed primarily in the region where normal strength concrete was used to form the plastic hinge. Bond failure

between normal concrete and UHPC was not observed, which indicated appropriate bond between the materials.

Figure 4-7 Plastic hinge damage at different displacement levels.

4.3.4.2 Mode of Failure

Longitudinal bar buckling in the plastic hinge region of the test specimen followed by bar fracture was the mode of failure that occurred at $5\Delta_y$. During the first cycle of $5\Delta_y$ a huge sound was heard, which could be attributed to the first rebar rupture resulting in load drop, and the test machine was quickly stopped. The failure was marked by the rupture of three more longitudinal bars at the 4th cycle of $5\Delta_y$ with strength degradation of more than 25%. Three of the fractured bars were located at the bottom and one in the top face of the column. Fracture of all bars were located around the middle of the plastic hinge. Spalling of concrete at $5\Delta_y$ developed inside the core of the concrete.

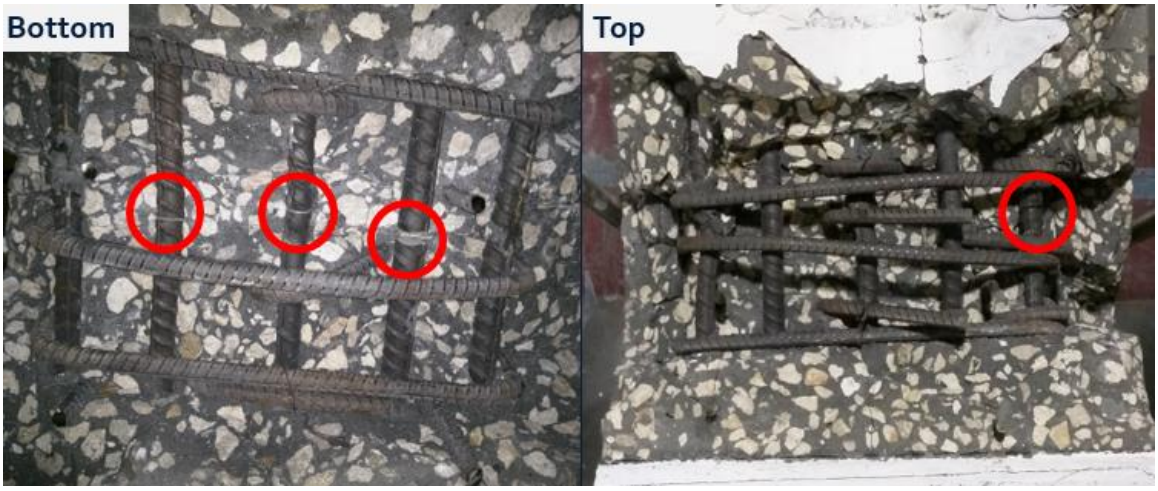

Figure 4-8 Fracture in bars located in the middle of the plastic hinge.

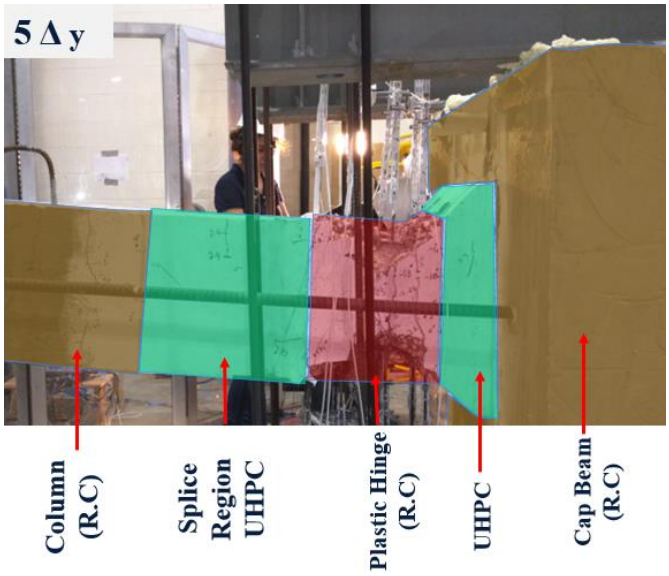

Figure 4-9 Failure mode and location of the plastic hinge.

4.3.4.3 Moment–Displacement Relationship

As mentioned, to calculate the idealized yield displacement of the column (Δ_y), several cycles were applied to the specimen. Based on first cycles, Δ_y was measured 1.8 in. The moment–displacement hysteretic curves of the specimen are shown in Figure 4-10. The measured moment includes the weight of the column and P-Δ effect. Based on this

figure, the maximum capacity of the system was 6500 kip.in. However, the nominal capacity of the column considering 200 kips axial load, was estimated 5840 kip.in.

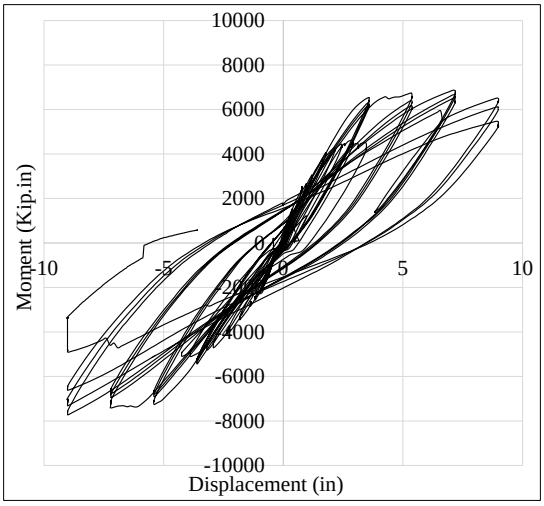

Figure 4-10 Experimental moment-displacement result.

4.3.4.4 Measured Curvatures

The specimen was instrumented with two rows of 8 potentiometers to measure the curvature of the column. The potentiometers were mounted on steel rods that passed through the column at four different distances from the cap beam face. The maximum curvature profile at each displacement versus the column height is presented in Figure 4-11. Results show that the plastic hinge was placed in the desired location in the column and curvature had uniform distribution in 2 and $3\Delta_y$ displacement level. At $4\Delta_y$ displacement level, the maximum curvature was measured between the second and third rows of the potentiometers, which were located approximately at the middle of the plastic hinge zone. By losing potentiometers at $5\Delta_y$ displacement, measuring curvature of the column was not possible.

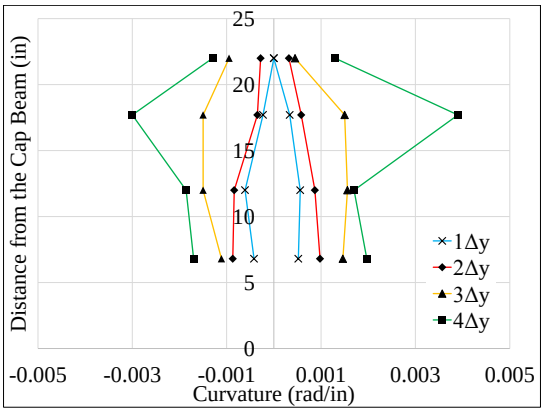

Figure 4-11 Plastic hinge curvature profiles for each displacement.

4.3.4.5 Measured Strains

The longitudinal bars were instrumented with six strain gauges at the middle of the plastic hinge. The peak tensile strain profiles of bars were measured at different displacement levels. No yielding of the shear reinforcement was observed even at $5\Delta_y$ displacement. By losing strain gauges at $5\Delta_y$ displacement, measuring strains of the bars was not possible.

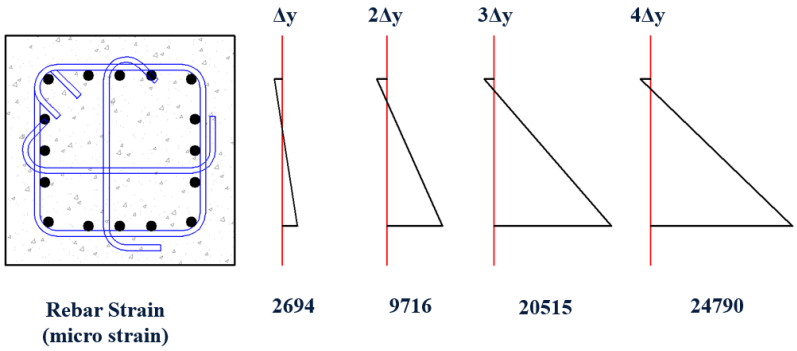

Figure 4-12 Peak tensile strain profiles of bars measured in the middle plastic hinge.

4.4 Summary and Conclusions

A layer of Ultra-High Performance Concrete (UHPC) was used to connect a large scaled precast concrete column to the cap beam. In order to force forming plastic hinge in the desired location in the column, another layer of UHPC was added below the cap beam.

A cyclic testing on cantilever configuration of the column was carried out. Results of the test led to the following conclusions:

This connection is proposed as a suitable precast column-to-cap beam or footing connection for high seismic zones in which formation of the plastic hinge in columns without any damage in cap beam or connection is guaranteed.

No damage such as pull out or spalling was observed in UHPC parts. The plastic hinge was located in the desired location and the second UHPC layer prevents development of plastic hinge into the cap beam.

Bond failure between normal concrete and UHPC was not observed, which indicated appropriate adhesive bond between the materials.

CHAPTER 5 INVESTIGATION ON CIRCULAR SECTION: FEASIBILITY STUDY ON DETAIL 1 AND PARAMETRIC STUDY ON DETAIL 2

5.1 Introduction

The objective of this chapter is to investigate the proposed UHPC based connection between the cap beam and circular columns which can potentially be used in ABC application for both seismic and non-seismic regions. The connection made primarily with UHPC and designed for a target plastic hinge location. The formation of plastic hinge provides ductility to the system and dissipates the seismic energy. The properly detailed and closely spaced transverse reinforcement in reinforced concrete columns can ensure ductile behavior during earthquakes. According to the current seismic design methods, forming the plastic hinge in the column should provide the ductility to the bridge in seismic regions.

The feasibility study of this research was described in chapter 4. In this phase of the study, four scaled columns with the proposed details were tested under cyclic loading and the structural behavior of the specimens was highlighted. The variables were the axial load rate and transverse reinforcement details in both plastic hinge and splice regions.

5.2 Experimental Program

In this phase of the study, four scaled connections between a precast column and cap beam were constructed and tested under combined axial and reversed cyclic loading. Three seismic and one non-seismic details were investigated. The column and cap beam

were designed based on common provisions for seismic regions [6,8,9]. The length of the splice region was large enough to ensure that slip failure in this region would not occur.

5.2.1 Description of the Test Specimens

Four columns to cap beam connection were designed for testing under lateral loading and constant axial load and designated as specimen S-2.5-10, S-4-10, S-2.5-20 and NS-2.5-10. Details of the test specimens and their variables including axial load are given in Table 5-1. S-2.5-10, S-4-10, S-2.5-20 had Detail 2 with different axial load rate and transverse rebar ratio in splice and plastic hinge zone. The axial load varied from 10% to 20% of its pure axial capacity. In addition, specimen NS-2.5-10 having Detail 1 with one layer of UHPC. In all specimens the length of the UHPC were equal to the lap splice length. Previous researches indicated that sufficient steel fibers in concrete may increase shear capacity, section confinement and provide more ductility [114]. Therefore, to study the confinement effect of UHPC, different transverse reinforcement ratios in the splice region were used. The preliminary investigation showed that the moment capacity of UHPC section is much higher than column section with regular concrete [115].

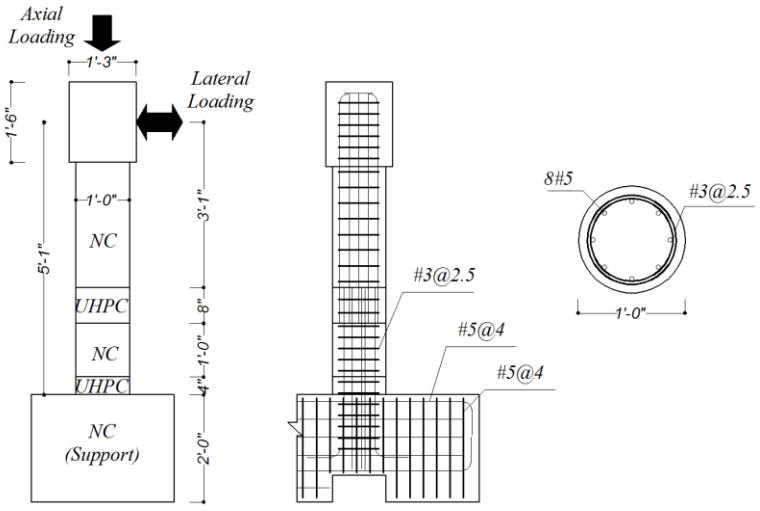

Figure 5-1 Specimens S-2.5-10, S-4-10, S-2.5-20 typical dimensions and reinforcement details.

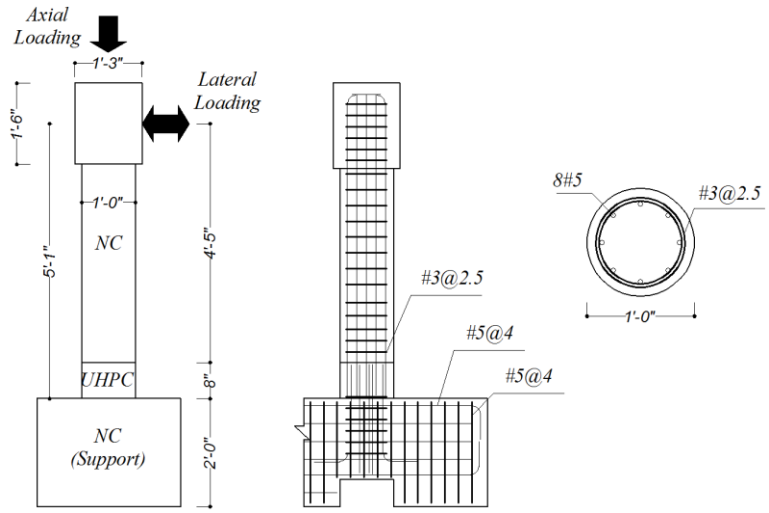

Figure 5-2 Specimen NS-2.5-10 dimensions and reinforcement details (No stirrups at splice region).

Figure 5-1 and 5-2 shows the reinforcement and dimensions of each specimen in detail. The column height was 61 in. with a circular cross-section having diameter of 12 in. The column was typically reinforced longitudinally with 8-No. 5 rebars. Longitudinal reinforcement ratio was 2.19% for all specimens. Clear cover of the rebars was 1.5 in. The axial load of the reference specimen (S-2.5-10) was 56 kips which resulted in approximately 10% of the nominal pure axial load capacity of the column section. The lap splice length of rebar in UHPC was 8 in., equals to 13 times of the rebar diameter; although, previous studies have shown that shorter lap splice lengths can be used if adequate cover concrete is provided [62].

Table 5-1 Details of the specimen.

Specimen ID	Geometry detail	Transverse Reinforcement detail	Axial Load Ratio
S-2.5-10 (Reference)	As shown in Fig 5-2 (Detail 2)	#3@2.5 in. in plastic hinge and splice region	10%
S-4-10	As shown in Fig 5-2 (Detail 2)	#3@4 in. in plastic hinge and no strips splice region	10%
S-2.5-20	As shown in Fig 5-2 (Detail 2)	#3@2.5 in. in plastic hinge and one stirrups at splice region	20%
NS-2.5-10	As shown in Fig 5-3 (Detail 1)	#3@2.5 in. in plastic hinge and no stirrups at splice region	10%

5.2.2 Construction of the Test Specimens

The first step of the construction procedure of the specimens having Detail 2, was casting the cap beam (support) followed by casting the first layer of UHPC and plastic hinge part. Casting splice region and column part were carried out 11 days later. In order to minimize the cold joint between the Normal Concrete (NC) and UHPC, the surface of the concrete was textured. Moreover, around 1 in. of the first layer of UHPC was embedded in the support to prevent any local damage at the concrete support. For the specimen having Detail 1, the first step of the construction procedure was casting of the cap beam (support) followed by casting the lap splice of UHPC and then the column part.

During casting of these series of the specimens, because of using more superplasticizers than needed, which happened by mistake, steel fibers in the UHPC regions did not achieve uniform distribution. However, as it will be discussed, the test outcome was not significantly affected. Also, the rebar cage shifted during casting and the concrete cover was not the same for all side of the specimens which created unsymmetrical arrangement of the cage.

Figure 5-3 Specimen construction procedures a) Formwork of the support, b) Casting support, c) Casting first layer of UHPC, d) Casting plastic hinge, e) Reinforcement of the column, f) Casting splice region with UHPC and g) Casting column with N.C.

5.2.3 Test Setup and Loading Procedure

The experimental test was carried out six months after casting the specimens. A cyclic loading test was carried out to evaluate the performance of the connection. A 150-kip hydraulic ram was used for cyclic testing of the cantilever column. A constant predetermined axial load was applied using two hydraulic rams. Initially, low displacement cycles were applied to the column to estimate the idealized yield displacement of the column (Δ_y).

a) b)

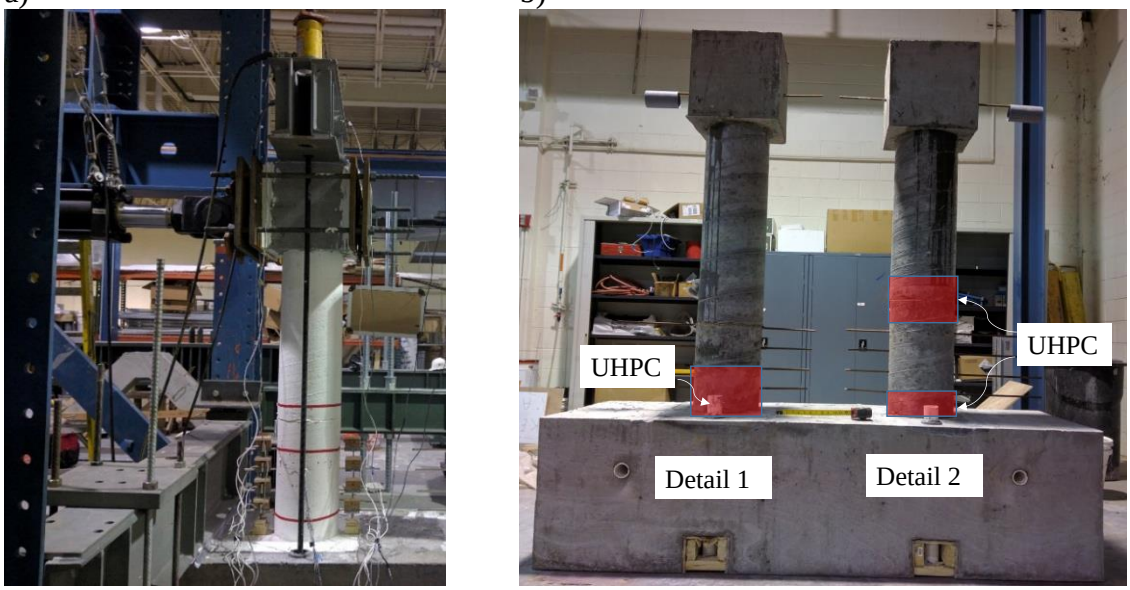

Figure 5-4 Constructed specimens and loading setup a) Loading setup overview b) Constructed specimens.

The yielding displacement (Δ_y) was defined by assuming the bilinear model, equivalent elasto-plastic system with the same elastic stiffness and ultimate load as the real system, by following the procedure suggested by R. Park [116]. After obtaining Δ_y, the column was subjected to three cycles of $2\Delta_y$, $3\Delta_y$, $4\Delta_y$ and etc. At the end of each cycle, the displacement was paused to observe the damages and trace the cracks. Yielding displacement of the specimens (S-2.5-10, S-4-10 and S-2.5-20) was 0.65 in. The yielding displacement of specimen (NS-2.5-10) was calculated to be 0.8 in. To evaluate the behavior of the specimens, the test setup was instrumented with string pots, load cells, strain gauges, potentiometers, and pressure transducers. To calculate the curvature of the column, potentiometers were employed at four levels in plastic hinge regions. Cylinder test was used to measure the compressive strength of normal concrete and UHPC a day after the experimental test. The actual material properties are reported in Table 5-2.

Table 5-2 Actual material properties of the material.

Concrete Material	
Concrete of Supports and Plastic hinge location	f_c=7.1 ksi
Concrete of the columns	f_c=6.4 ksi
UHPC of the first layer	f_c= 20.1 ksi
UHPC of the splice region	f_c= 24.9 ksi
Steel Bars	
f_y= 68 ksi	f_u= 113 ksi

5.3 Experimental Results

5.3.1 Observed Damage

The development of cracks and spalling of the concrete in the plastic hinge region at different displacement levels are shown in Figure 5-5 for each specimen. For all specimens having Detail 2 (S-2.5-10, S-4-10 and S-2.5-20), the first cracks formed in the plastic hinge area followed by development of limited cracks in the column and no crack was observed in the cap beam. For these specimens the spalling of the cover concrete was first observed at $2\Delta_y$ and damage was limited to the plastic hinge zone, which consisted of normal strength concrete. No spalling or cracking was observed in UHPC portions of all specimens. No bond failure between normal concrete and UHPC was observed, which indicates the sufficient bond between UHPC and normal concrete. The spalling of the cover concrete of the specimen having Detail 1 (NS-2.5-10) was first observed at the first cycle of $2\Delta_y$. In the specimen which had Detail 1, only limited concrete cracking was found on the surface of the cap beam of the specimen.

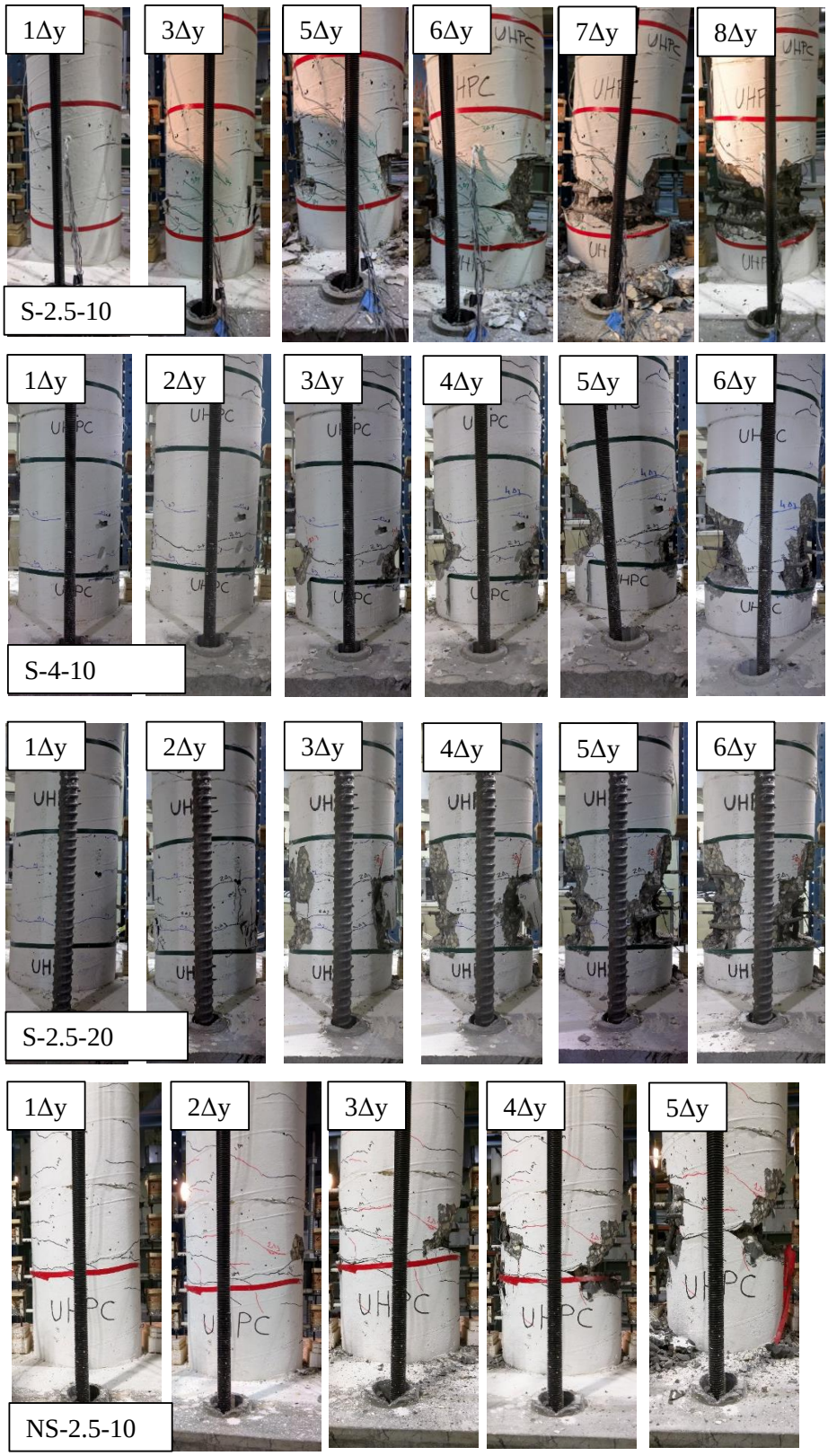

Figure 5-5 Plastic hinge damage at different displacement levels for all specimens.

5.3.2 Mode of Failure

The specimens failed when one of the longitudinal bars ruptured after development of buckling between stirrups due to spalling of the concrete cover. The concrete cover in the plastic hinge zone spalled off and then the core concrete crushed. Fracture of the rebar was located around 2 inches above the UHPC layer for specimens having Detail 2. The displacement ductility of the specimens is shown in Table 5-3 indicating their performance in seismic zones based on common seismic provisions. Results of the test show that by increasing the stirrup spacing or axial load the ductility will decrease. By comparing reference specimen (S-2.5-10) with specimens S-4-2.5 (with less transverse reinforcement ratio) and S-2.5-20 (higher axial load), it was concluded that the ductility of the specimens was most influenced by the space between the stirrups in the plastic hinge region.

a) S-2.5-10 b) S-4-10

c) S-2.5-20 d) NS-2.5-10

Figure 5-6 Failure pattern, longitudinal rebar fracture and location of the plastic hinge in the specimens.

5.3.3 Moment Displacement Curve

Table 5-3 shows the maximum displacement for each specimen. The specimen having Detail 1 was subjected to the cyclic loading to show its capability for seismic area as well. Compared with the monotonic loading, cyclic loading can provide severe loading condition. Figure 5-7 shows the hysteresis moment displacement curve of the specimens. Note that the moment was measured at the base of the column including P delta effect. As mentioned in construction section, in all specimens rebar cages were shifted approximately half inches during the casting. The lateral load decreased gradually after the peak load, indicating the spall off of cover concrete and p-Δ effects. Lateral load reduction after peak

load of specimen S-4-10 (with a larger distance between stirrups) and specimen with Detail 1 (NS-2.5-10), were more than other specimens. Specimens with higher ductility ratio had more capacity to absorb and dissipate energy under extreme loads, such as earthquakes, by showing a limited loss of serviceability. However, it should be noted that the residual drifts of the specimen S-2.5-20 (with 20% axial load) was smaller than those of columns with 10% axial load.

Due to the applied axial load, specimen S-2.5-20 had a higher load capacity compared to other details. It is also worth noticing, as the distance between load and critical section in the specimen with Detail 1 (NS-2.5-10) was less than other specimens, the specimen could experience a higher level of lateral load.

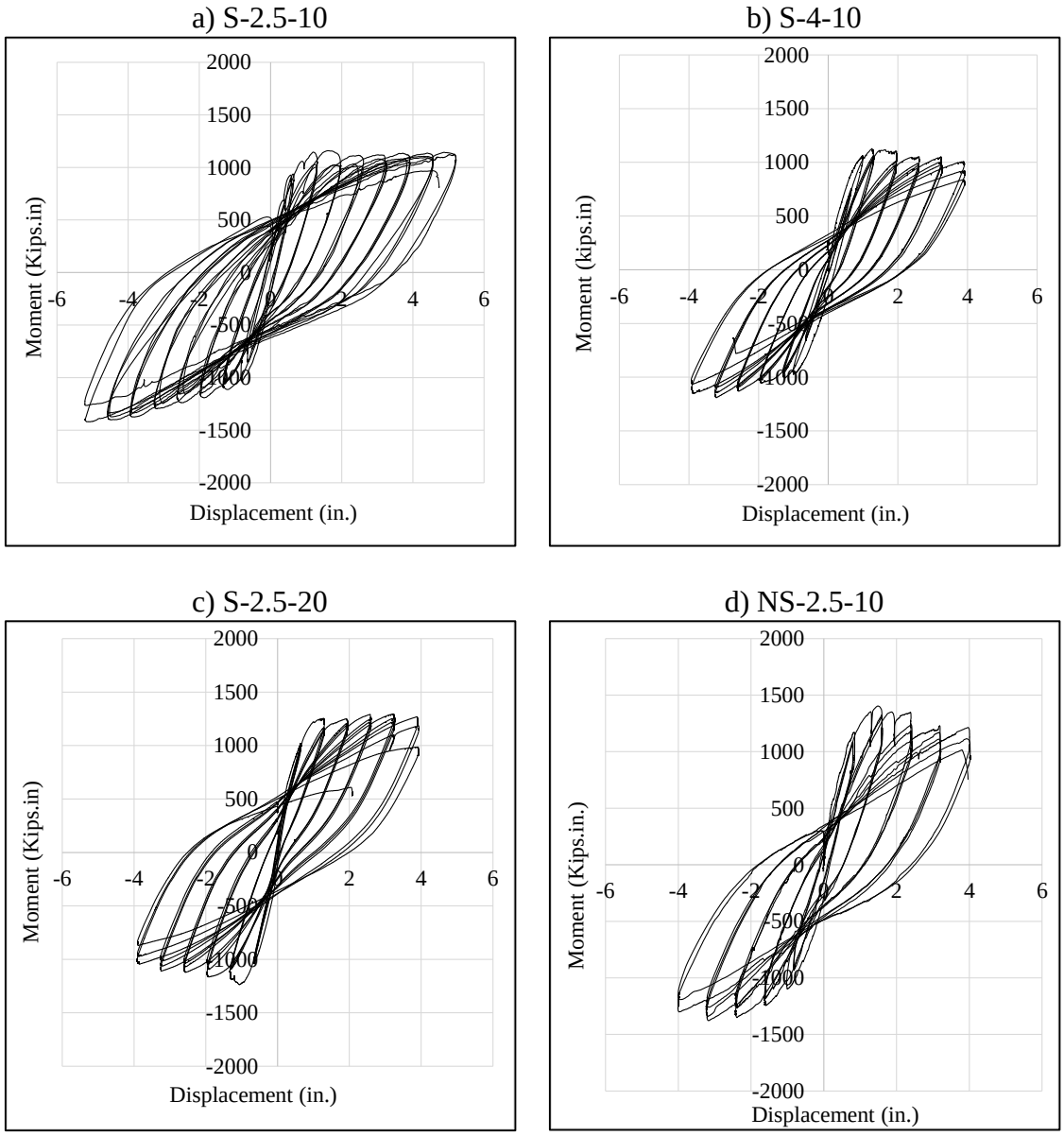

Figure 5-7 Hysteric moment displacement curve of the specimens.

Table 5-3 Ductility and maximum drift of the specimens.

Specimen ID	Maximum drift	Displacement ductility
S-2.5-10	8.5 %	8
S-4-10	5.3 %	5
S-2.5-20	6.4%	6
NS-2.5-10	6.5%	5

5.3.4 Measured Curvatures

The specimens were instrumented with 8 potentiometers to measure the curvature of the column. The potentiometers were mounted on steel bars that passed through the column at four different distances (4 in. space) from the cap beam face. Some potentiometers stopped working at high displacement levels and further measurement of curvature was not possible. The maximum average curvature profile at each displacement level versus the column height is shown in Figure 5-8. Results show that in the details 2, the plastic hinge was placed at the desired location (between two layers of UHPC). For Detail 1 (NS-2.5-10) the plastic hinge formed above the splice region and the results show that the use of UHPC in splice region prevented development of plastic hinge to the cap beam as well. This shows the capability of this specimen for seismic area as well.

By comparing the curves plotted in Figure 5-8, the effects of axial load in the plastic hinge can be investigated. In the specimen S-2.5-20 with higher axial load ratio the maximum curvature was less than other specimens. It is worthwhile to notice that the UHPC splice region in Detail 1 prevented forming the plastic hinge in the cap beam.

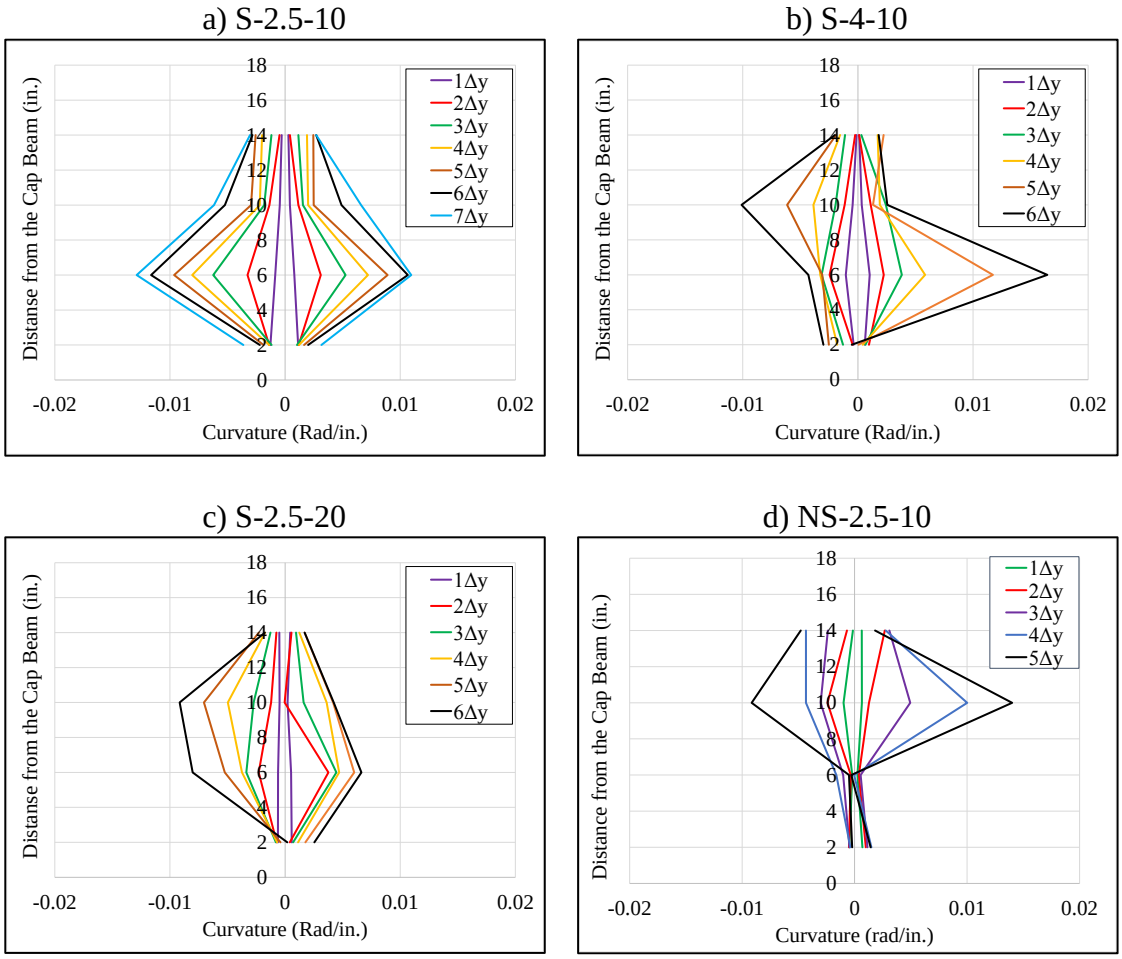

Figure 5-8 Plastic hinge curvature profiles for each displacement.

5.4 Moment Curvature Analysis

As it will be discussed in the next chapters, the behavior of the specimens are governed by normal strength concrete section and only the location of the plastic hinge (critical section) is changing. Therefore in this section, the moment capacity of the specimens was calculated using a Moment-Curvature section analysis. For this analysis, the curves were obtained with corresponding axial load and the idealized curves were derived according to Caltrans [8]. Considering the equivalent analytical plastic hinge length and the length of the column, the local displacement capacity of a member can be

calculated based on its moment-curvature analysis which includes idealized yield and plastic displacement due to rotation of the plastic hinge.

The effect of expected properties of the rebar, confinement of concrete and shifting the rebar due to construction imperfection were considered in the moment-curvature analysis. The idealized yield displacement and moment capacity of the specimen (S-2.5-10) calculated 0.54 in. and 836 kip.in. , respectively. The ductility of the specimen (S-2.5-10), based on Caltrans, was 9. Figure 5-9 shows the relation between experimental and analytical load-displacement curves of the column using Caltrans and moment curvature analysis.

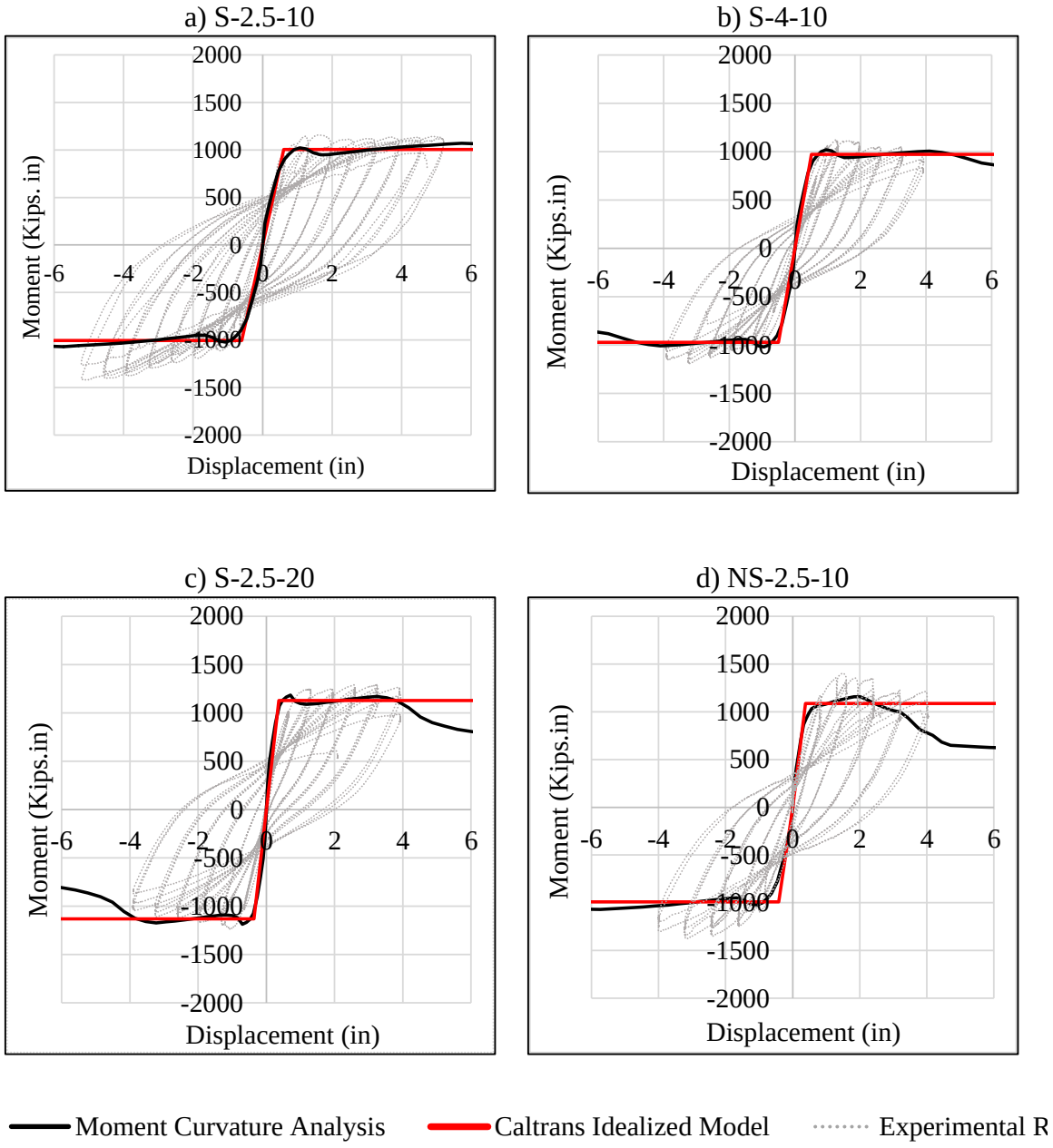

Figure 5-9 Load-displacement curves of the specimens, based on moment curvature analysis and idealized Caltrans curve.

5.5 Summary and Conclusions

In this chapter two types of connection for precast concrete column to cap beam for seismic and non-seismic region were investigated. A layer of Ultra-High Performance Concrete (UHPC) was used to connect precast elements. In order to force forming plastic

hinge in the desired location, another layer of UHPC was added below the cap beam. Four specimens in cantilever configuration were tested under combined constant axial load and cyclic lateral load. Various responses of the connection were highlighted in this chapter. Influence of transverse reinforcement and axial load on the behavior of the connections were investigated. The results of this chapter have led to the following conclusions:

All specimens having Detail 2 showed ductile behavior and the plastic hinge formed in the desired location. High workability of the UHPC and large tolerance of bars in the proposed detail can facilitate and accelerate the on-site construction. Designers should consider the shifting of the plastic hinge which can affect the behavior of the structure.

Judging from the observed ductility and failure mode of specimens, the main characteristic of the proposed connection is influenced by transverse rebar ratio in the plastic hinge region. The distance between the stirrups plays a major role in preventing longitudinal bars buckling. Results show that increasing axial load can provide more capacity but less ductility for the specimen.

In both details, no major crack was observed in the cap beam. Therefore Detail 1, with a seismic design consideration can be an alternative detail even for seismic regions. This detail is preferred as it is easier to build and is less expensive.

No significant damage was found in splice region even in the absence of the transverse reinforcement in this region. Observing no failure in splice region indicates that UHPC can provide a good confinement and shear capacity. Eliminating the need for stirrups in the splice region can facilitate the construction procedure in the field. Moreover, in comparison with conventional concrete, even a short lap splice of bars in UHPC can

transfer forces between spliced bars, which lead to a decrease in casting volume while saving time in the field.

CHAPTER 6 INVESTIGATION ON CIRCULAR SECTION: PARAMETRIC STUDY ON DETAIL 1

6.1 Introduction

As it was discussed in chapter 5, Detail 1, with a seismic design consideration can be an alternative detail for both seismic and non-seismic regions and protects cap beam from damage. No significant damage was observed in splice region even in the absence of the transverse reinforcement and UHPC provided sufficient confinement. This detail is preferred as it is easier to build and is less expensive. This phase of the research focuses on Detail 1 and no transverse reinforcement was placed in the splice region. Having no stirrups can accelerate and facilitate the construction procedure. In this detail the plastic hinge forms in the column. Four more specimens having Detail 1 with different rebar sizes and splice lengths were constructed and tested. In addition, two control specimens the same as the conventional method were cast and employed as the reference point.

6.2 Description of the Connection

As it was mentioned, in Detail 1, UHPC is used to simply join the precast elements in the field.

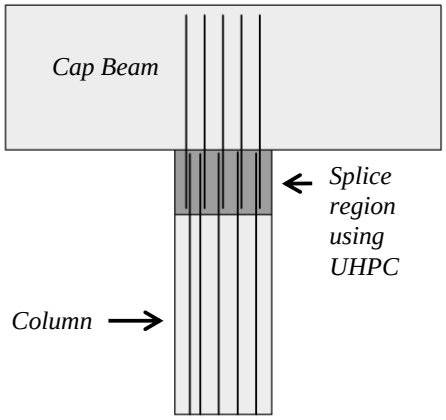

Figure 6-1 Details of the concept of the Detail 1.

The simplicity of the detail, gain of strength of UHPC over a short time and large tolerances for construction of this detail, can provide a rapid method of bridge construction. The merits of the proposed connection system are large tolerance for construction, prevention of rebar yield in the cap beam in the case of a large seismic event, and ease of construction and transportation of the precast elements. In order to investigate the structural behavior of this connection, the effects of the rebar size and lap splice length, a set of experiments were conducted.

6.3 Experimental Program

Four additional specimens having Detail 1 were constructed and tested. In addition, two control specimens with connections as constructed with conventional method were cast. The column and cap beam were designed based on common provisions [8,9] and previous series of test. In this part of the research, the length of the overlap in the splice region and rebar size were the parameters.

6.3.1 Description of the Test Specimens

Four column to cap beam connection were designed for testing under lateral loading and constant axial load. In addition, two specimens were cast as a reference without Detail 1. The investigated parameters included rebar size (Rebar No. #5 and #6) and rebar lap splice length ($8d_b$ and $12d_b$). In all specimens the length of the UHPC were equal to the lap splice length. Details of the test specimens and their variables are given in Table 6-1. In this series of the test, the axial load ratio was 10%. Two specimens were constructed as the reference for bar size #5 and #6 (S-5-R, S-6-R). Each test specimen consisted of two column which were cast over a single support but tested was conducted separately.

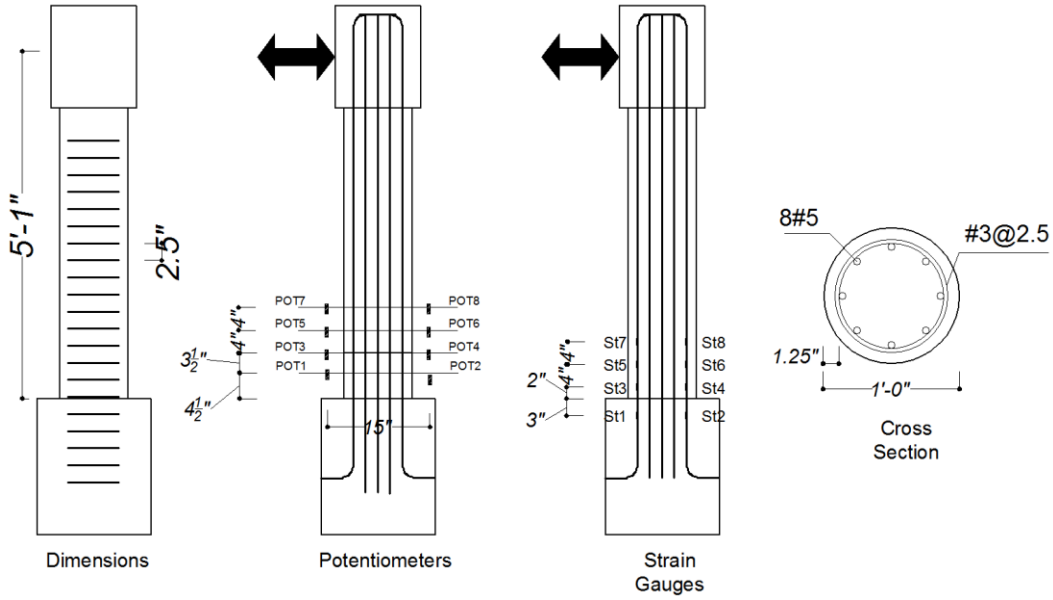

Figure 6-2 Specimens S-5-R details, dimensions, reinforcement and installed measurement tools.

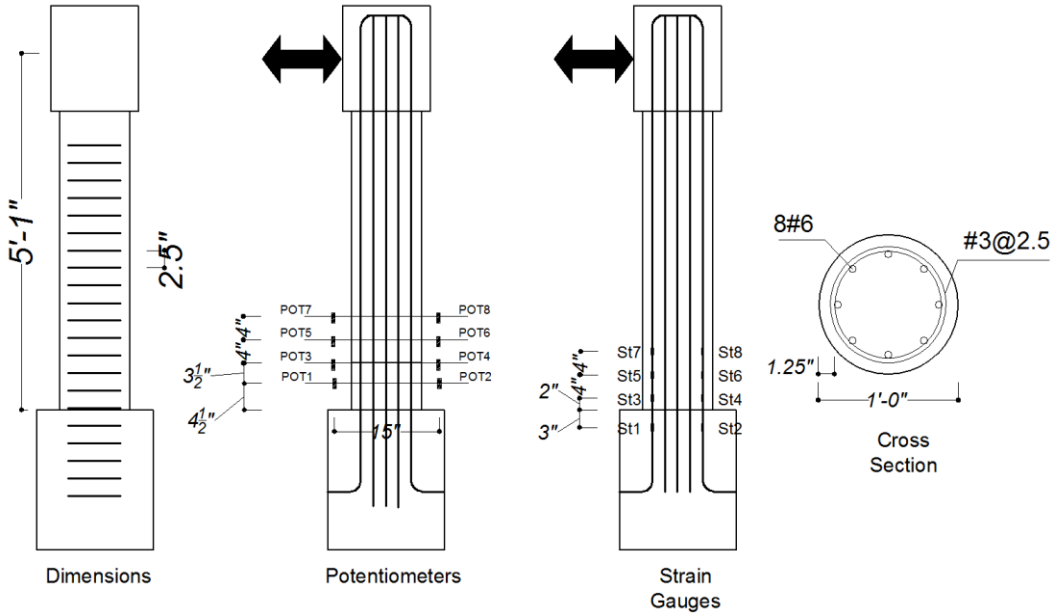

Figure 6-3 Specimen S-6-R details, dimensions, reinforcement and installed measurement tools.

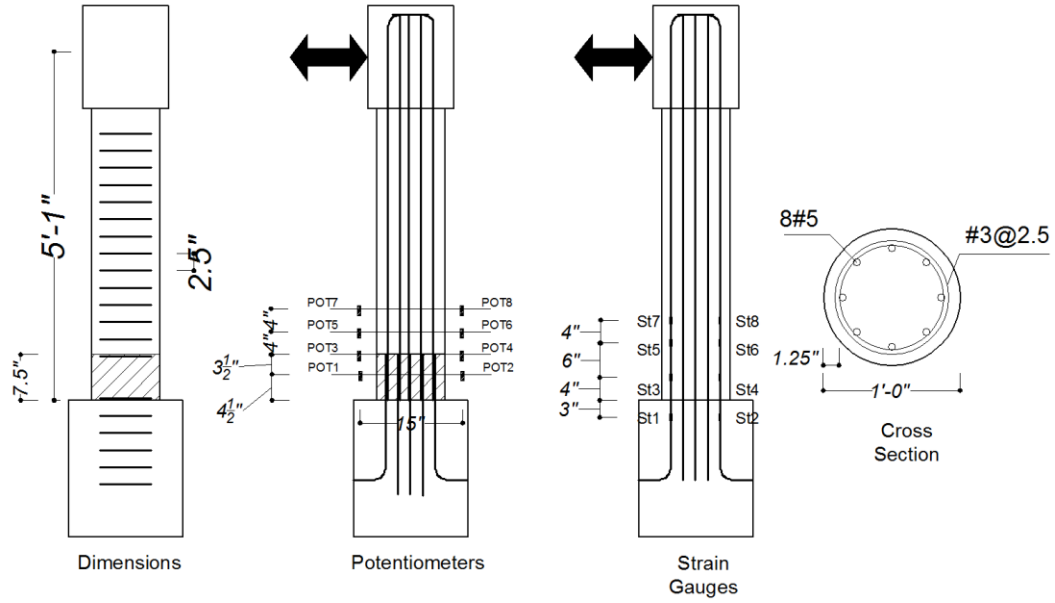

Figure 6-4 Specimen S-5-12 details, dimensions, reinforcement and installed measurement tools. (No stirrups at splice region).

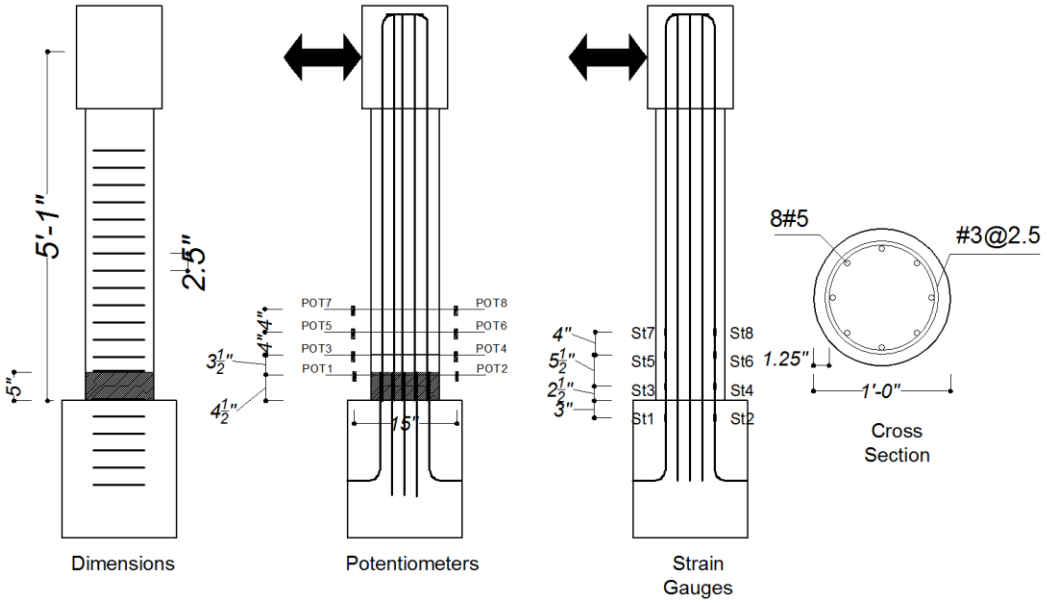

Figure 6-5 Specimen S-5-8 details, dimensions, reinforcement and installed measurement tools. (No stirrups at splice region).

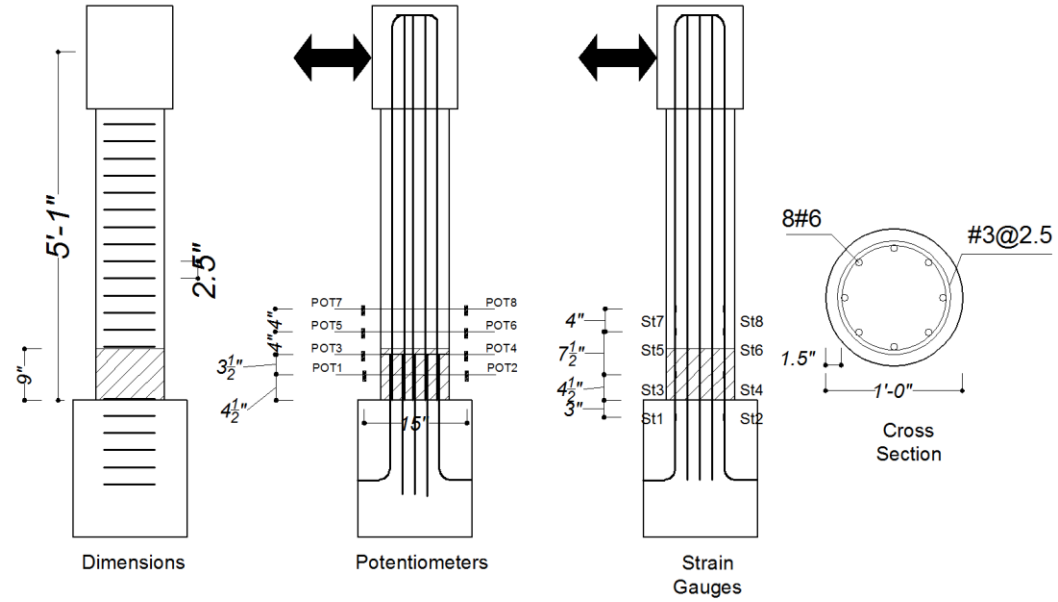

Figure 6-6 Specimen S-6-12, dimensions, reinforcement and measurement tools details (No stirrups at splice region).

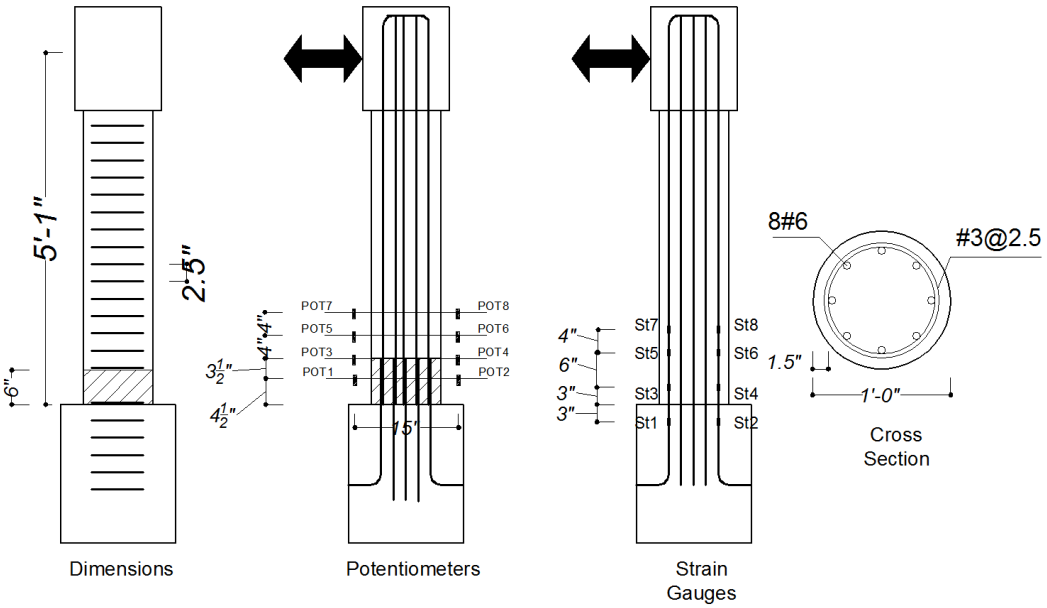

Figure 6-7 Specimen S-6-8, dimensions, reinforcement and measurement tools details (No stirrups at splice region).

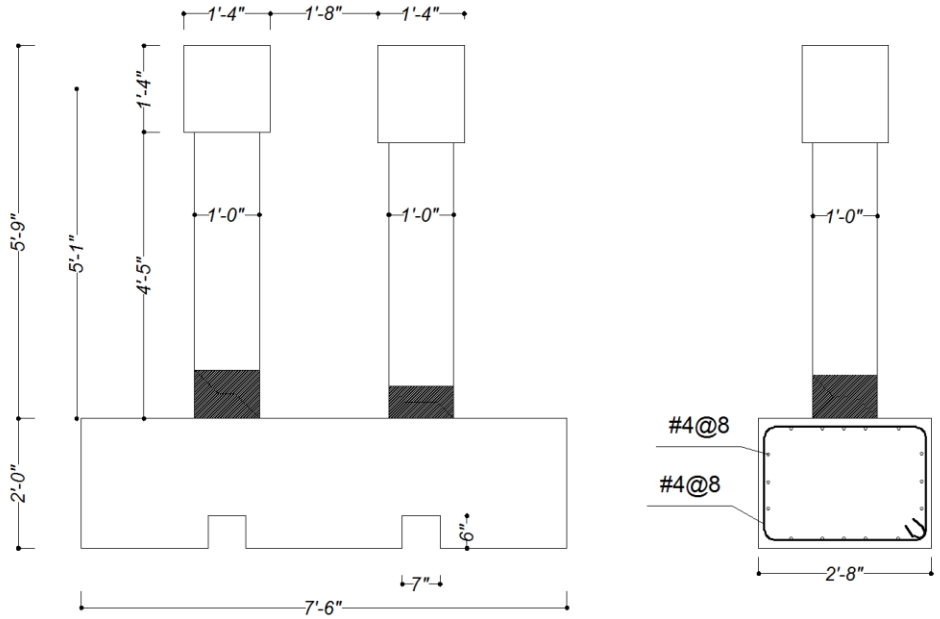

Figure 6-8 General dimensions and reinforcement of the supports.

Figure 6-2 through 6-8 show the specimens dimensions in detail. The column height was 61 in. with a circular cross-section having diameter of 12 in. (30.5 cm). Depending on the design, the columns were reinforced longitudinally with either 8-No. 5 or 6 rebars.

Longitudinal reinforcement ratio was 2.19% for the sections with No 5 and 3.1% for the section with No 6. Clear cover of the rebars was $2d_b$. The axial load of the specimens was approximately 10% of the pure axial load capacity of the column section. The lap splice length of rebar in UHPC were 8 d_b and 12 d_b where d_b is the bar diameter. Note that no transverse reinforcement was placed in the splice region.

Table 6-1 Details of the specimen.

Specimen ID	Geometry detail	Parameter Detail	Axial Load Ratio
S-5-R	As shown in Fig 6-2	Reference rebar size #5	10%
S-6-R	As shown in Fig 6-3	Reference rebar size #6	10%
S-5-12	As shown in Fig 6-4	Splice Length $12d_b$ rebar size #5	10%
S-5-8	As shown in Fig 6-5	Splice Length $8d_b$ rebar size #5	10%
S-6-12	As shown in Fig 6-6	Splice Length $12d_b$ rebar size #6	10%
S-6-8	As shown in Fig 6-7	Splice Length $8d_b$ rebar size #6	10%

6.3.2 Construction of the Test Specimens

First step of the construction procedure was casting of the cap beam (support). In order to minimize the cold joint between the Normal Concrete (NC) and UHPC, the surface of the concrete was textured by sandblasting and UHPC was embedded in the support to prevent any localized damage at the concrete support. Casting splice region and column portion was carried out 15 days later.

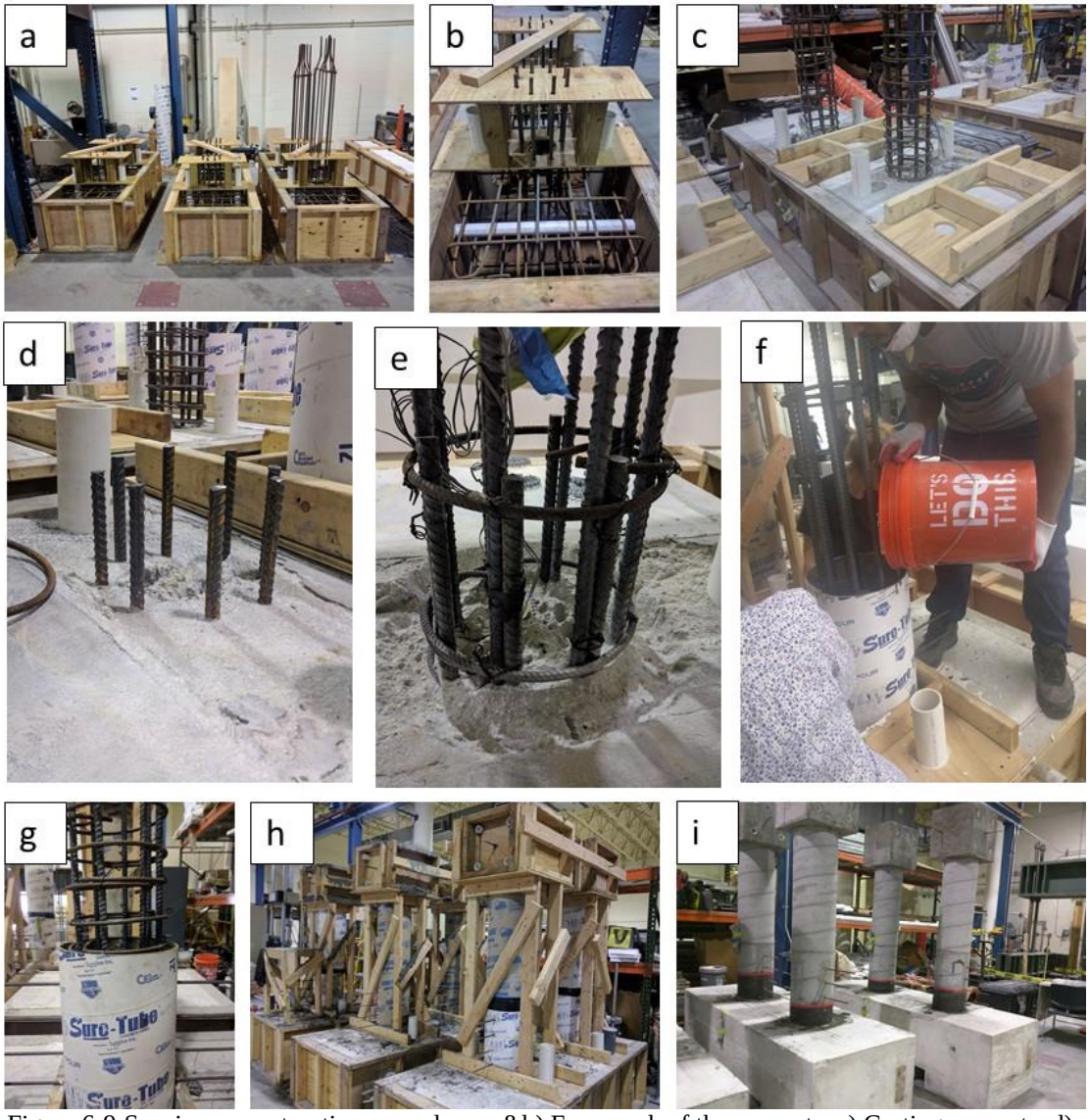

Figure 6-9 Specimen construction procedures a&b) Formwork of the supports, c) Casting supports, d) exposed rebar, d) Splicing rebar and sand blasting, f) Casting UHPC, g) Placing column stirrups, h) Casting column, and i) Removing formworks.

6.3.3 Test Setup and Loading Procedure

The experimental test was carried out one month after casting the columns. A cyclic loading was employed to evaluate the structural behavior of the connection. A 150-kip hydraulic ram was used for cyclic testing of the cantilever column. A constant predetermined axial load was applied using two hydraulic rams. Initially, low displacement

cycles were applied to the column to estimate the idealized yield displacement of the column (Δ_y).

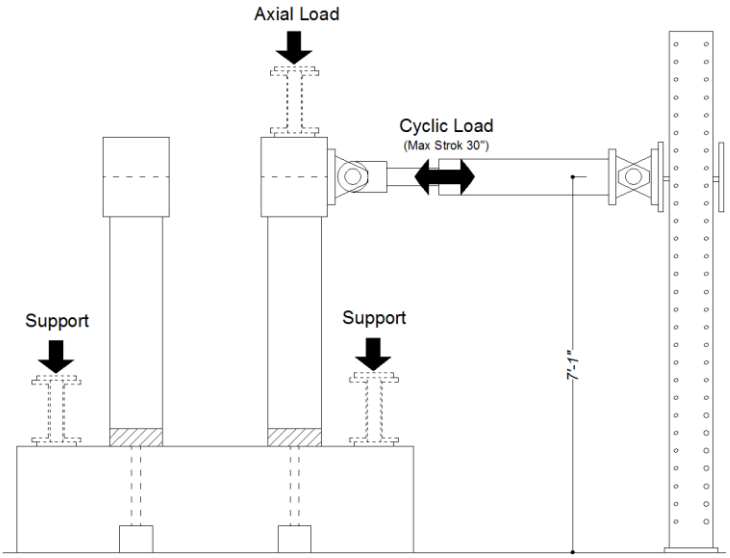

Figure 6-10 Loading setup overview.

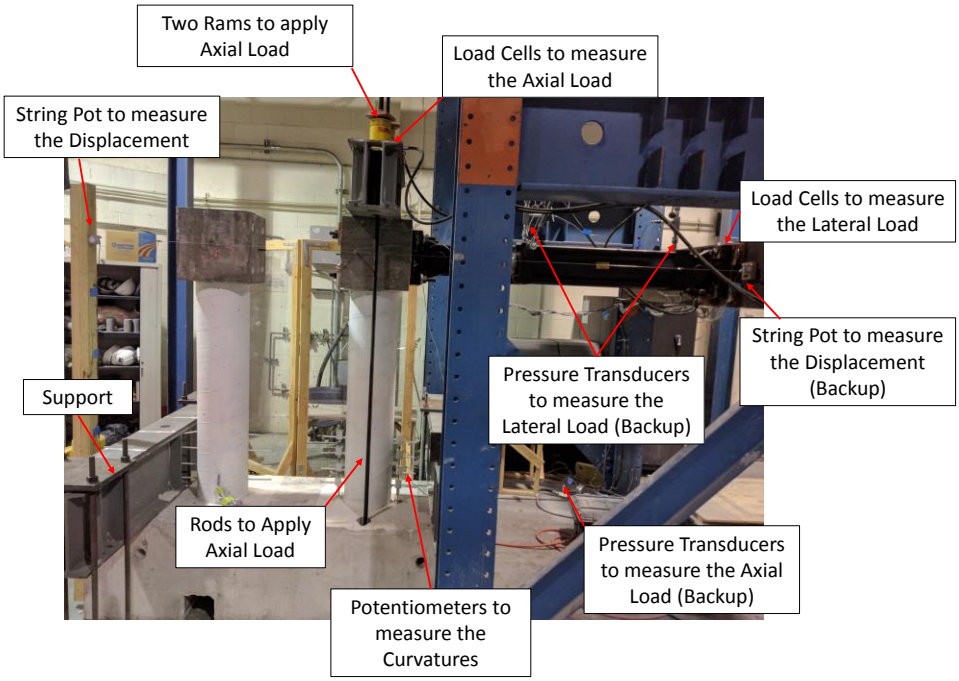

Figure 6-11 Loading setup and measurement tools overview 1.

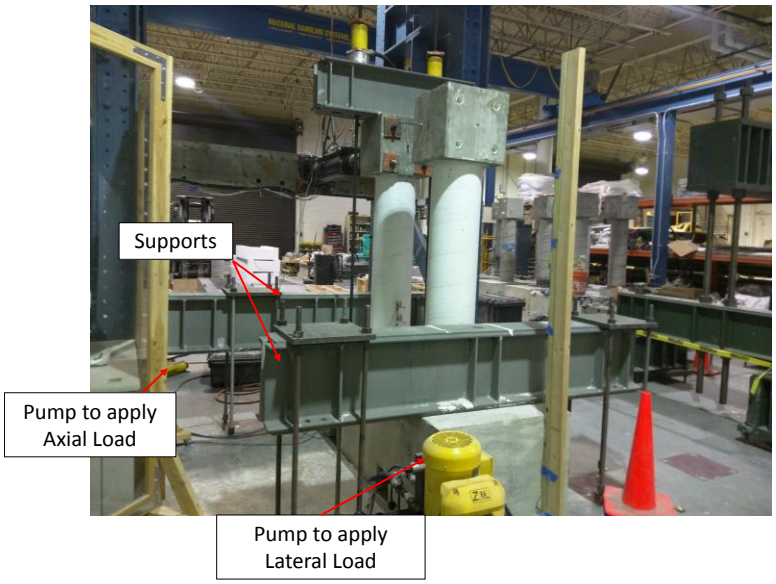

Figure 6-12 Loading setup and measurement tools overview 2.

The yielding displacement (Δ_y) was defined by assuming the bilinear model the same as the previous test. The column was subjected to three cycles of 1 in., 2 in., 3 in. and etc. displacement. At the end of each cycle, the displacement was paused to observe the damages and trace the cracks.

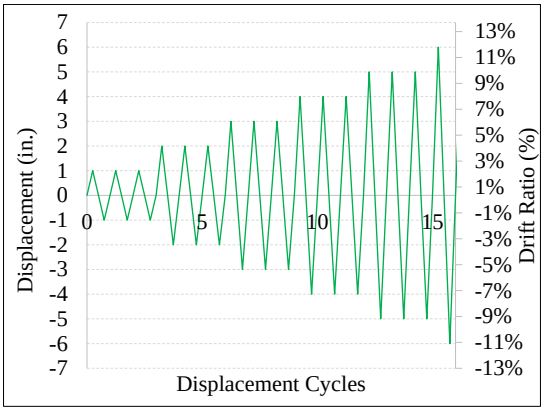

Figure 6-13 Loading Protocol.

To evaluate the behavior of the specimens, the test setup was instrumented with string pots, load cells, strain gauges, potentiometers, and pressure transducers. To calculate the curvature of the column, potentiometers were employed at four levels in plastic hinge

regions. Cylinder test was used to measure the compressive strength of normal concrete and UHPC a day after the experimental test. The actual material properties are reported in Table 6-2.

Table 6-2 Actual material properties of the material.

	Material Properties
Concrete of Supports	fc=5.3 ksi
Concrete of the columns (Slump)	fc=5.8 ksi (5 in.)
UHPC (Flowability)	fc= 25 ksi (8 in.)

6.4 Experimental Results

6.4.1 Observed Damage

The development of cracks and crushing of the concrete in column are shown in Figure 6-14 to 6-25 for each specimen. In all specimens having Detail 1, the first cracks formed in the column above the splice region. In the case of references specimens (S-5-R and S-6-R), first cracks formed in the column followed by cracks in the cap beam (support). In the reference columns, the spalling of the cover concrete in the column was first observed at 3.3% of drift followed by damages to the cap beam at higher level of displacement. In all specimens having Detail 1, no spalling or cracking or bond failure was observed in UHPC portions which indicates the sufficient bond between UHPC, normal concrete. No major damage was observed in the cap beam.

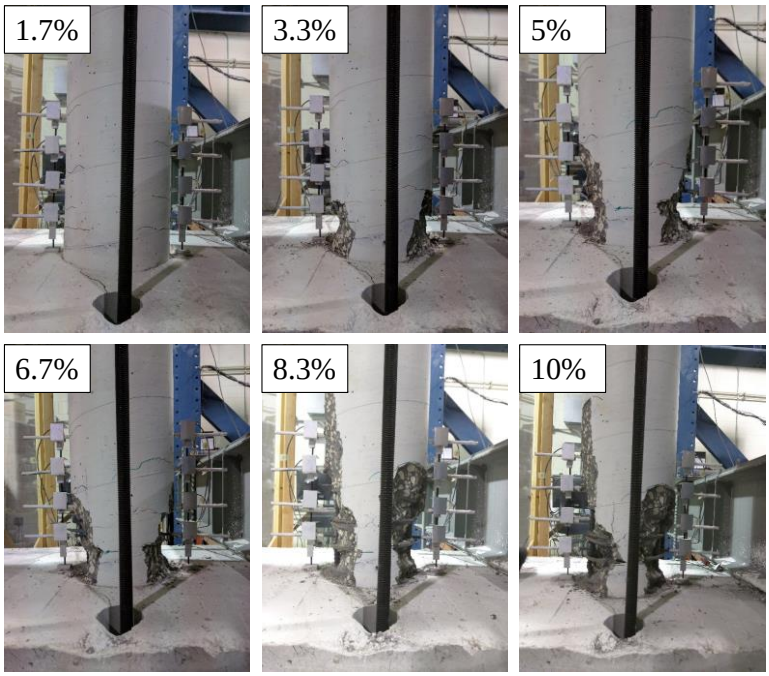

Figure 6-14 Damage at different displacement drift for specimen S-5-R (side 1).

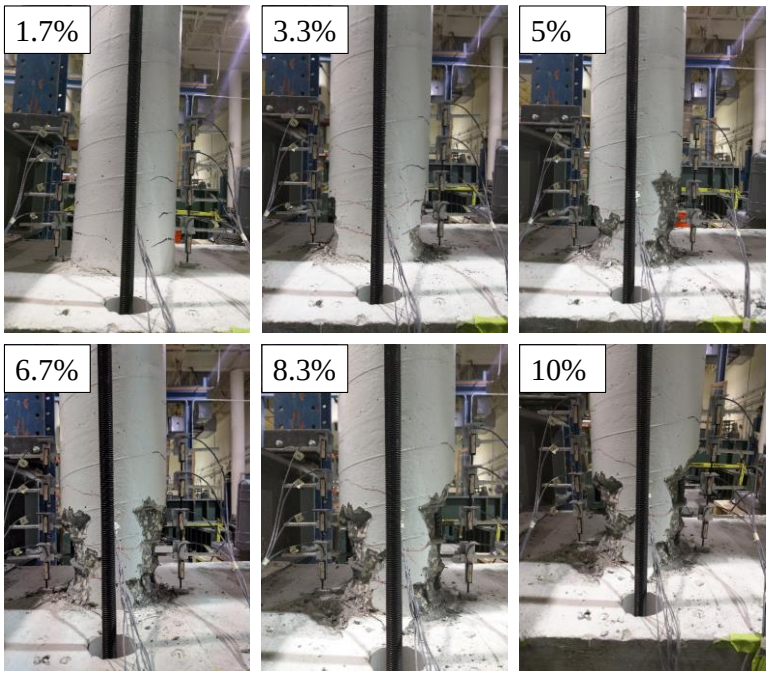

Figure 6-15 Damage at different displacement drift for specimen S-5-R (side 2).

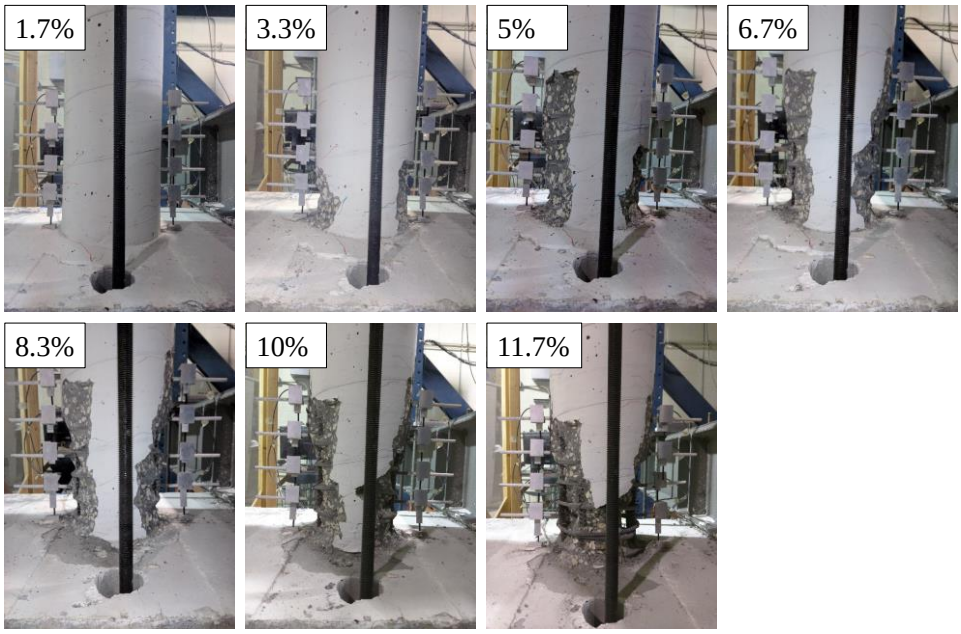

Figure 6-16 Damage at different displacement drift for specimen S-6-R (side 1).

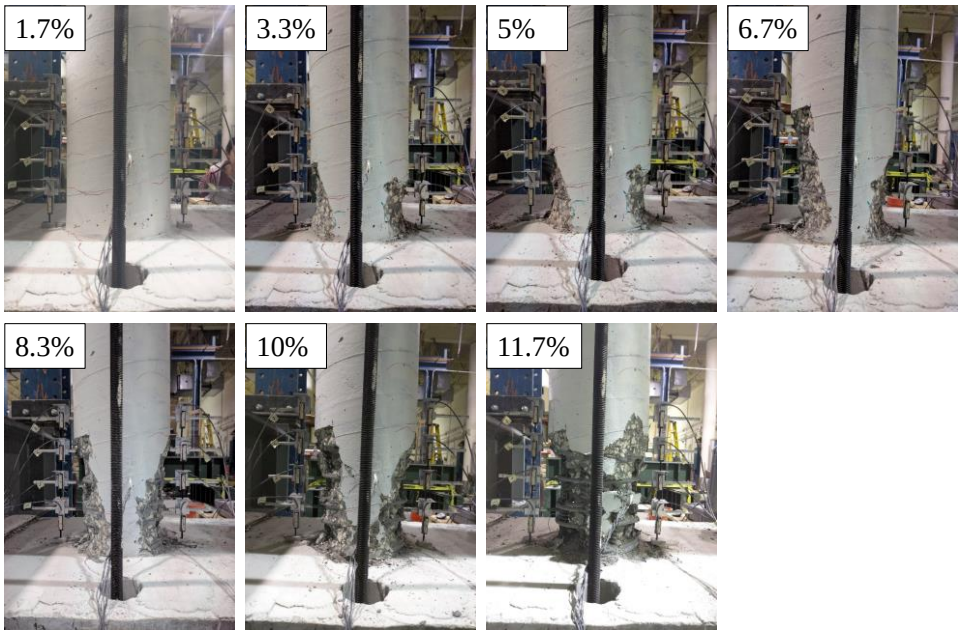

Figure 6-17 Damage at different displacement drift for specimen S-6-R (side 2).

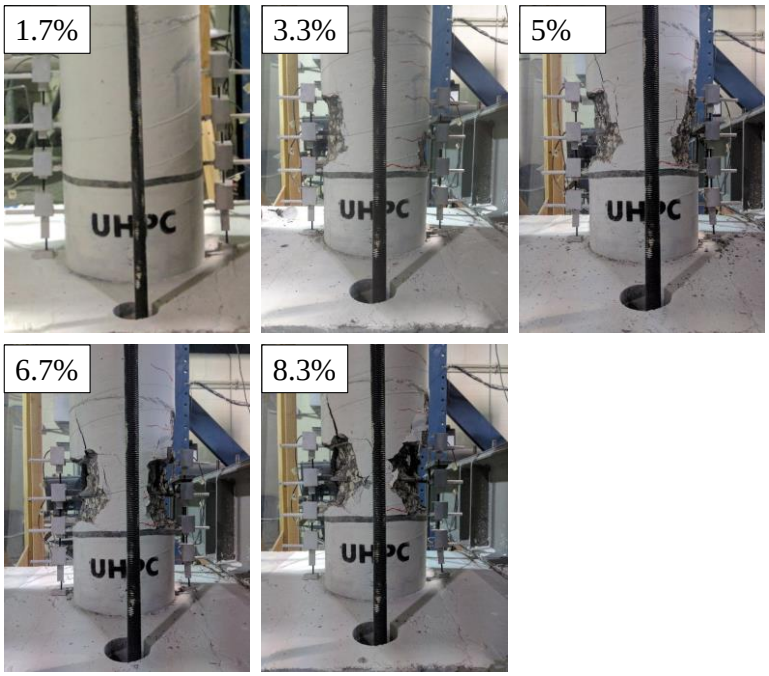

Figure 6-18 Damage at different displacement drift for specimen S-5-12 (side 1).

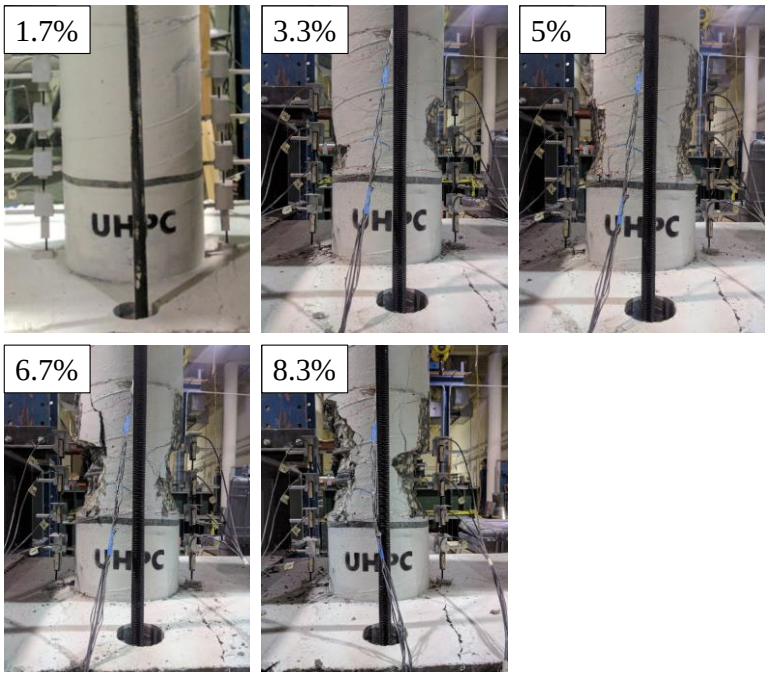

Figure 6-19 Damage at different displacement drift for specimen S-5-12 (side 2).

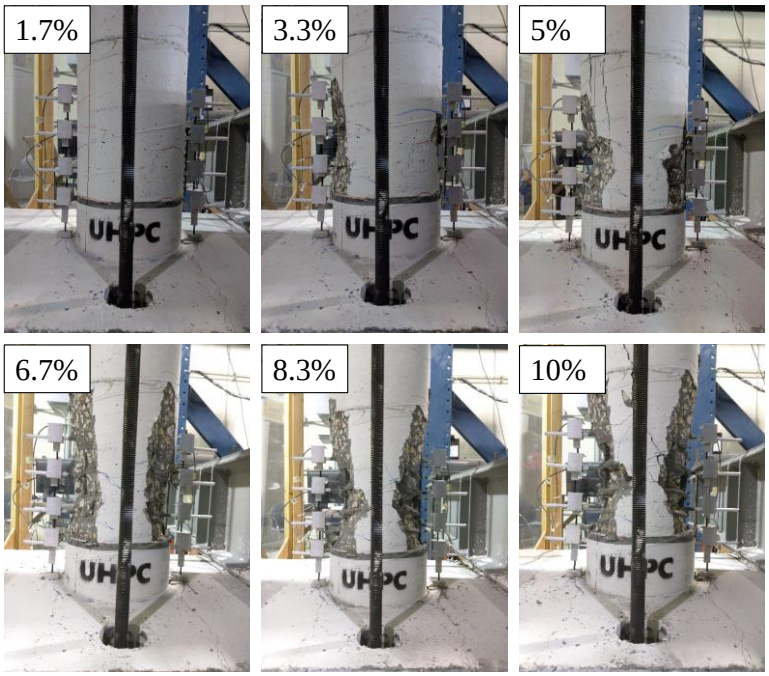

Figure 6-20 Damage at different displacement drift for specimen S-5-8 (side 1).

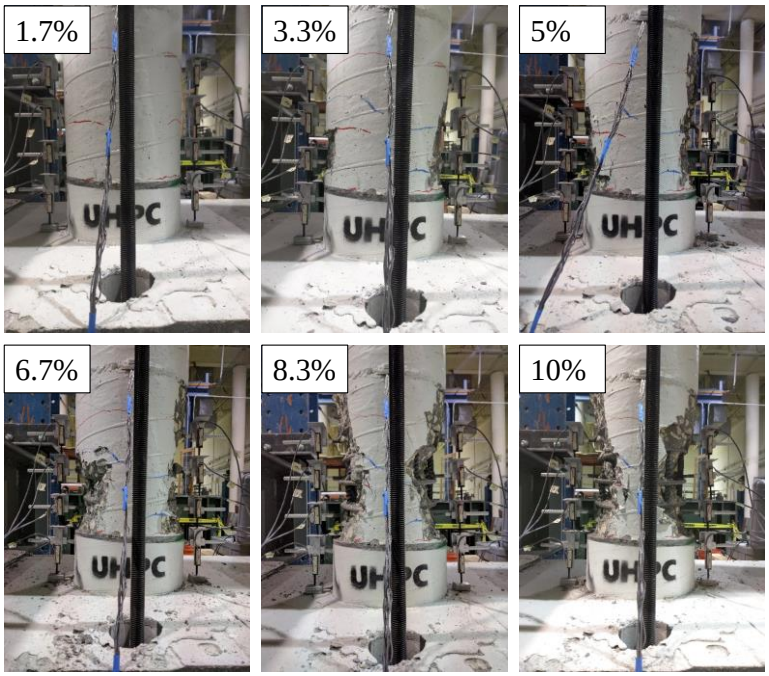

Figure 6-21 Damage at different displacement drift for specimen S-5-8 (side 2).

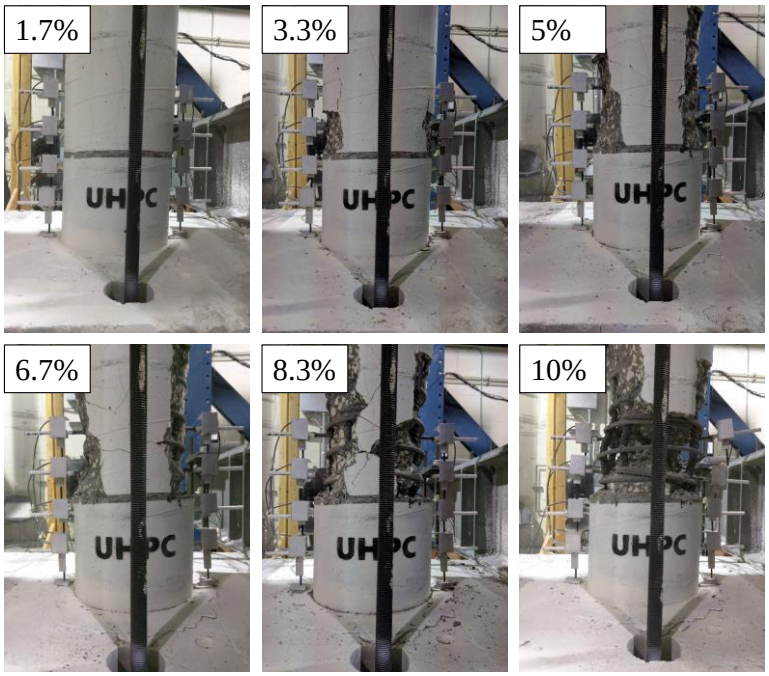

Figure 6-22 Damage at different displacement drift for specimen S-6-12 (side 1).

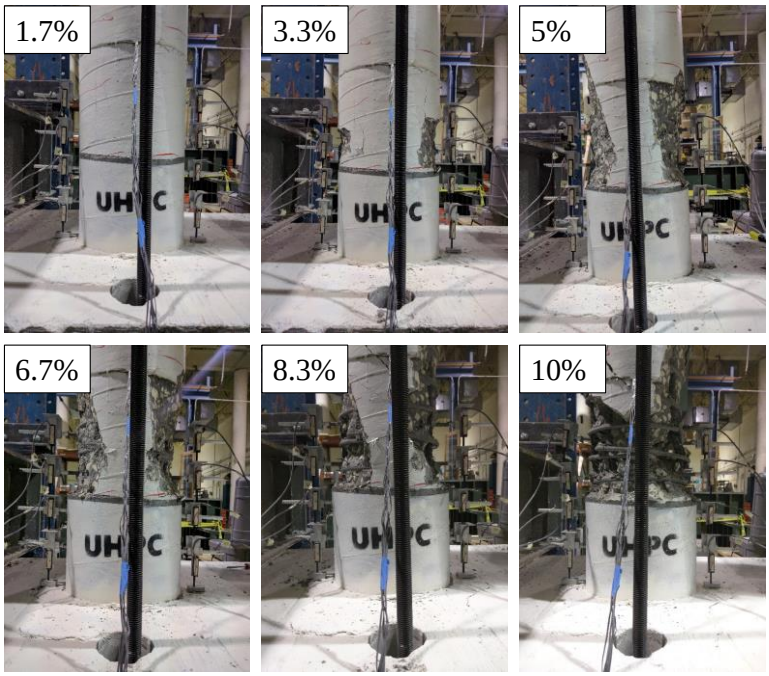

Figure 6-23 Damage at different displacement drift for specimen S-6-12 (side 2).

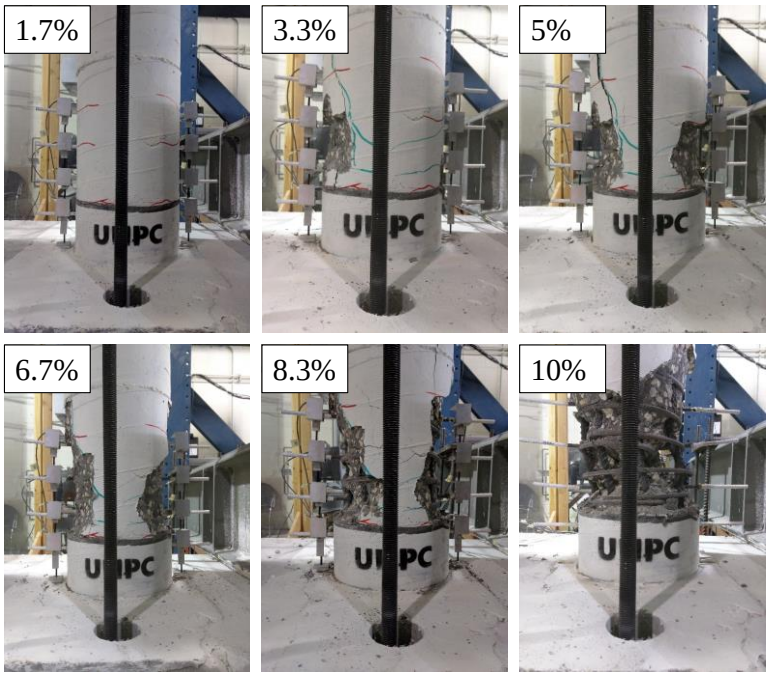

Figure 6-24 Damage at different displacement drift for specimen S-6-8 (side 1).

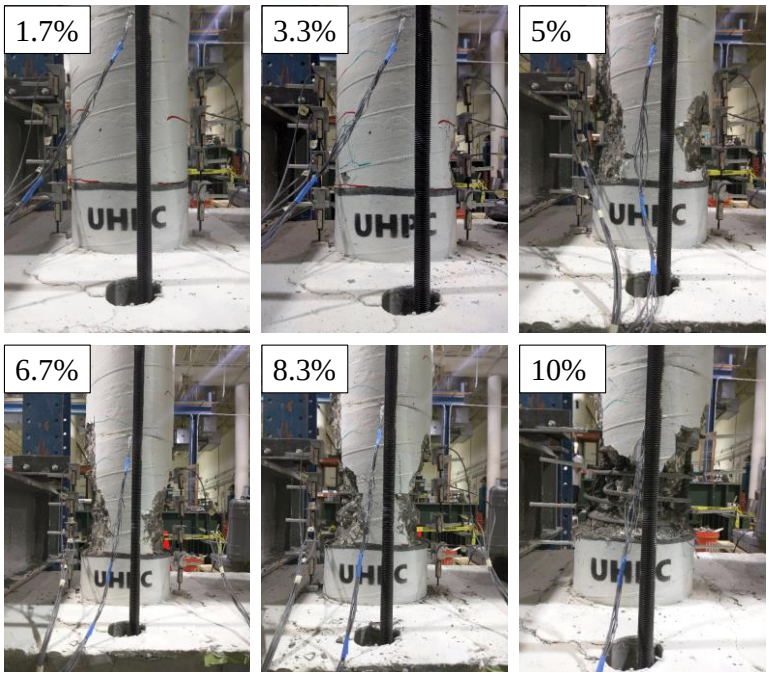

Figure 6-25 Damage at different displacement drift for specimen S-6-8 (side 2).

6.4.2 Mode of Failure

Specimens having rebar No. 5 failed when one of the longitudinal bars ruptured by buckling between stirrups after spalling of the concrete cover. In the case of specimens having rebar No. 6, when one of the longitudinal bars buckled between stirrups due to spalling of the concrete cover, the core concrete crushed at high displacement drifts. Fracture of the rebar was generally located around 2-3 inches above the UHPC layer. The displacement ductility of the specimens is shown in Table 6-3 indicating their performance in seismic zones based on common seismic provisions. Comparing reference specimen (S-5-R), specimens S-5-8 and S-5-8, show that in the case of No. 5 bar size with a side cover of $2d_b$, $8d_b$ can be considered a lap splice length. Also, comparing reference specimen (S-6-R), specimens S-5-8 and S-6-8, show that in the case of No. 6 bar size with a side cover of $2d_b$, $8d_b$ can be also considered a lap splice length. Note that d_b is the bar diameter.

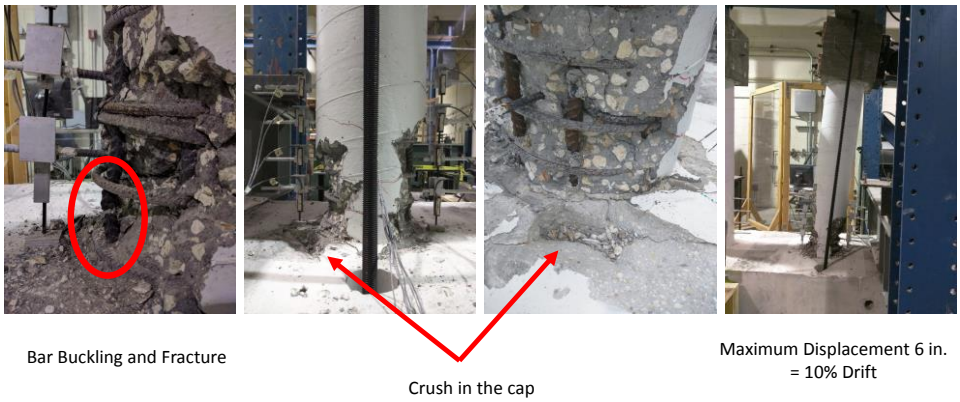

Figure 6-26 Failure pattern, longitudinal rebar fracture and location of the plastic hinge in the S-5-R.

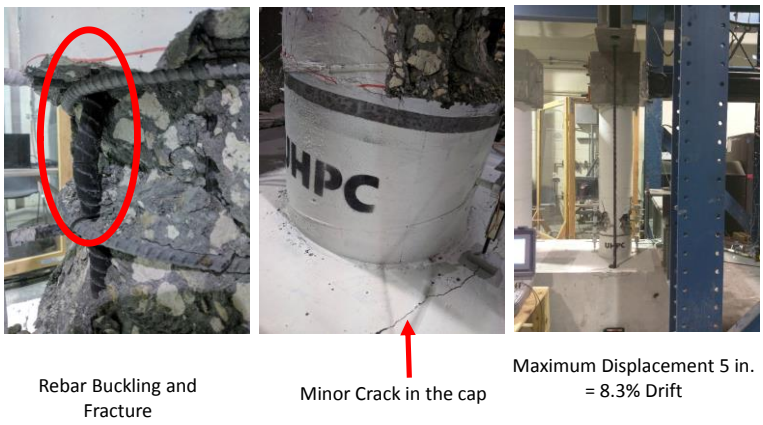

Figure 6-27 Failure pattern, longitudinal rebar fracture and location of the plastic hinge in the S-5-12.

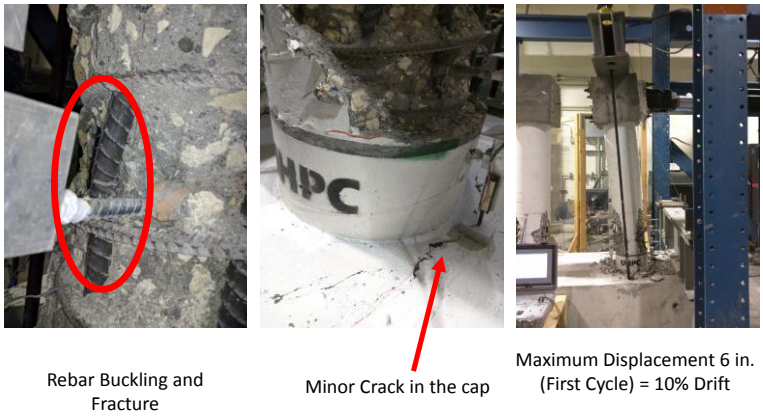

Figure 6-28 Failure pattern, longitudinal rebar fracture and location of the plastic hinge in the S-5-8.

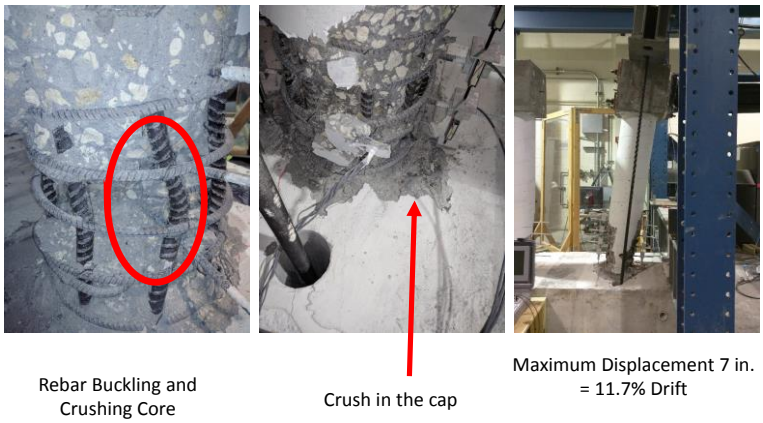

Figure 6-29 Failure pattern, rebar backing, crushing core concrete and location of the plastic hinge in the S-6-R.

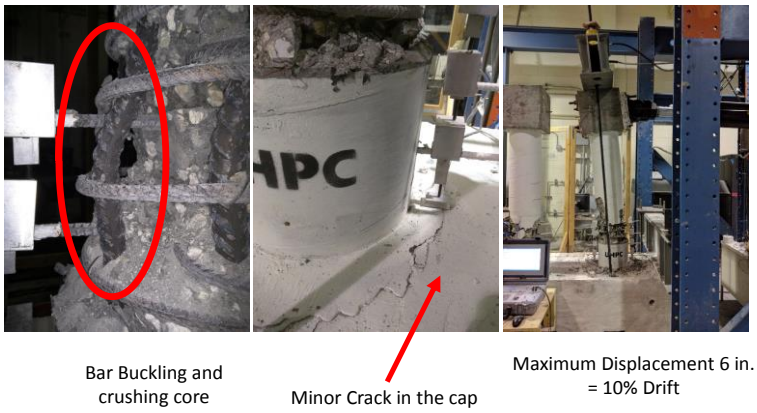

Figure 6-30 Failure pattern, rebar backing, crushing core concrete and location of the plastic hinge in the S-6-12

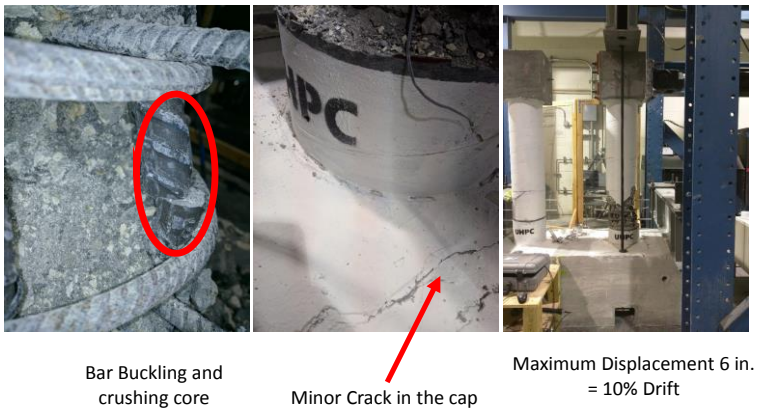

Figure 6-31 Failure pattern, rebar backing, crushing core concrete and location of the plastic hinge in the S-6-12

6.4.3 Moment- Displacement Curve

Table 6-3 shows the maximum displacement of the specimens. All specimens were subjected to the cyclic loading to show their capability for seismic area. Figure 6-32 and 6-33 show the hysteresis moment deflection curve of the specimens. The measured value shows the moment at the base of the column including P-Δ effect. The lateral load decreased gradually after the peak load, indicating the spalling of cover concrete and p-Δ effects.

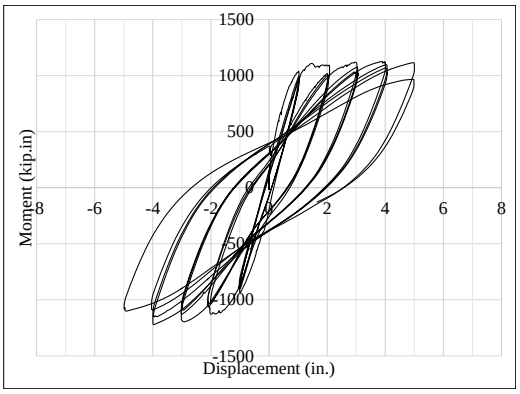

S-5-12

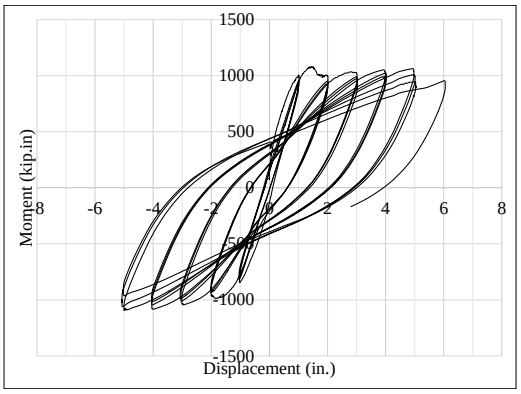

S-5-8

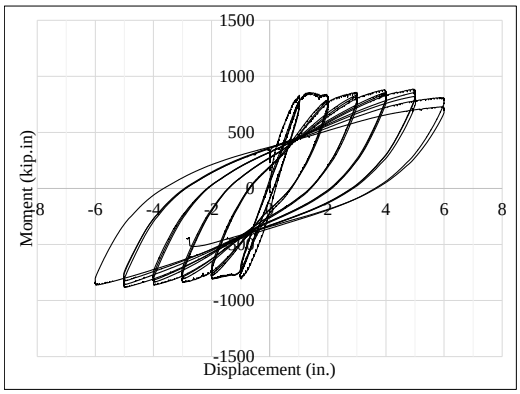

S-5-R

Figure 6-32 Hysteresis moment-displacement curve of the specimens, bar size #5.

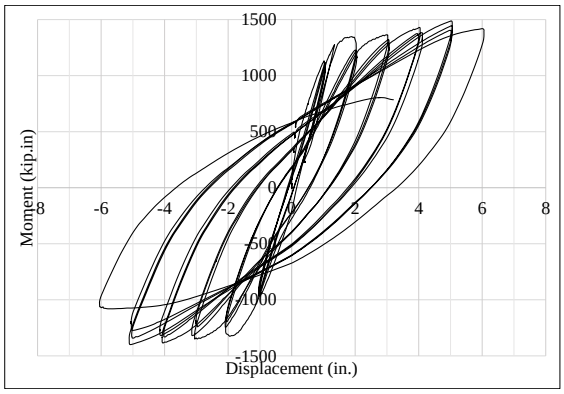

S-6-12

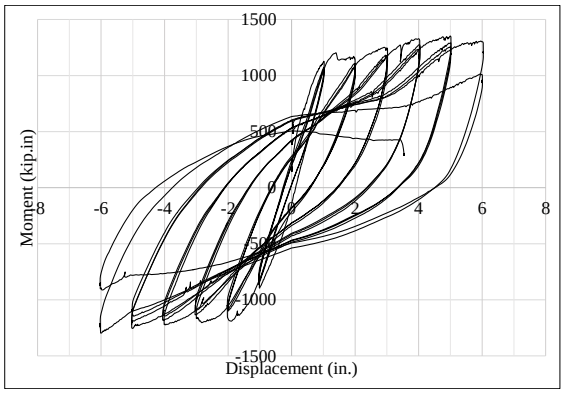

S-6-8

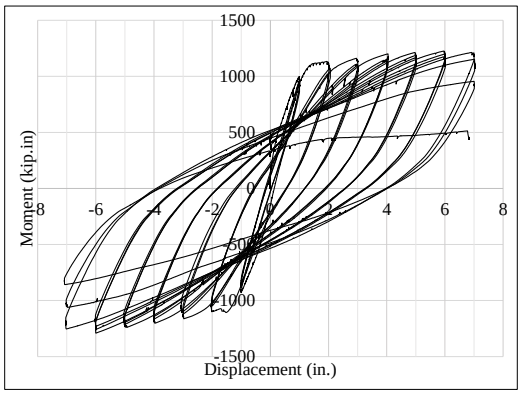

S-6-R

Figure 6-33 Hysteresis moment-displacement curve of the specimens, bar size #6.

Table 6-3 Ductility and maximum drift of the specimens (Rebar Size: #5).

	S-5-R (#5 Rebar, Reference)	S-5-8 (#5 Rebar, $8d_b$ Splice)	S-5-12 (#5 Rebar, $12d_b$ Splice)
Maximum Moment at Base (kip.in.)	850	1050	1100
Maximum Displacement (%Drift)	6 in. (10%)	6 in. (10%)	5 in. (8.3%)
Failure	Second Cycle of 6 in.	First Cycle of 6 in.	Second Cycle of 5 in.
Calculated yield displacement (Δ_y)	0.6 in.	0.65 in.	0.65 in.
Displacement Ductility (μ_d)	10	9	7.5

Table 6-4 Ductility and maximum drift of the specimens (Rebar Size: #6).

	S-6-R (#6 Rebar, Reference)	S-6-8 (#6 Rebar, $8d_b$ Splice)	S-6-12 (#6 Rebar, $12d_b$ Splice)
Maximum Moment at Base (kip.in.)	1060	1340	1470
Maximum Displacement (%Drift)	7 in. (11.6%)	6 in. (10%)	6 in. (10%)
Failure	First Cycle of 8 in.	Third Cycle of 6 in.	Second Cycle of 6 in.
Calculated yield displacement (Δ_y)	0.60 in.	0.65 in.	0.70 in.
Displacement Ductility (μ_d)	11	9	9

6.4.4 Measured Curvatures

The specimens were instrumented with 8 potentiometers to measure the curvature of the column. The potentiometers were mounted on steel bars that passed through the column at four different distances (≈4 in. space) from the cap beam face. At very high displacement levels, some potentiometers stopped working and further measurement of curvature was not possible. The maximum curvature profile at different displacement level versus the column height is shown in Figure 6-34 and Figure 6-35. Results show that in the proposed detail, the plastic hinge was placed in the column and the cap beam was damage free. This shows the capability of this connection for the seismic region as well.

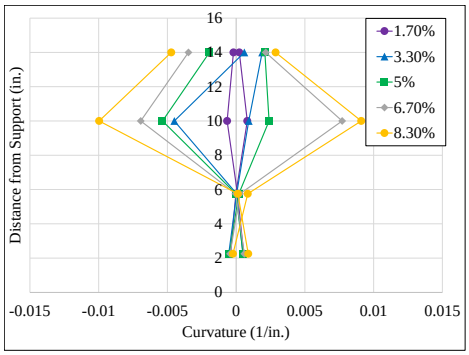

S-5-12

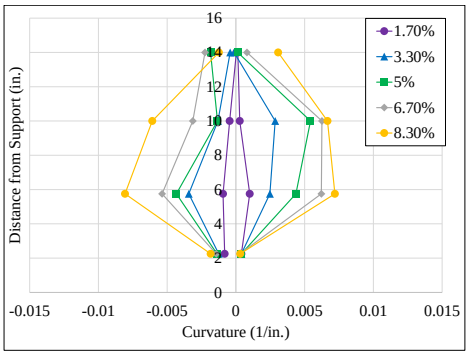

S-5-8

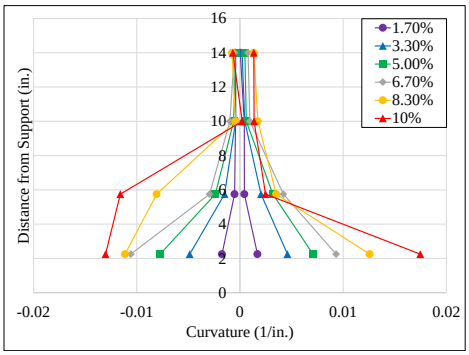

S-5-R

Figure 6-34 Plastic hinge curvature profiles for each displacement (Specimens Rebar size: #5).

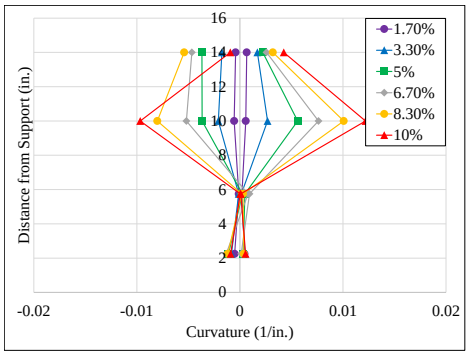

S-6-12

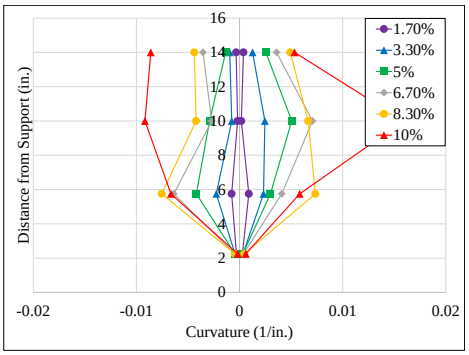

S-6-8

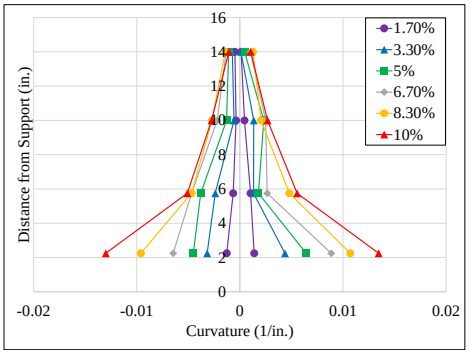

S-6-R

Figure 6-35 Plastic hinge curvature profiles for each displacement (Specimens Rebar size: #6).

6.5 Rebar Strain

The longitudinal bars were instrumented with 8 strain gauges from the cap beam to the column. The peak tensile strain profiles of bars were measured at different displacement levels. By losing strain gauges at high level of displacement, measuring strains of the bars was not feasible. Results show that rebar did not yield in the UHPC lap splice length.

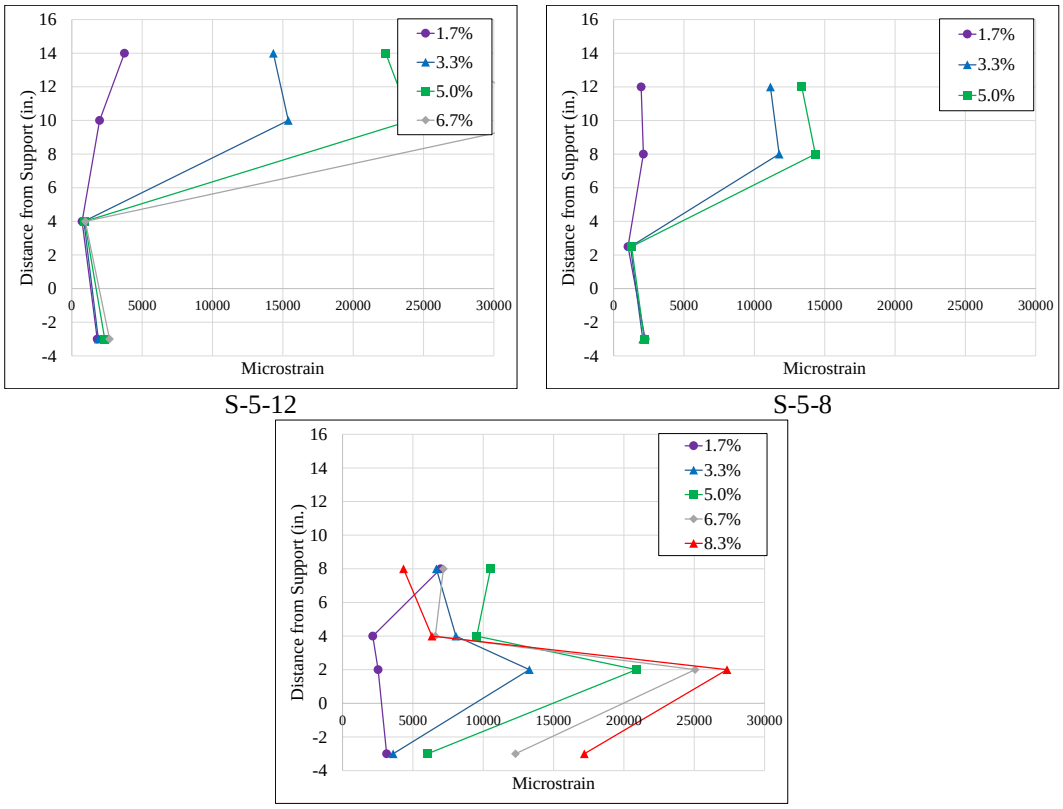

Figure 6-36 Plastic hinge curvature profiles for each displacement (Specimens Rebar size: #5).

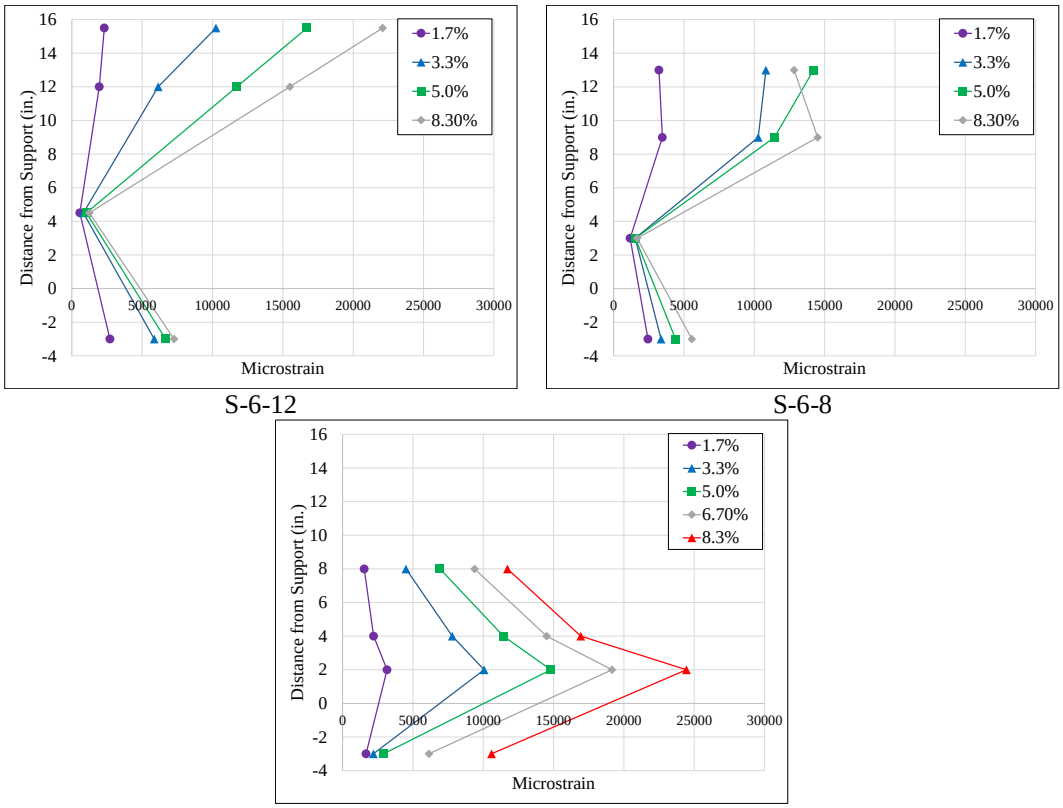

Figure 6-37 Plastic hinge curvature profiles for each displacement (Specimens Rebar size: #6).

6.6 Impulse Response Test

The Impulse-Response system uses a hammer, to send impact waves through the tested specimen. The impact causes the specimen to vibrate in a bending mode and a geophone placed adjacent to the impact point and measures responses. The hammer load cell and geophone are connected to a computer with software for data acquisition, signal processing and storage (Figure 6-38). The outcome of the test expressed as the mobility of the specimen. Generally higher mobility indicated lower stiffness and can be considered as a sign of damages.

Figure 6-38 Measuring the mobility of the column.

In this research, an equipment (Olson SE/IR), was used to measure the mobility of the tests after each cycle of the applying load. The results are shown in the in Figure 6-39 and Figure 6-40. The measurement was done at different level of the column and at the last cycle of loading. Increase in the mobility is a result of decrease in stiffness of the column after each cycle. In all specimens because of the crushing after 3 inch displacement (3.3% Drift), no more measurement was possible. Generally, the mobility of the specimen increased 70% in the first cycle and 110% for the third cycle compared the original specimen.

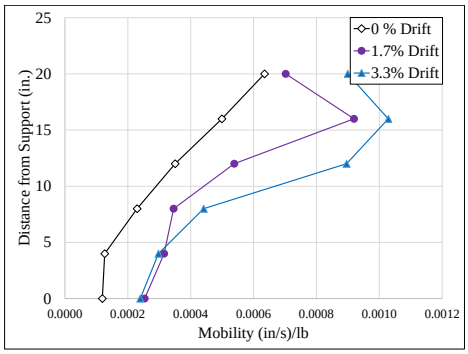

S-5-12

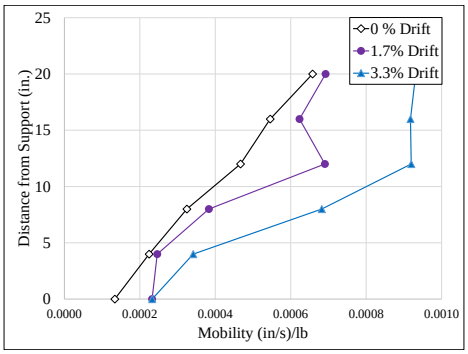

S-5-8

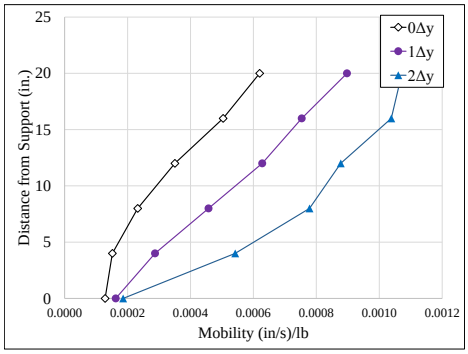

S-5-R

Figure 6-39 Specimens mobility after each cycle (Specimens Rebar size: #5).

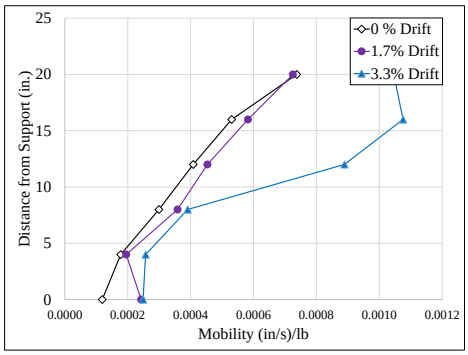

S-6-12

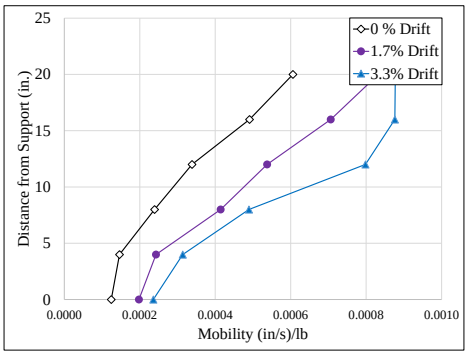

S-6-8

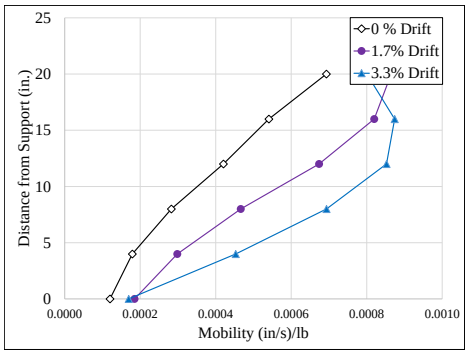

S-6-R

Figure 6-40 Specimens mobility after each cycle (Specimens Rebar size: #6).

6.7 Moment Curvature Analysis

The moment capacity of the specimens was calculated using a Moment-Curvature section analysis. For this analysis, the curves were obtained with related axial load and the idealized curves were derived according to Caltrans [8]. Considering the equivalent analytical plastic hinge length and the length of the column, the local displacement capacity of a member can be calculated based on its moment-curvature analysis which includes idealized yield and plastic displacement due to rotation of the plastic hinge.

The effect of the expected properties of the rebar, confinement of concrete was considered in the analysis. Figure 6-41 and 6-42 show the relation between experimental and analytical load-displacement curves of the column using moment-curvature analysis.

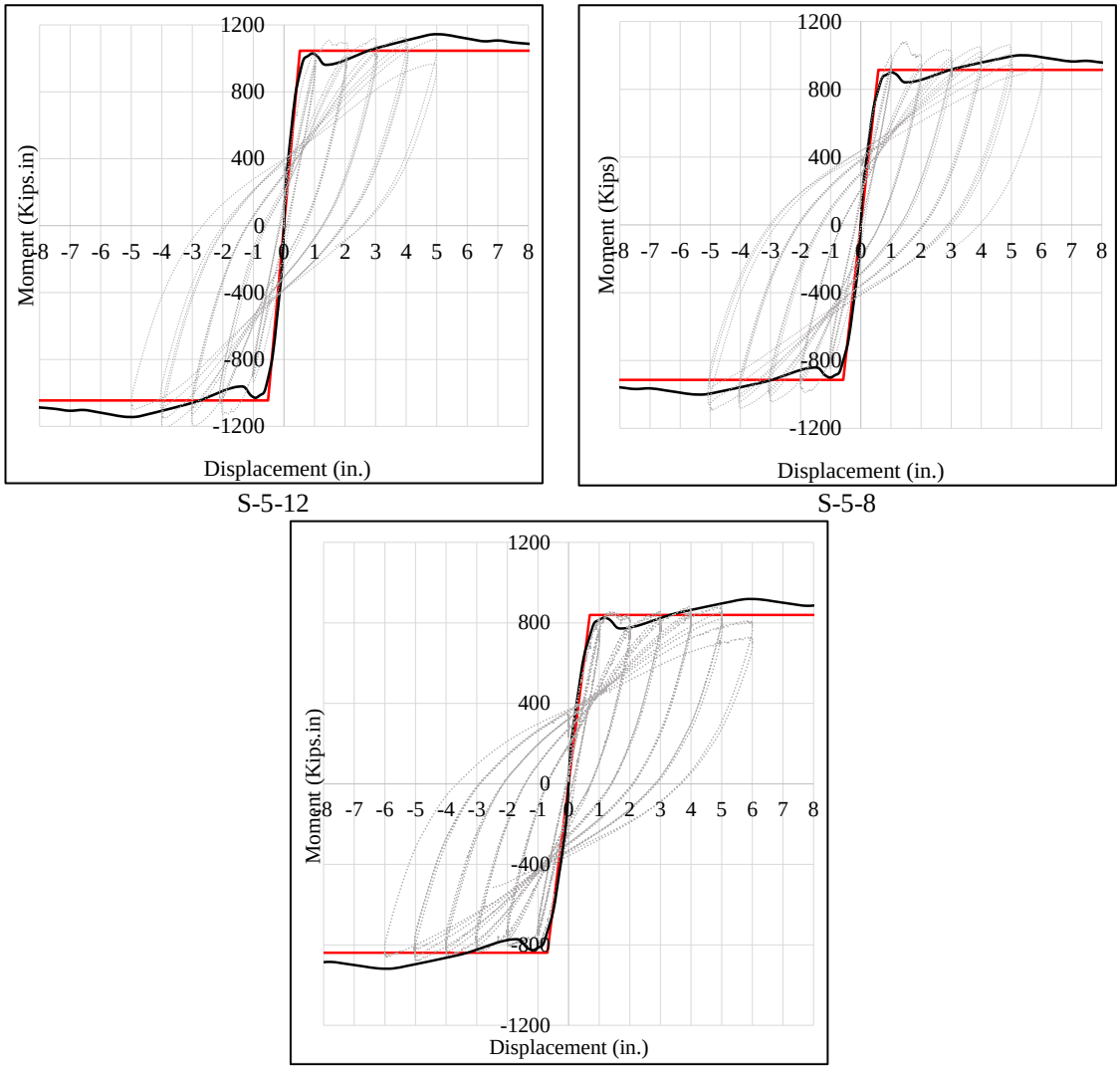

Figure 6-41 Moment-displacement curves of the specimens, based on moment curvature analysis and idealized Caltrans curve (rebar size #5).

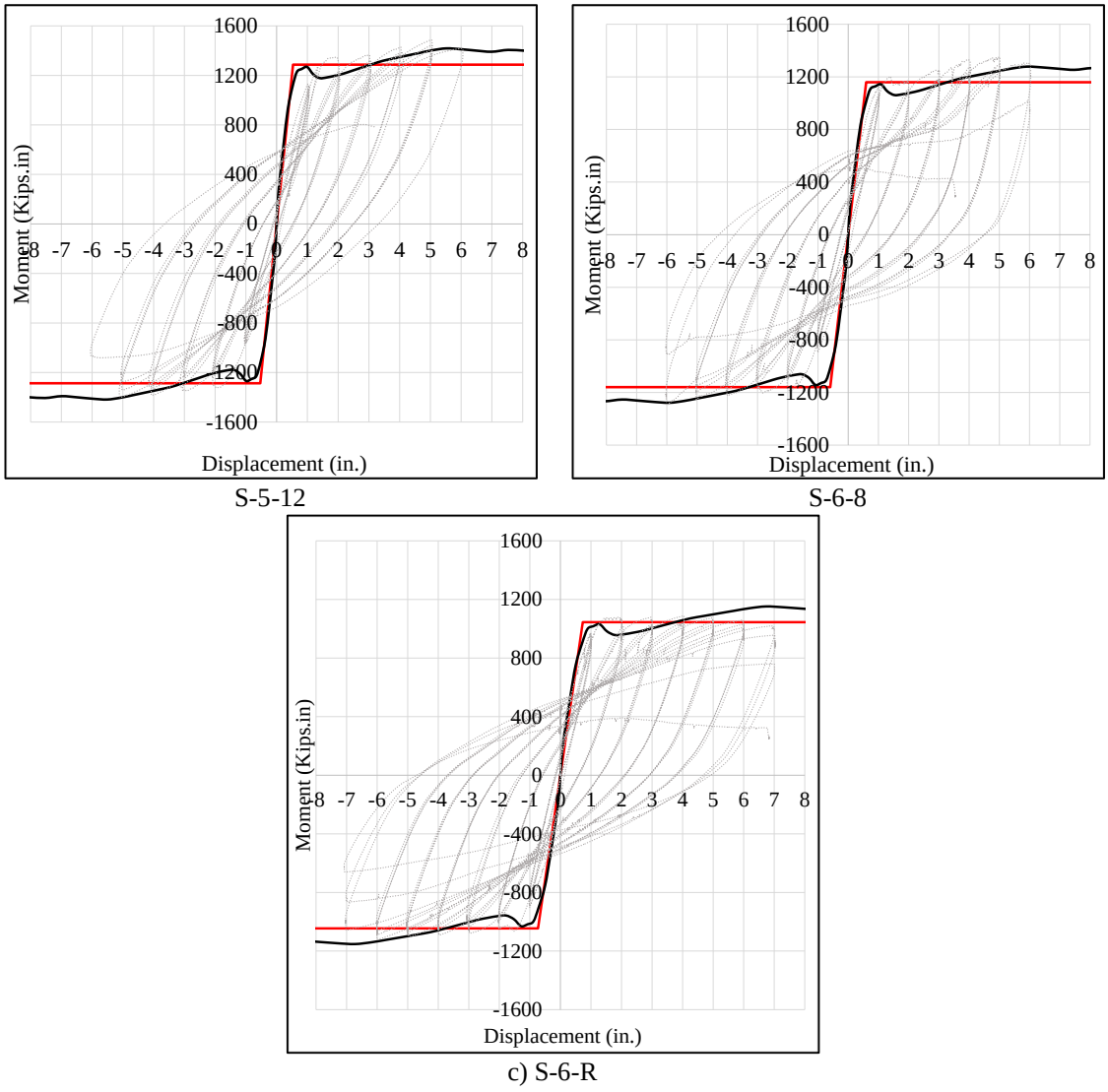

Figure 6-42 Moment-displacement curves of the specimens, based on moment curvature analysis and idealized Caltrans curve (rebar size #6).

6.7.2 Results and Discussion

In all tested specimens, the critical section was located in the section having normal strength concrete and the behavior of the specimen generally governed by these sections. Note that in different specimen the distance between the loading point and the critical

section was different so the maximum applied load and consequently the moment at the base was different.

To have a better comparison, normalized displacements and moment in the critical section were employed. Figure 6-43 shows the comparison between the specimens. Note that L' is the distance between the load applied and the critical section. The comparison shows that the behavior of specimens having Detail 1 are the same as their corresponding references considering the fact that the critical section shifted adjacent to UHPC in the column.

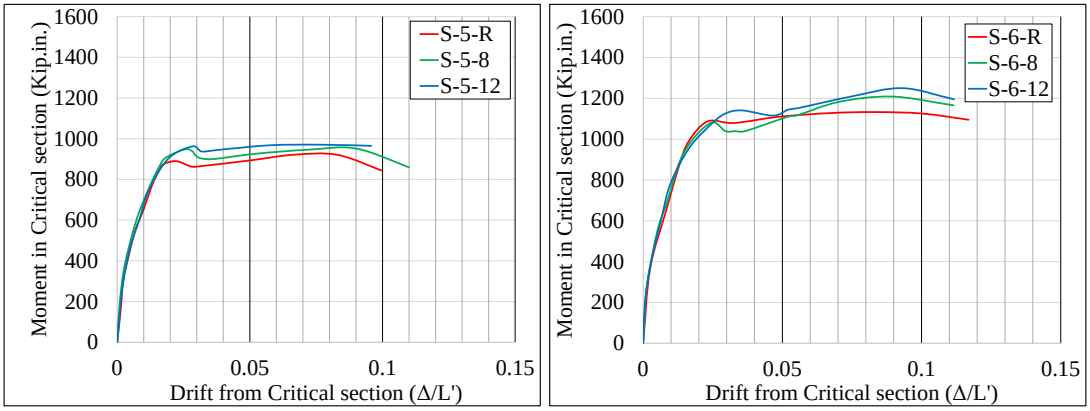

Figure 6-43 Comparison between the tested specimens.

6.8 Summary and Conclusions

In this chapter, the structural behavior of Detail 1 was investigated. In this detail, a layer of Ultra-High Performance Concrete (UHPC) was used to connect precast elements. Six specimens, including two references, in cantilever configuration, were tested under combined constant axial load and reversed lateral load. Various responses of the connection were highlighted. Lap splice length and rebar sizes were the variables. The results show that $8d_b$ of the lap splice for rebar No. 5 & 6 can prevent slipping of the rebars and developing damage into the cap beam. Simplicity and large tolerance of bars using high

workability of UHPC in the proposed detail can facilitate and accelerate the on-site construction.

No significant damage was found in the splice region even in the absence of the transverse reinforcement in this region. Observing no failure in splice region indicates that UHPC can provide a good confinement and shear capacity. Eliminating the need for stirrups in the splice region can facilitate the construction procedure in the field. Moreover, in comparison with conventional concrete, even a short lap splice of bars in UHPC can transfer forces between spliced bars, which leads to a decrease in casting volume while saving time in the field. Comparing the results of the tested specimens and references shows that the proposed connection just shifts the plastic hinge location in the column from the surface or even in the cap beam to the column adjacent to the UHPC layer and protect cap beam from damage. The behavior of the system is governed by the section having normal strength concrete. This is because of the fact that capacity of the UHPC section using lap splice is much higher than the column with normal strength concrete.

CHAPTER 7 NUMERICAL INVESTIGATION

7.1 Introduction

In this chapter, modeling of the tested specimens and effect of parameters such as axial load and splice length are investigated. The geometric details and boundary conditions were similar to the experimental test conditions. The simulation of experimental conditions is not only important for comparison of tested data with numerical results but also validates the results of the parametric study.

Two concrete models are available in ABAQUS/Standard: Concrete Smeared Cracking (CSC) and the Concrete Damaged Plasticity (CDP) model. CSC model does not consider the effects of steel-concrete interface, such as bond slip. Based on the Abaqus documentation, the model may only be used for monotonic loadings under fairly low confining pressures. The CDP model can be used for a general analysis of the concrete structures under cyclic and/or dynamic loading and high confining pressures.

Both CDP and CSC models can be used for modeling conventional concrete. Based on previous studies on UHPC [82] CDP model replicates the observed strain and deflection response of UHPC specimens better than the CSC model. Since UHPC is remarkably different from normal strength concrete, typical values for a normal concrete may not accurately reflect the behavior of UHPC. Therefore, the parameters of the models must be calibrated based on an available experimental data.

At the first step of this research, a FE material model was generated and calibrated with the experimental results. The modeling details, calibration process, and accuracy of the UHPC material were described in Chapter 2 and 3. In these chapters, the modeling

details, calibration, and their accuracy to predict the behavior of the proposed connections were discussed.

The objective of this chapter is to develop FE analysis modeling techniques which is applicable for the proposed connection. In this study, only three-dimensional, and static model with a monotonic loading were used. Most of the modeling aspects such as material properties of UHPC and steel bar, mesh, and element types are very similar to that implemented and detailed in previous chapters.

7.2 Numerical Modeling Details

A quasi-static analysis with small load increments was used for the numerical study. The models were subjected to a monotonic displacement control loading. In all models, the cap beam and the support was restricted in all three directions. Similar to the experimental test conditions, first axial load was applied as a pressure and then a displacement was applied to the end of the column as a lateral load. These boundary conditions enabled rotation of the model while the load was being applied.

An eight-node solid element (C3D20) was used to model the normal concrete and UHPC, while the truss elements (T3D2) were selected for embedded reinforcement bars. The material strength was based on the measured compressive strength of regular concrete and UHPC.

7.3 Modeling the Bond Behavior of the Bars

In order to model the spliced bars, a spring element was used (see Figure 7-1). In this model, the interaction between the steel bars are assumed as a non-linear element (spring) and the properties of the non-linear element were calibrated by experimental test.

Rebar diameter and type, clear cover and the strength of the concrete can affect the overlap splice length and consequently the assumptions of the spring properties.

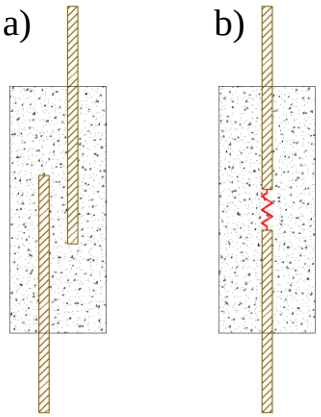

Figure 7-1 Splice modeling technique a) Overlap spliced rebar, b) Concept of the modeling.

To calibrate the proposed model, the experimental data of Peruchini performed at the University of Washington was used [113]. In that study, the behavior of a lap spliced UHPC joint between two precast concrete elements (deck panels) with No. 5 bar was evaluated. The specimens were loaded in a three-point bending setup placed on the joint until the lap spliced connection failed (Figure 7-2). Joint width (thus splice lengths) and the clear cover over the main tension reinforcement and the offset between opposing reinforcing bars were the main parameters. It is worth to mention that, in their experiments, the compressive and tensile strength of UHPC were 15.95 ksi and 1.9 ksi, respectively.

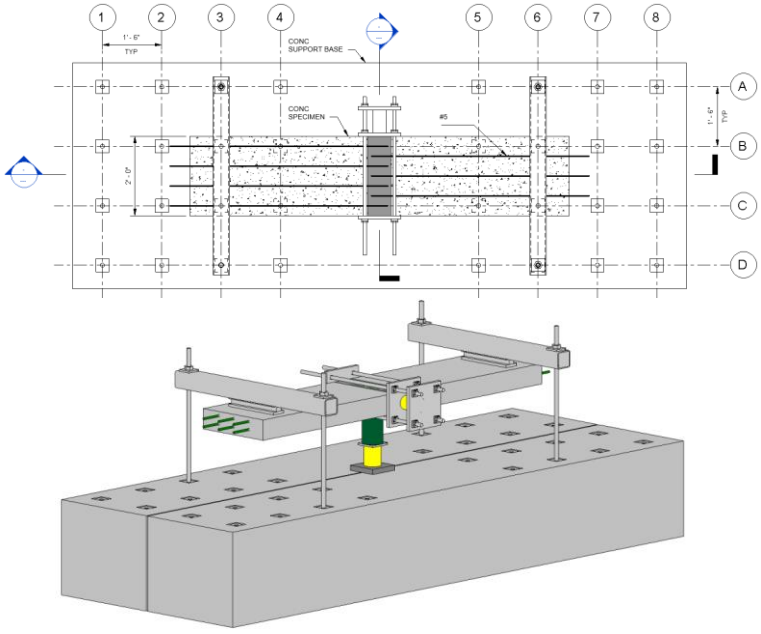

Figure 7-2 Plan view and 3D model of the test by Peruchini [113].

Considering the material properties of the tested specimens, the beam with a 4 in. overlap ($4d_b$) were modeled and employed to calibrate the spring properties. Figure 7-3 shows the calibrated FE modeling results compared to the experimental results.

a)

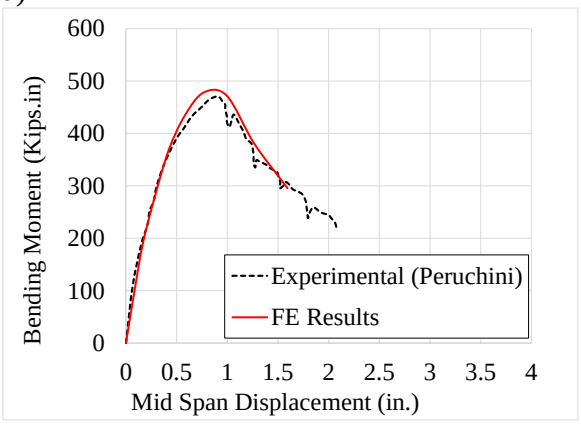

b)

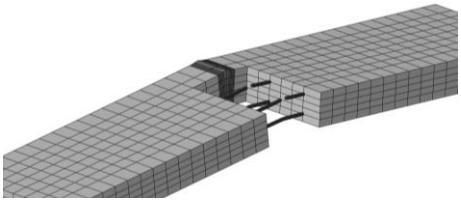

Figure 7-3 Modeling results of Peruchini test a) Comparison between calibrated FEM results and experimental test b) Deformed modeled specimen.

7.4 Numerical Model of the Large Scale Rectangular-Section Specimen (Feasibility Study)

As discussed in chapter 4, a large-scaled connection between a precast column and cap beam was constructed and tested under combined axial compression and reversed cyclic loading to form the plastic hinge and failure. The column length from the footing surface to the center of the loading point was 10.5 ft with a cross section of 20×20 in. The column was reinforced longitudinally with 16 No. 6 bars and transversely with No. 4 stirrups at a 3-in. spacing. The axial load of the column was 200 kips which resulted into approximately 10% of the pure axial load capacity of the column section.

Figure 7-4 shows the numerical model and mesh density in detail. Global seeds of 2-inch were used to mesh the column except in the plastic hinge area. For mesh in plastic hinge area, 1-inch global seeds were used. However, this model showed low sensitivity to mesh size. The material model was as adopted from the test specimen described in chapter 2 and 3.

The values used for uniaxial compressive strength of concrete materials in models were the actual values taken from cylinder test on the day after the experimental test was performed. The uniaxial compressive strength was 7.1 ksi for normal concrete and 21.7 ksi for UHPC. The bars material considered to be elastic-perfectly plastic material in both tension and compression. Steel material input data in the model for all rebars was taken from the actual tensile test. The yield and ultimate stresses were found to be 68.1 ksi and 112.2 ksi, respectively. Modulus of elasticity and Poisson's ratio of steel were assumed 29000 ksi and 0.2.

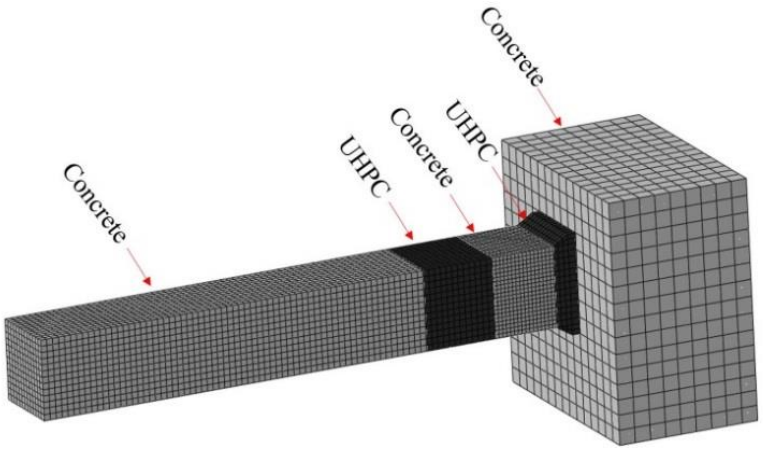

Figure 7-4 Column numerical model details.

7.4.2 Simulation Results

The measured hysteretic curves of the experimental model are compared with analytically determined moment-displacement are shown in Figure 7-5. As indicated in this figure, the initial stiffness of the system in FE model is higher than the stiffness obtained from the experimental study. This difference can be attributed to the variation in material properties and boundary condition defined in FE model. However, a good correlation of the maximum load capacity was observed between FE model and experiment.

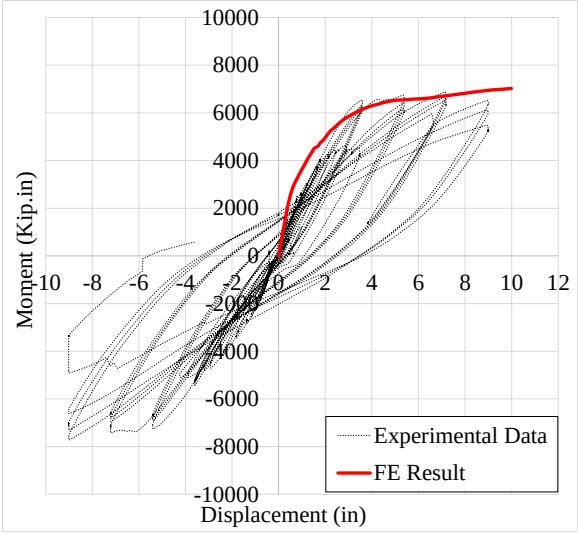

Figure 7-5 Measured hysteretic curves and calculated Moment–displacement.

The numerical results of the crack formation and bars stresses are depicted in Figure 7-6. The model was able to reproduce the column behavior with reasonable accuracy. As illustrated, the results of FE analysis could predict crack formation, critical sections, and yielding development in bars.

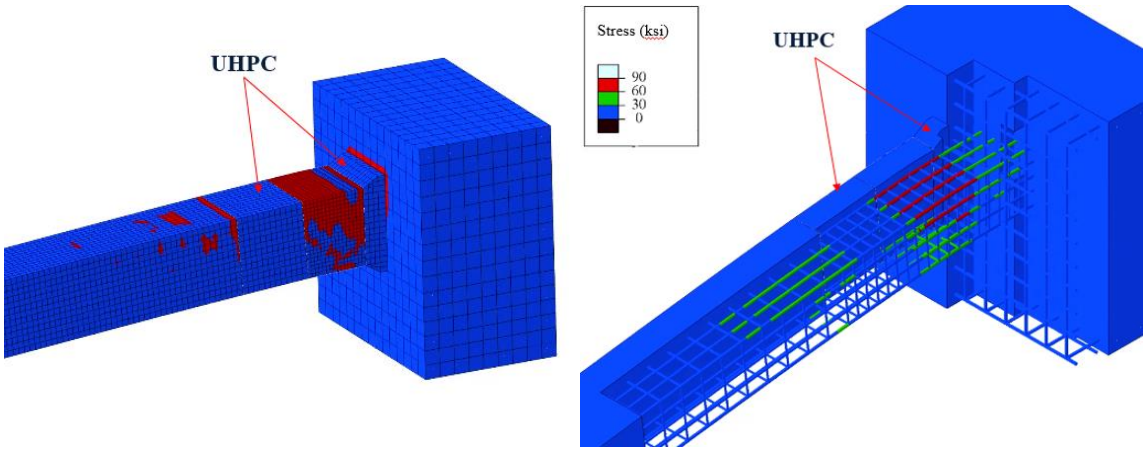

Figure 7-6 Crack formations and rebar stresses in the numerical model.

7.4.3 Axial Load Effect

The validated model was used to investigate the effect of axial load on the connection behavior. The FE model was subjected to different axial load from 10 to 25

percent of the pure axial load capacity of the column. Results show that increasing the axial load, increases the ultimate capacity of the column.

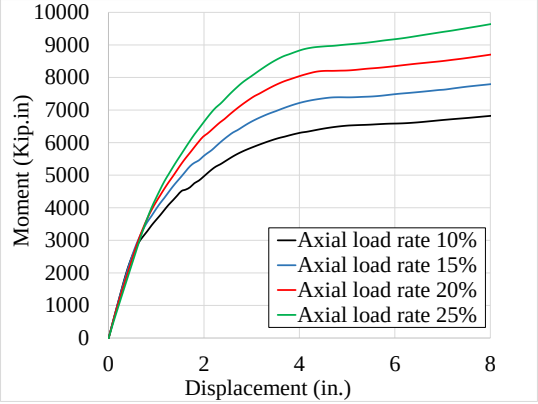

Figure 7-7 Effect of axial load on the behavior of the connection.

7.5 Numerical Model of the Circular-Section Specimens (Phase I)

Four columns to cap beam connection were tested under lateral loading and constant axial load as discussed in chapter 5. Three of the columns had Detail 2 and one had Detail 1. Different axial load and transverse rebar ratio in splice and plastic hinge zone were the varying parameters. The axial load varied from 10% to 20% of its pure axial capacity.

The column height was 61 in. with a circular cross-section having a diameter of 12 in. The column was reinforced longitudinally with 8 No. 5 rebars which resulted into a reinforcement ratio of about 2.19% for all specimens.

In this section, the FE models were based on the previous model and were revised as illustrated in Figure 7-8. The column was meshed with 1.5-inch global seeds. The procedure for material modeling was similar to one discussed earlier in chapter 2 and 3.

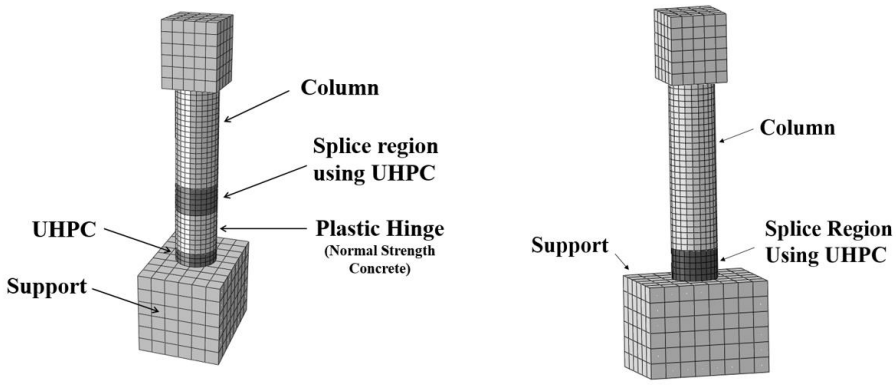

Figure 7-8 Column numerical model and mesh density details.

The values used for uniaxial compressive strength of concrete materials in models were the actual values taken from cylinder test at the day after the experimental test. The uniaxial compressive strength was 6.4 ksi for normal concrete and 20.1 ksi for UHPC. The bars material considered to be elastic-perfectly plastic material in both tension and compression. Steel material input data in the model for all rebars were taken from actual tensile test. Yield and ultimate stresses were 68 ksi and 113 ksi, respectively. Modulus of elasticity and Poisson's ratio of steel were assumed 29000 ksi and 0.2.

7.5.2 Simulation Results

A comparison of the results of the simulated specimens and experimental moment-displacement curve are plotted in Figure 7-9. A good correlation between the maximum load capacity and initial stiffness was observed between FE model and experiments.

The numerical results for the bars stresses are depicted in Figure 7-10. The model was able to simulate the column behavior with reasonable accuracy. As illustrated, the results of FE analysis could specify critical sections, and yielding development in rebars. The results of FE model show no rebar yielding or damage in the cap beam.

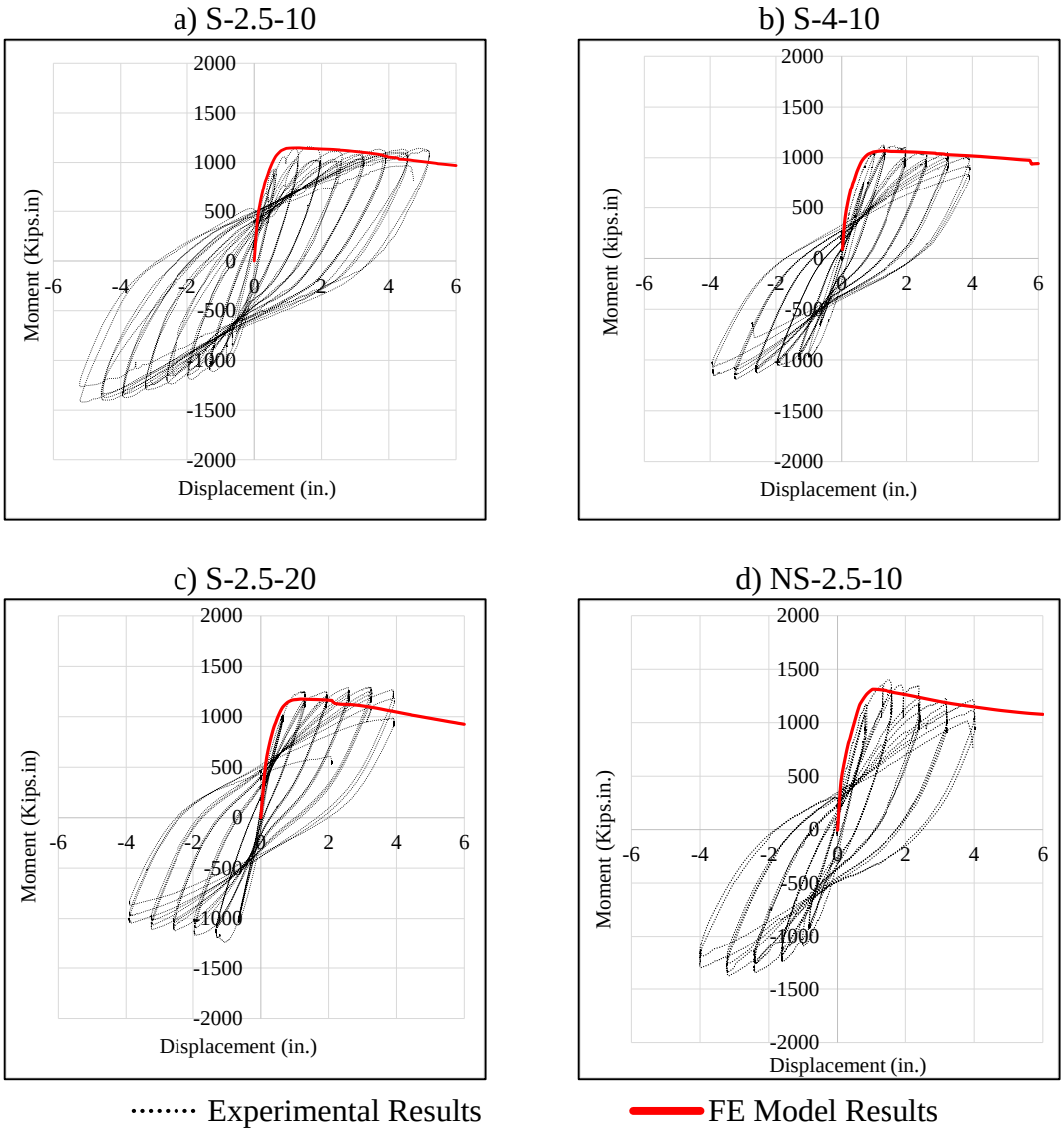

Figure 7-9 Measured hysteretic curves and numerical results of the specimens.

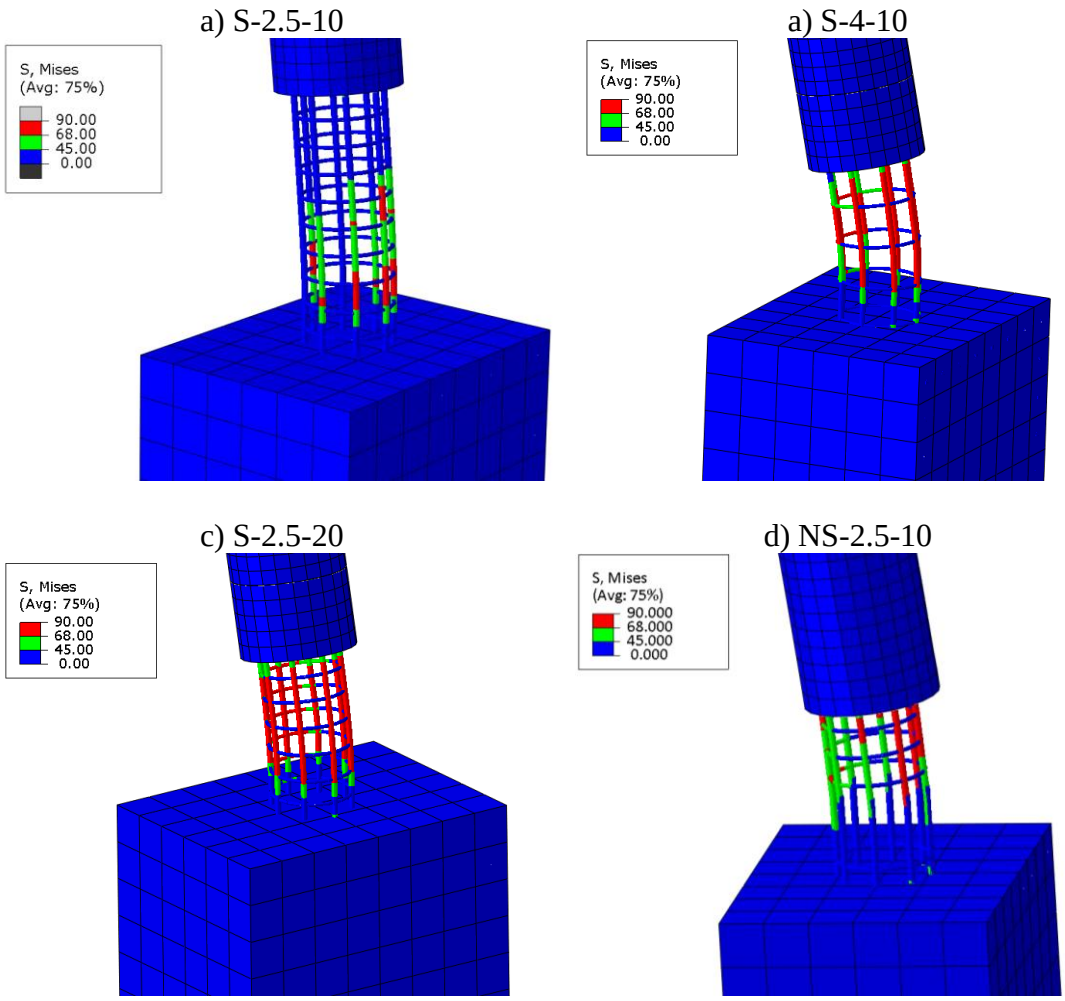

Figure 7-10 Rebar stresses in the numerical models.

7.6 Numerical Model of the Circular-Section Specimens (Phase II)

Four more specimens having Detail 1 were tested under the same loading condition as phase I. In addition, two reference specimens that were constructed using conventional methods were cast. The investigated parameters included rebar size (Rebar No. #5 and #6) and rebar lap splice length (8 d_b and 12 d_b). In this series of the test, the axial load ratio was 10%.

The column height was 61 in. with a circular cross-section having diameter of 12 in. The columns were reinforced longitudinally with either 8 No. 5 or 6 rebars. A monotonic

displacement control loading was applied to the model. 1.5-inch global seeds were used to mesh the whole column. However, results showed that the mesh sensitivity of this model is quite low.

7.6.1 Simulation Results

A comparison of the results of the simulated specimens and experimental moment-displacement curve are plotted in Figure 7-11 and 7-12. The model was able to simulate the column behavior with reasonable accuracy. As illustrated, the results of FE analysis could specify critical sections, and yielding development in rebars.

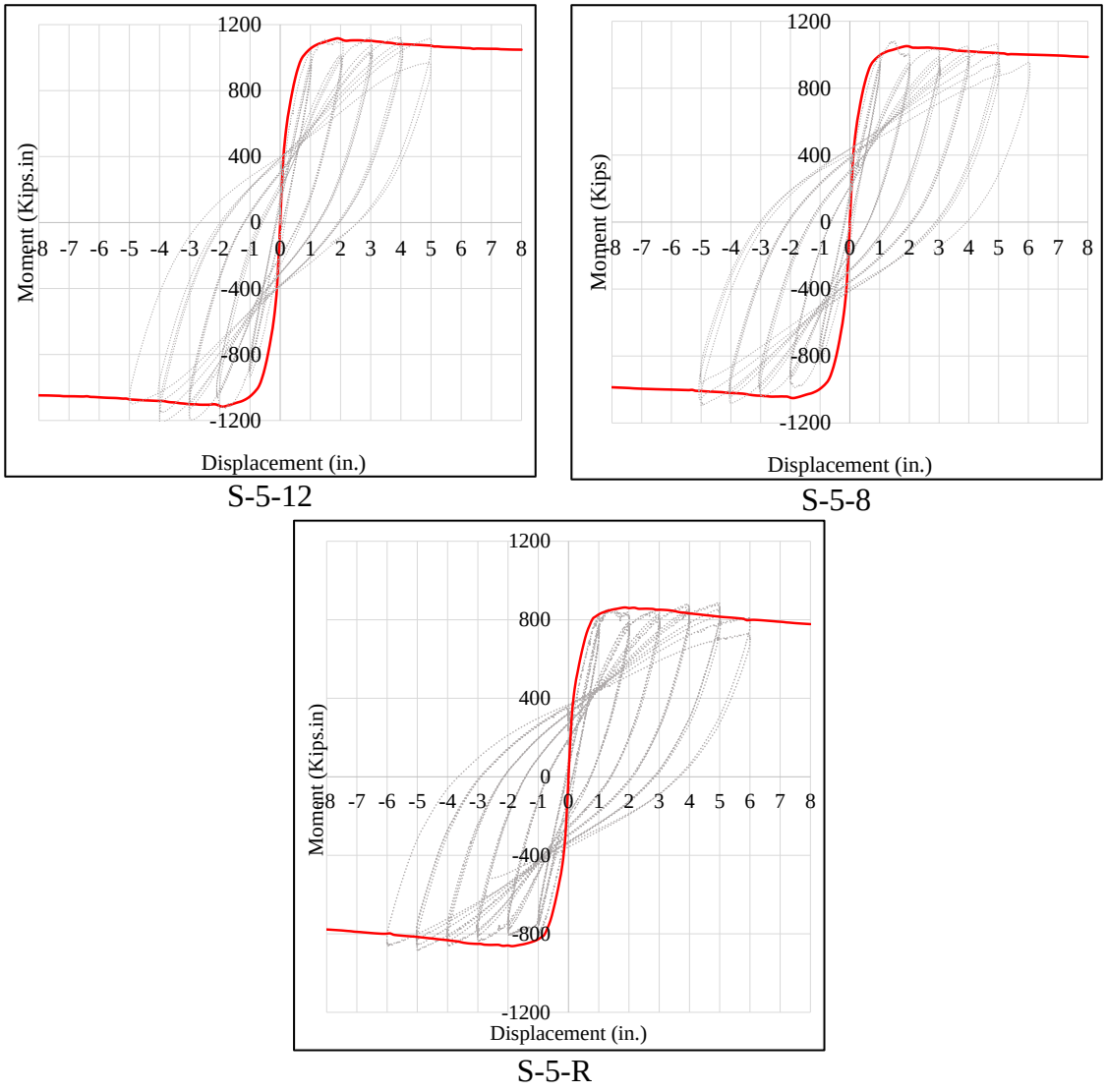

Figure 7-11 Measured hysteretic curves and numerical results of the specimens (Rebar Size: #5).

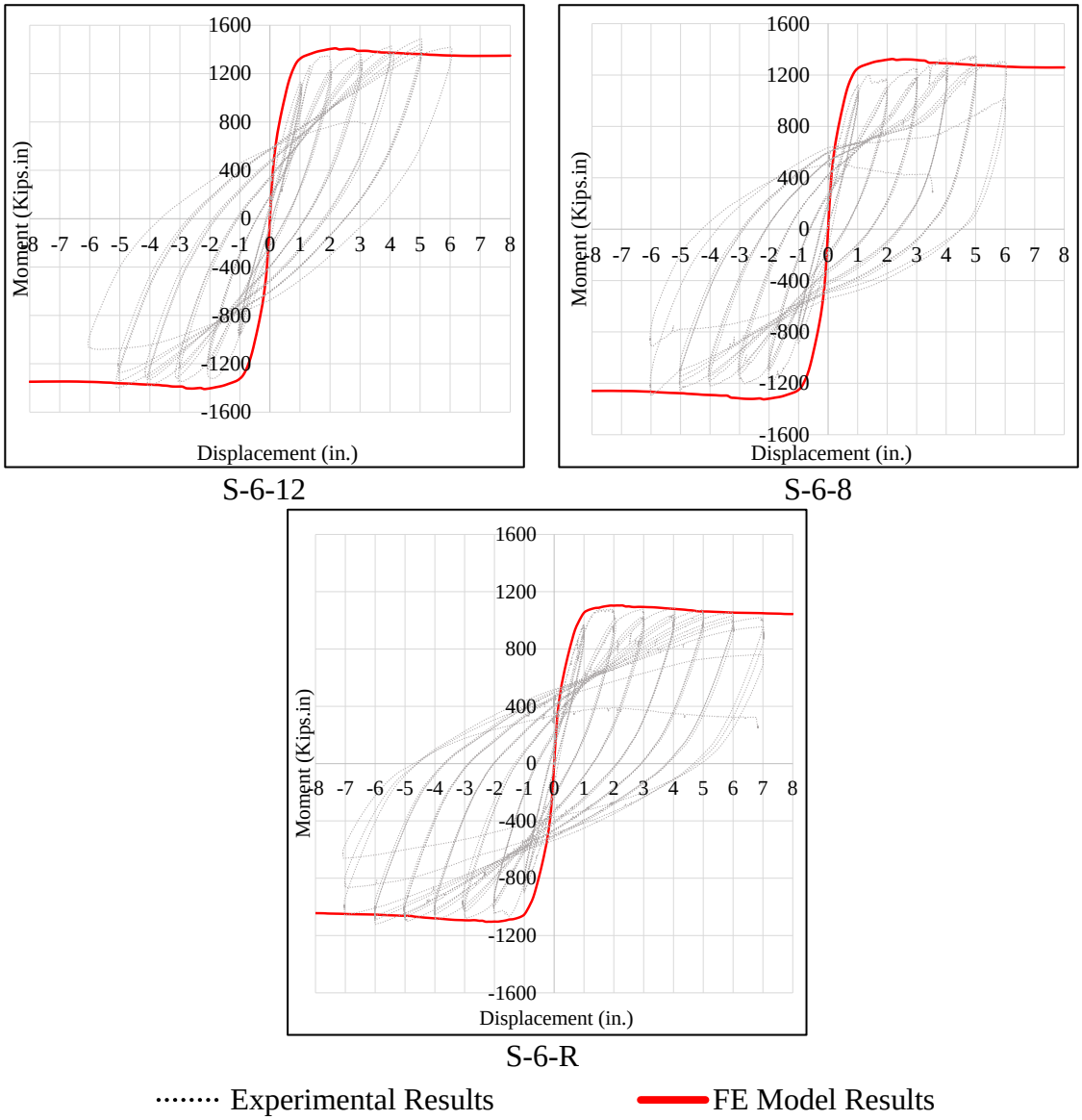

Figure 7-12 Measured hysteretic curves and numerical results of the specimens (Rebar Size: #6).

7.6.2 Effects of Axial Load

Table 7-1 shows the sensitivity of the moment capacity of the connections to the axial load ratio. Models with higher axial load showed more capacity. These observations were similar in all the analyses. The parametric study on the effect of the axial load showed that increasing axial load from 10% to 20% may increase in the capacity of the system around 7%.

Table 7-1 Moment capacity of the column with different axial load ratios (designations and geometry described in chapter 6)

Specimen name	Moment capacity (Axial load ratio 10%)	Moment capacity (Axial load ratio 20%)
S-5-R	839 Kips.in	928
S-5-8	914 Kips.in	1010
S-5-12	1045 Kips.in	1068
S-6-R	1058 Kips.in	1122
S-6-8	1159 Kips.in	1244
S-6-12	1286 Kips.in	1316

7.6.3 Mesh Sensitivity

Different global seeds of 0.5, 1, 1.5 and 3 were used to mesh the column. Figure 7-13 demonstrate that both meshes accurately predict the response for specimen S-5-8. At the same time, the 0.5-inch seeded model required 22 times more execution time of the 1.5-inch seeded model using the same computational machine. The 1-inch seeded model required 1.6 times of running time of the 1.5-inch seeded model and finally, the 3-inch seeded model required 0.4 times of running time of the 1.5-inch seeded model.

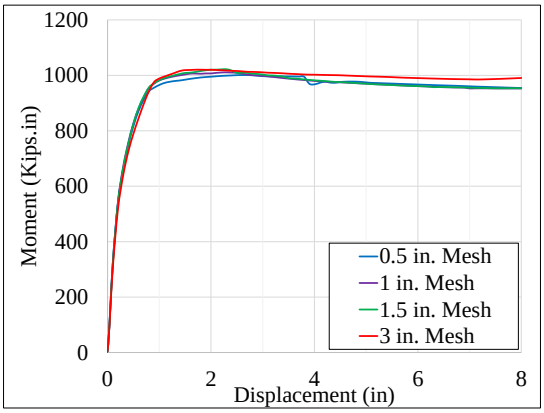

Figure 7-13 Effect of mesh size on the moment displacement curve (S-5-8).

7.7 Effect of Lap Splice Length

In this section, the behavior of the connection, when the sufficient length of lap splice is not provided, is investigated. The study done by Peruchini [113] showed that 5.11

in. (8 d_b) for No. 5 bar is satisfactory to fracture the reinforcement within the connection. Therefore, a specimen originated from the second phase (S-5-8) was modeled with 4 d_b overlap using the calibrated spring model discussed in section 7.3. The values used for uniaxial compressive strength of concrete materials in models were the actual values taken from the reported data by Peruchini [113]. Figure 7-14 shows the slippage failure between longitudinal reinforcements when the lap splice length is $4d_b$. Figure 7-15 shows the moment displacement result of the simulated connection. The results showed that when the lap splice length is around $4d_b$ the maximum capacity of the system will decrease by 25% compared to the case of 8 d_b.

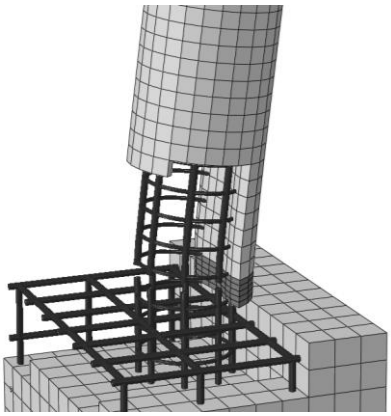

Figure 7-14 Deformed shape of the connection when the lap splice length is not provided.

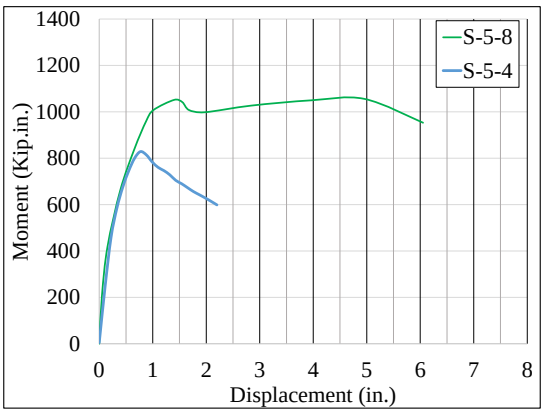

Figure 7-15 Moment-Displacement curves of the modeled specimens when lap splice length is not provided compared to the specimen S-5-8.

7.8 Conclusion

The following conclusions were drawn based on the results of this chapter:

1. The Concrete Damaged Plasticity (CDP) model for both normal concrete and UHPC was able to predict with reasonable accuracy different responses of the proposed connection.
2. Generally, good convergence was achieved for the model and the results had low mesh sensitivity. A coarse 2-inch seeded mesh could capture the connection behavior reasonably well. There was minimal difference between the results of 2-inch and 1-inch seeded meshes.
3. The parametric study on the effect of the axial load showed that increasing axial load from 10% to 20% may increase the capacity of the connection by 7%.
4. A model was proposed for lap splice which demonstrated the slippage failure in the splice region when the sufficient length of lap splice was not provided.
5. The numerical results showed that decreasing the overlap length from 8 d_b to 4d_b could result in 25% reduction in moment capacity of the investigated system.

CHAPTER 8 DESIGN GUIDE

Both details (Detail 1 and 2) are designed to form the plastic hinge far from the cap beam and applicable to both seismic and non-seismic regions. The use of UHPC layer adjacent to the cap beam ensures that the plastic hinge is formed at a desired location which is away from the cap beam. One of the advantages of the proposed detail is its ability to adopt provisions of existing design specifications without extensive modifications. The design procedure of both details are summarized in the flowcharts shown in Figure 8-1 and 8-2.

In both details, a key factor to design the splice region is provision of sufficient overlap splice length to prevent the bond failure. Based on the results of experiments, 8-times diameter of the rebar length for lap splice provides sufficient bond strength. It should be noted that the experimental data is limited to bar No. 5 and 6 with a clear cover of 2-times diameter of the reinforcement.

Although the maximum moment may occur in the UHPC sections, the strength of UHPC in both compression and tension provides higher capacity and confinement. The results of this study indicated that there is no need to place transverse reinforcement in the splice region. Eliminating transverse reinforcement facilitates the construction process.

The main difference between Detail 1 and two is the region of column where plastic hinge can form. Using two layers of UHPC in Detail 2, prevents development of plastic hinge to a larger area. The advantage of Detail 1 is its simplicity and its ability to protect the cap beam. Since both details can be used in seismic and non-seismic regions, the selection of either details is at the discretion of designer. Moreover, in Detail 2, the distance

between the cap beam and plastic hinge, in the column, is controlled by changing the thickness of the layer of UHPC adjacent to the cap beam.

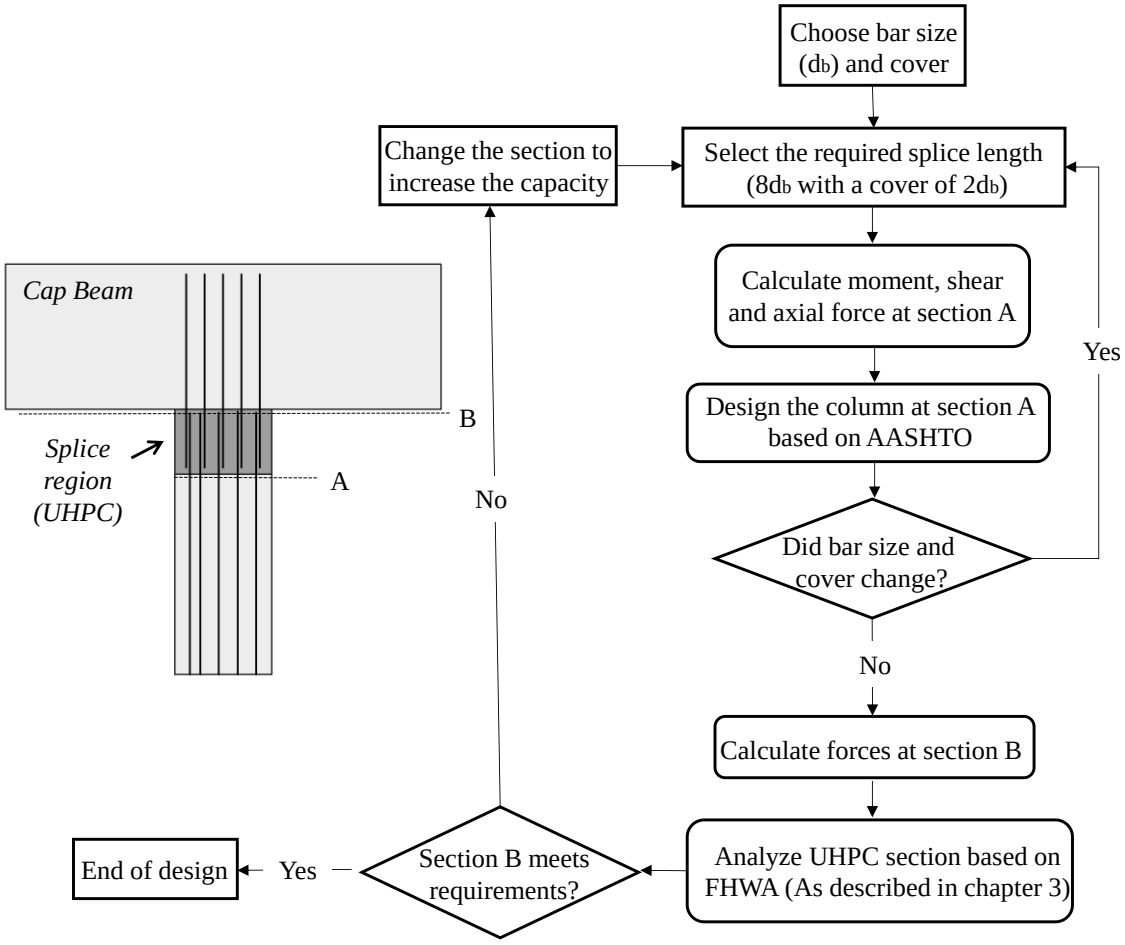

Figure 8-1 Design flowchart- Detail 1.

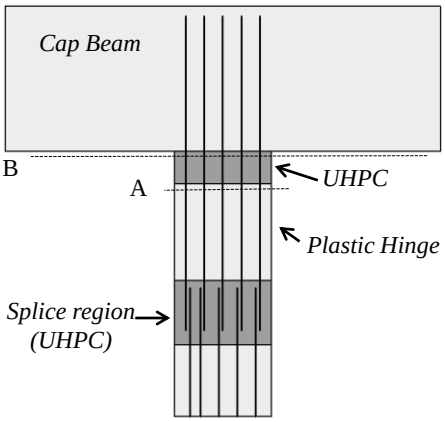

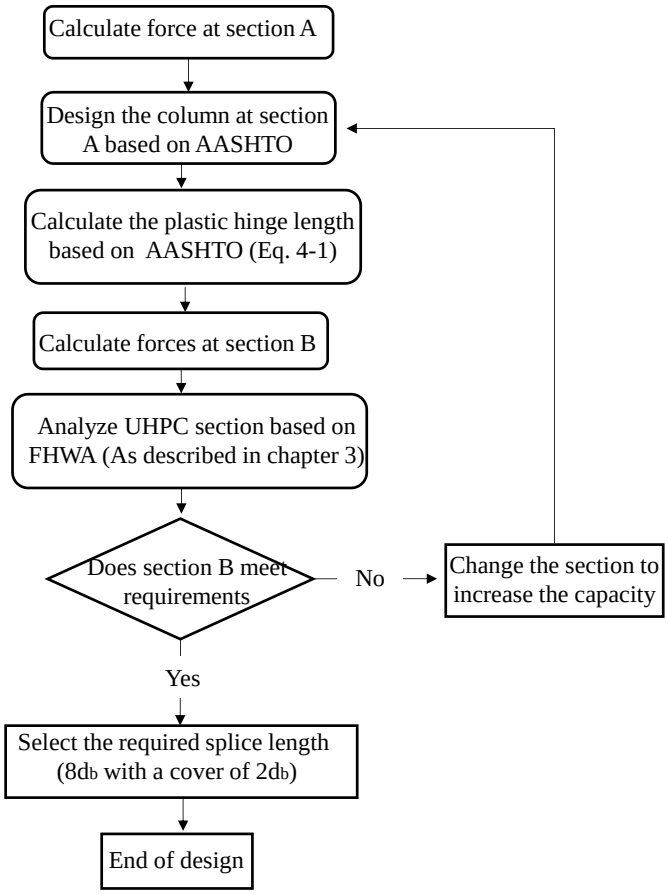

Figure 8-2 Design flowchart- Detail 2.

CHAPTER 9 CONCLUSION

9.1 Conclusion

In this research, two new connection details for seismic and non-seismic regions were proposed and tested. Both details completely prevent penetrating connections into the cap beam. The proposed connections are constructed outside the cap beam within the precast column. In both details, the reinforcements of the cap beam and the column are spliced in the column and joined with a layer of Ultra High Performance Concrete (UHPC). UHPC offers material benefits such as high workability and the inherent large tolerances within the suggested details can facilitate and accelerate the on-site construction.

The primary goal of this research was to provide a description of the newly developed connection detail and verifying their structural performance. This goal was achieved through a comprehensive experimental and numerical program. The following conclusions were drawn based on the results of this research:

1- Both proposed details are easy to implement and the high workability of the UHPC and large construction tolerances, accelerates the construction process.

2- Results show that both details are applicable to seismic and non-seismic regions and able to achieve adequate levels of ductility.

3- The UHPC layer in both details, prevents development of yielding into the cap beam which is capacity protected. Detail-2 guaranties the formation of the plastic hinge, in the limited length of the column, between the UHPC layers. Detail-1 shifts the damage far from the cap beam.

4- In comparison with conventional concrete, even a short lap splice of bars in UHPC can transfer forces between spliced bars, which leads to a decrease in casting volume. According to the results of the experiments performed in this research, 8-times diameter of the bar length for lap splice can provide sufficient bond strength. It should be noted that the experimental data was limited to bar No. 5 and 6and the clear cover was 2-times diameter of the bars.

5- No significant damage was found in splice region even in the absence of the transverse reinforcement in that area. Observing no failure in splice region indicates that UHPC can provide a good confinement and shear capacity. Eliminating the need for stirrups, in the splice region, can facilitate the on-site construction.

6- The use of Concrete Damaged Plasticity (CDP) model for modeling UHPC and concrete, simulates the observed deflections, strain and damages responses of the proposed connection. The mesh sensitivity of the model was quite low. The proposed model for lap splice could demonstrate the slippage failure in the splice region when the sufficient length of lap splice was not provided. The numerical results showed that decreasing the overlap length from 8 d_b to 4d_b could result in 25% reduction in moment capacity of the investigated system.

9.2 Future Study

This dissertation provides a comprehensive experimental and numerical study of two detailing methods used for connecting precast column to precast cap beam. Cap beams are designed to be damage free and capacity protected elements in bridges. The finite

element analysis and moment curvature analysis generally give a very good estimate of structural behavior of the whole system. As the next step, it is important to propose a construction method and introducing a technique to hold the cap beam before the UHPC casting. The implementation and feasibility of this approach and its structural performance may need some experimental test.

In the next step, a complete bridge incorporating all the connection details can be constructed and subjected to a shake table test. The shake table will allow the designer to monitor the performance of the connection under a simulated seismic event. Another area of interest which requires further experimental testing is finding minimum lap splice length in the absence of the stirrups. This task may focus on several parameters such as rebar size and type, clear cover etc. There is a need to test the connection at full scale to understand the field implementation, constructability and possible monitoring of connections for structural performance and longevity under real conditions.

REFERENCES

[1] M. P. Culmo, "Accelerated Bridge Construction Manual - Experience in Design, Fabrication and Erection of Prefabricated Bridge Elements and Systems," 2011.

[2] PCI Northeast Bridge Technical Committee, "Guidelines For Accelerated Bridge Construction Using Precast / Prestressed Concrete Elements Including Guideline Details," 2014.

[3] A. Jahromi, A. Valikhani, and A. Azizinamini, "Toward Development of Best Practices for Closure Joints in ABC Projects," 2018.

[4] N. R. Council, "Innovative Bridge Designs for Rapid Renewal: ABC Toolkit," 2013.

[5] E. Matsumoto, M. Waggoner, M. Kreger, J. Vogel, and L. Wolf, "Development of a precast concrete bent-cap system," *PCI Journal*\, vol. 53.3, 2008.

[6] *AASHTO Guide Specifications for LRFD Seismic Bridge Design, 2nd Edition*. 2011.

[7] *AASHTO LRFD Bridge Design specifications*. 2012.

[8] California Department of Transportation, *Seismic design of concrete bridges*. 2015.

[9] *AASHTO LRFD Bridge Desgin Specification 7th edition*. 2014.

[10] A. Birely, J. Mander, J. Lee, C. McKee, and K. Yole, "Precast, Prestressed Concrete Bent Caps: Volume 1, Preliminary Design Considerations and Experimental Test Program," 2018.

[11] A. Birely, J. Mander, C. McKee, and J. Lee, "Precast, Prestressed Concrete Bent Caps: Volume 2, Design Recommendations and Design Examples," 2018.

[12] M. Culmo, "Connection details for prefabricated bridge elements and systems," 2009.

[13] M. Marsh, M. Wernli, B. E.Garrett, J. F. Stanton, M. O. Eberhard, and M. D. Weinert, "Application of Accelerated Bridge Construction Connections in Moderate-to-High Seismic Regions (NCHRP Report 698)," 2011.

[14] J. Restrepo, M. Tobolski, and E. Matsumoto, "Development of a Precast Bent Cap System for Seismic Regions (NCHRP Report 681)," 2011.

[15] S. Rowell, C. Grey, S. Woodson, and K. Hager, "High strain-rate testing of mechanical couplers," 2009.

[16] Z. B. Haber, "Precast column-footing connections for accelerated bridge construction in seismic zones," University of Nevada, Reno, 2013.

[17] B. Z. Haber, M. S. Saiidi, and D. Sanders, "Seismic Performance of Precast Columns with Mechanically Spliced Column-Footing Connections," *ACI Structural Journal*, 2014.

[18] H. Qu, T. Li, Z. Wang, H. Wei, J. Shen, and H. Wang, "Investigation and verification on seismic behavior of precast concrete frame piers used in real bridge structures: Experimental and numerical study," *Engineering Structures*, vol. 154, no. May 2017, pp. 1–9, 2018.

[19] M. Tazarv and M. S. Saiidi, "UHPC-filled duct connections for accelerated bridge construction of RC columns in high seismic zones," *Engineering Structures*, vol. 99, pp. 413–422, 2015.

[20] D. Raynor, D. Lehman, and J. Stanton, "Bond-Slip Response of Reinforcing Bars Grouted in Ducts," *ACI Structural Journal*, vol. 99, pp. 568–576, 2002.

[21] J. F. Steuck, Kyle P and Eberhard, Marc O and Stanton, "Anchorage of Large-Diameter Reinforcing Bars in Ducts.," *ACI Structural Journal*, vol. 106, pp. 506–513, 2009.

[22] J. F. Pang, Jason BK and Steuck, Kyle P and Cohagen, Laila and Eberhard, Marc O and Stanton, "Rapidly Constructible Large-Bar Precast Bridge-Bent Connection," 2008.

[23] F. Brenes, S. Wood, and M. Kreger, "Anchorage requirements for grouted vertical-duct connectors in precast bent cap systems," *Report No. FHWA/TX-06/0-4176-1, Center for Transportation Research, University of Texas at Austin*, 2006.

[24] B. Khaleghi, E. Schultz, S. Seguirant, L. Marsh, O. Haraldsson, M. Eberhard, and J. Stanton, "Accelerated bridge construction in Washington state: From research to practice," *PCI Journal*, vol. 57, no. 4, pp. 34–49, 2012.

[25] A. Mohebbi, M. S. Saiidi, and A. M. Itani, "Shake Table Studies and Analysis of a PT-UHPC Bridge Column with Pocket Connection," *Journal of Structural Engineering*, vol. 144, p. 4018021, 2018.

[26] A. Mehrsoroush and M. S. Saiidi, "Cyclic Response of Precast Bridge Piers with Novel Column-Base Pipe Pins and Pocket Cap Beam Connections," *Journal of Bridge Engineering*, vol. 21, p. 4015080, 2016.

[27] Y. Osanai, F. Watanabe, and S. Okamoto, "Stress Transfer Mechanism of Socket Base Connections with Precast Concrete Columns," *ACI Structural Journal*, vol. 93, no. 3, pp. 266–276, May 1996.

[28] O. S. Haraldsson, T. M. Janes, M. O. Eberhard, and J. F. Stanton, "Seismic Resistance of Socket Connection between Footing and Precast Column," *Journal of Bridge Engineering*, vol. 18, no. 9, pp. 910–919, 2013.

[29] S. Motaref, "Seismic Response of Precast Bridge Columns with Energy Dissipating Joints," University of Nevada, Reno, 2011.

[30] S. Motaref, M. . Saiidi, and D. H. Sanders, "Seismic Response of Precast Bridge Columns with Energy Dissipating Joints," *Center for Civil Engineering Earthquake Research, Department of Civil and Environmental Engineering, University of Nevada, Reno, Nevada, Report No. CCEER-11-01*, 2011.

[31] P. . Ziehl, J. M. Caicedo, D. Rizos, T. Mays, A. Larosche, M. ElBatanouny, and B. Mustain, *Testing of Connections between Prestressed Concrete Piles and Precast Concrete Bent Caps*. Department of Civil and Environmental Engineering, University of South Carolina, South Carolina Department of Transportation, 2011.

[32] A. Palermo, ; S Pampanin, and D. Marriott, "Design, Modeling, and Experimental Response of Seismic Resistant Bridge Piers with Posttensioned Dissipating Connections," *Journal of Structural Engineering*, vol. 133(11), pp. 1648–1661, 2007.

[33] J. Stanton, W. C. Stone, and G. S. Cheok, "A Hybrid Reinforced Precast Frame for Seismic Regions," *PCI Journal*, vol. 42, no. 2, 1997.

[34] S. L. Billington and J. K. Yoon, "Cyclic Response of Unbonded Posttensioned Precast Columns with Ductile Fiber-Reinforced Concrete," *Journal of Bridge Engineering*, vol. 9, no. 4, pp. 353–363, Jul. 2004.

[35] A. Palermo, S. Pampanin, and G. M. Calvi, "Concept and Development of Hybrid Solutions for Seismic Resistant Bridge Systems," *Journal of Earthquake Engineering*, vol. 9, no. 6, pp. 899–921, 2005.

[36] Y.-C. Ou, M.-S. Tsai, K.-C. Chang, and G. C. Lee, "Cyclic Behavior of Precast Segmental Concrete Bridge Columns with High Performance or Conventional Steel Reinforcing Bars as Energy Dissipation Bars," *Earthquake Engineering & Structural Dynamics*, vol. 39, no. 11, pp. 1181–1198, 2010.

[37] J. Hewes, "Seismic Tests on Precast Segmental Concrete Columns with Unbonded Tendons," *Bridge Structures*, vol. 3, pp. 215–227, 2007.

[38] W. Stone, G. Cheok, and S. JF, "Performance of hybrid moment-resisting precast beam-column concrete connections subjected to cyclic loading," *Structural Journal*, vol. 92.2, pp. 229–249, 1995.

[39] G. Cheok, W. Stone, and S. Kunnath, "Seismic response of precast concrete frames with hybrid connections," *Structural Journal*, vol. 95.5, pp. 527–539, 1998.

[40] A. Sadeghnejad, "Extending Application of Simple for Dead and Continuous for Live Load Steel Bridge System to ABC Applications in Seismic Regions- Phase II-Experimental," 2018.

[41] R. Taghinezhadbilondy, "Extending Use of Simple for Dead Load and Continuous for Live Load (SDCL) Steel Bridge System to Seismic Areas," Florida International University, 2016.

[42] A. Asnaashari, R. Grafton, and M. Johnnie, "Precast Concrete Design-Construction of San Mateo-Hayward Bridge Widening Project," *PCI journal*, vol. 50, no. 1, 2005.

[43] C. E. Chalioris, "Steel fibrous RC beams subjected to cyclic deformations under predominant shear," *Engineering Structures*, vol. 49, pp. 104–118, 2013.

[44] H. Russel, G and B. a. Graybeal, "Ultra-High Performance Concrete : A State-of-the-Art Report for the Bridge Community," 2013.

[45] M. Farzad, D. Garber, A. Azizinamini, and K. Lau, *Corrosion Macrocell Development in Reinforced Concrete With Repair UHPC*. NACE International, 2018.

[46] B. Graybeal, "Material Property Characterization of Ultra-High Performance Concrete," 2006.

[47] M. Shafieifar, M. Farzad, and A. Azizinamini, "New Connection Detail to Connect Precast Column to Cap Beam using Ultra-High-Performance Concrete in Accelerated Bridge Construction Applications," *Transportation Research Board 97th Annual MeetingTransportation Research Board*, no. 18–04892, 2018.

[48] P. Richard and M. Cheyrezy, "Composition of Reactive Powder Concretes," *Cement and concrete research*, vol. 25, no. 7, pp. 1501--1511, 1995.

[49] B. H. Oh, "Flexural Analysis of Reinforced Concrete Beams Containing Steel Fibers," *Journal of Structural Engineering*, vol. 118, no. 10, pp. 2821–2835, 1992.

[50] S. Ashour and F. Wafa, "Flexural behavior of high-strength fiber reinforced concrete beams," *Structural Journal*, vol. 90, no. 3, pp. 279–287, 1993.

[51] G. Campione and M. Mangiavillano, “Fibrous reinforced concrete beams in flexure: experimental investigation, analytical modelling and design considerations,” *Engineering structures*, vol. 30, no. 11, pp. 2970–2980, 2008.

[52] D. Lim and B. Oh, “Experimental and theoretical investigation on the shear of steel fibre reinforced concrete beams,” *Engineering structures*, vol. 21, no. 10, pp. 937–944, 1999.

[53] A. Dili and M. Santhanam, “Investigations on reactive powder concrete: A developing ultra high-strength technology,” *Indian concrete journal*, vol. 78, no. 4, pp. 33–38, 2004.

[54] Z. B. Haber, I. De La Varga, and B. A. Graybeal, “Properties and Behavior of UHPC-Class Materials,” no. FHWA-HRT-18-036, p. 153, 2018.

[55] S. Han, Y. Liu, D. Liu, M. An, and Z. Yu, “The Modeling Research on the Early-Age Shrinkage of UHPFRC in Different Curing Conditions,” *Advances in Civil Engineering*, vol. 2018, 2018.

[56] S. Aaleti, B. Petersen, and S. Sritharan, “Design Guide for Precast UHPC Waffle Deck Panel System, including Connections,” vol. FHWA-HIF-1, no. June, p. 127, 2013.

[57] G. Parra-Montesinos, “Shear strength of beams with deformed steel fibers,” *Concrete international*, vol. 28.11, 2006.

[58] *AFGC Betons fibres a ultra-hautes performances Ultra High Performance Fibre-Reinforced Concretes Recommendations*. 2013.

[59] B. A. Graybeal, “Characterization of the behavior of ultra-high performance concrete,” 2005.

[60] D. Harris and C. Roberts-Wollmann, “Characterization of the punching shear capacity of thin ultra-high performance concrete slabs,” 2005.

[61] W. Fuchs, R. Eligehausen, and J. Breen, “Concrete capacity design (CCD) approach for fastening to concrete,” *Structural Journal*, vol. 92.1, pp. 73–94, 1995.

[62] J. Yuan and B. Graybeal, “Bond behavior of reinforcing steel in ultra-high performance concrete,” 2014.

[63] V. S. Ronanki, S. Aaleti, and D. B. Valentim, “Experimental investigation of bond behavior of mild steel reinforcement in UHPC,” *Engineering Structures*, vol. 176, no. August, pp. 707–718, 2018.

[64] V. De la, Z. Igor, H. B., and B. A. Graybeal, “Performance of Grouted Connections for Prefabricated Bridge Elements—Part I: Material-Level Investigation on Shrinkage and Bond,” 2016.

[65] D. Harris, M. Muñoz, A. Gheitasi, and T. Ahlborn, “The challenges related to interface bond characterization of ultra-high-performance concrete with implications for bridge rehabilitation practices,” *Advances in Civil Engineering Materials*, vol. 4.2, pp. 75–101, 2014.

[66] A. Sadeghnejad, S. F. Fancy, A. Valikhani, B. Chunn, R. Mohammadi, Alireza Taghinezhadbilondy, M. Moravej, J. Gull, A. Yakel, and K. Lau, “Non-Destructive Testing (NDT) of a Segmental Concrete Bridge Scheduled for Demolition, with a Focus on Condition Assessment and Corrosion Detection of Internal Tendons,” 2017.

[67] D. Garber, J. Gull, M. Sheifiefar, and N. Rezaei, “Compilation of Accelerated Bridge Construction (ABC) Bridges,” 2016.

[68] A. Jahromi, M. Dickinson, A. Valikhani, and A. Azizinamini, “Assessing Structural Integrity of Closure Pours in ABC Projects,” 2018.

[69] A. Valikhani, A. J. Jahromi, and A. Azizinamini, “Experimental Investigation of High-Performing Protective Shell Used for Retrofitting Bridge Elements,” 2018.

[70] A. Valikhani, A. Jahromi, and A. Azizinamini, “Retrofitting Damaged Bridge Elements Using Thin Ultra High Performance Shell Elements,” 2017.

[71] J. Resplendino and F. Toutlemonde, *Designing and Building with UHPFRC*. 2013.

[72] “Federal Highway Administration Research and Technology.” [Online]. Available: https://www.fhwa.dot.gov/research/resources/uhpc/bridges.cfm.

[73] Y. Park, A. Abolmaali, Y. H. Kim, and M. Ghahremannejad, “Compressive strength of fly ash-based geopolymer concrete with crumb rubber partially replacing sand,” *Construction and Building Materials*, vol. 118, pp. 43–51, Aug. 2016.

[74] M. Mandavi, A. Abolmaali, and M. Ghahremannejad, “The Effects of pH and Temperature on Compressive Strength of Synthetic Fiber-Reinforced Concrete Cylinders Exposed to Sulfuric Acid,” *Advances in Civil Engineering Materials*, vol. 7.1, pp. 403–413, 2018.

[75] M. Ghahremannejad, M. Mahdavi, A. E. Saleh, S. Abhaee, and A. Abolmaali, “Experimental investigation and identification of single and multiple cracks in synthetic fiber concrete beams,” Case Studies in Construction Materials,vol. 9, pp. e00182, 2018.

[76] Shafieifar, Mohamadreza, Mahsa Farzad, and Atorod Azizinamini. “Alternative ABC Connection Utilizing UHPC.” No. 17-03398. 2017.

[77] M. Farzad, M. Shafieifar, and A. Azizinamini, “Accelerated Retrofitting of Bridge Elements Subjected to Predominantly Axial Load Using UHPC Shell,” 2018.

[78] M. Farzad, A. Mohammadi, M. Shafieifar, H. Pham, and A. Azizinamini, “Development of Innovative Bridge Systems Utilizing Steel-Concrete-Steel Sandwich System,” 2017.

[79] *Annual Book of ASTM Standards*. 2012.

[80] “AASHTO T132, Standard Method of Test for Tensile Strength of Hydraulic Cement Mortars,” 2000.

[81] T. Jankowiak and T. Lodygowski, “Identification of parameters of concrete damage plasticity constitutive model,” *Foundations of civil and environmental engineering*, vol. 6, no. 1, pp. 53–69, 2005.

[82] L. Chen and B. Graybeal, “Finite element analysis of ultra-high performance concrete: Modeling structural performance of an AASHTO type II girder and a 2nd generation pi-girder,” 2010.

[83] S. Qom, Y. Xiao, and M. Hadi, “Evaluation of Cooperative Adaptive Cruise Control (CACC) vehicles on managed lanes utilizing macroscopic and mesoscopic simulation,” in *Transportation Research Board 95th Annual Meeting*, 2016.

[84] J. Shen, O. Seker, B. Akbas, P. Seker, S. Momenzadeh, and M. Faytarouni, “Seismic performance of concentrically braced frames with and without brace buckling,” *Engineering Structures*, vol. 141, pp. 461–481, Jun. 2017.

[85] M. Shafieifar and V. Khonsari, “A Numerical Investigation on Behavior of Column Base Plates with Different Configurations,” *Civil Engineering Journal*, vol. 4.6, pp. 1223–1239, 2018.

[86] M. Shafieifar and V. Khonsari, “Studying the Behaviour of Base Plates with High Degree of Rigidity,” in *15 WCEE*, 2012.

[87] Z. Andalib, M. Kafi, M. Bazzaz, and S. Momenzadeh, “Numerical evaluation of ductility and energy absorption of steel rings constructed from plates,” *Engineering Structures*, vol. 169, pp. 94–106, 2018.

[88] J. Sadeghi and M. Fesharaki, “Importance of nonlinearity of track support system in modeling of railway track dynamics,” *International Journal of Structural Stability and Dynamics*, vol. 13, no. 1, p. 1350008, Feb. 2013.

[89] M. Fesharaki and T. Wang, “The effect of rail defects on track impact factors,” *CivilCivil Engineering Journal*, vol. 2(9), pp. 458–473, 2016.

[90] M. Shafieifar, M. Farzad, and A. Azizinamini, “Experimental and numerical study on mechanical properties of Ultra High Performance Concrete (UHPC),” *Construction and Building Materials*, vol. 156, pp. 402–411, 2017.

[91] W. Pansuk, H. Sato, Y. Sato, and R. Shionaga, “Tensile behaviors and fiber orientation of UHPC,” in *Proceedings of second international symposium on ultra high performance concrete, Kassel, Germany*, 2008, pp. 161–168.

[92] S. W. Kim, S. T. Kang, J. J. Park, and G. S. Ryu, “Effect of filling method on fibre orientation and dispersion and mechanical properties of UHPC,” in *Proceedings of second international symposium on ultra high performance concrete, Kassel, Germany*, 2008, pp. 185–192.

[93] A. Bozorgzad, “Consistent distribution of air voids and asphalt and random orientation of aggregates by flipping specimens during gyratory compaction process,” *Construction and Building Materials*, vol. 132, pp. 376–382, 2017.

[94] A. Bozorgzad, S. Kazemi, and F. M. Nejad, “Evaporation-induced moisture damage of asphalt mixtures: Microscale model and laboratory validation,” *Construction and Building Materials*, vol. 171, pp. 697–707, 2018.

[95] A. Bozorgzad, B. Chon, A. Sampath, Y. Kim, and H. . Lee, “Impacts of WMA Additives on Viscosity and Cracking of Asphalt Binder,” *Environmental Engineering*, vol. 13, p. 1, 2018.

[96] J. Yuan and B. A. Graybeal, “Bond Behavior of Reinforcing Steel in Ultra-High Performance Concrete,” *Engineering Structures*, vol. 1, no. 6, pp. 228–235, 2011.

[97] ASTM, “Standard test method for flow of hydraulic cement mortar,” *ASTM International, Pennsylvania*, 2001.

[98] B. Bae, H. Choi, and C. Choi, “Flexural Strength Evaluation of Reinforced Concrete Members with Ultra High Performance Concrete,” *Advances in Materials Science and Engineering*, vol. 2016, 2016.

[99] B. A. Graybeal, “Compression Testing of Ultra-High-Performance Concrete,” *Advances in Civil Engineering Materials*, vol. 4, no. 2, pp. 102–112, 2017.

[100] D. Y. Yoo, N. Banthia, and Y. S. Yoon, “Predicting the flexural behavior of ultra-high-performance fiber-reinforced concrete,” *Cement and Concrete Composites*, vol. 74, pp. 71–87, 2016.

[101] *Building Code Requirements for Structural Concrete (ACI 318-14)*. 2014.

[102] S. P. Shah, "Design considerations for steel fiber reinforced concrete (ACI Committee 544)," *ACI Structural Journal*, 1988.

[103] A. N. Dancygier and Z. Savir, "Flexural behavior of HSFRC with low reinforcement ratios," *Engineering Structures*, vol. 28, no. 11, pp. 1503–1512, 2006.

[104] M. Imam, L. Vandewalle, and F. Mortelmans, "Shear--moment analysis of reinforced high strength concrete beams containing steel fibres," *Canadian Journal of Civil Engineering*, vol. 22, no. 3, pp. 462–470, 1995.

[105] S. Al-Ta'an and J. Al-Feel, "Evaluation of shear strength of fibre-reinforced concrete beams," *Cement and Concrete composites*, vol. 12, no. 2, pp. 87–94, 1990.

[106] S. Sritharan, B. J. Bristow, and V. H. Perry, "Characterizing an Ultra-High Performance Material For Bridge Applications Under Extreme Loads," in *3rd International Symposium on High Performance Concrete, Orlando, FL*, 2003.

[107] S. Momenzadeh, O. Seker, M. Faytarouni, and J. Shen, "Seismic performance of all-steel buckling-controlled braces with various cross-sections," *Journal of Constructional Steel Research*, vol. 139, pp. 44–61, Dec. 2017.

[108] M. Asl, B. Farivar, and S. Momenzadeh, "Investigation of the rigidity of welded shear tab connections," *Engineering Structures*, vol. 179, pp. 353–366, 2019.

[109] M. Ghahremannejad and A. Abolmaali, "Prediction of shear strength of reinforced concrete beams using displacement control finite element analysis," *Engineering Structures*, vol. 169, pp. 226–237, 2018.

[110] G. H. Mahmud, Z. Yang, and A. M. T. Hassan, "Experimental and numerical studies of size effects of Ultra High Performance Steel Fibre Reinforced Concrete (UHPFRC) beams," *Construction and Building Materials*, vol. 48, pp. 1027–1034, 2013.

[111] M. A. Saleem, A. Mirmiran, J. Xia, and K. Mackie, "Development Length of High-Strength Steel Rebars in Ultra-High Performance Concrete," *Journal of Materials in Civil Engineering*, vol. 25, no. 8, pp. 991–998, 2012.

[112] B. Graybeal, "Design and Construction of Field-Cast UHPC Connections," 2014.

[113] T. J. Peruchini, "Investigation of Ultra-High Performance Concrete for Longitudinal Joints in Deck Bulb Tee Bridge Girders Timothy," University of Washington, 2017.

[114] P. Paultre, R. Eid, Y. Langlois, and Y. Lévesque, "Behavior of Steel Fiber-Reinforced High-Strength Concrete Columns under Uniaxial Compression," *Journal of Structural Engineering*, vol. 136, no. 10, pp. 1225–1235, Oct. 2010.

[115] M. Shafieifar, M. Farzad, and A. Azizinamini, "A comparison of existing analytical methods to predict the flexural capacity of Ultra High Performance Concrete (UHPC) beams," *Construction and Building Materials*, vol. 172, pp. 10–18, 2018.

[116] R. Park, "Evaluation of ductility of structures and structural assemblages from laboratory testing," *Bulletin of the New Zealand national society for earthquake engineering*, vol. 22, no. 3, pp. 155–166, 1989.

VITA

MOHAMADREZA SHAFIEIFAR

Born, Tehran, Iran

2005-2009	B.Sc., Civil Engineering, Structural Engineering University of Tabriz Tabriz, Iran
2010-2012	M.S., Civil Engineering, Structural Engineering Sharif University of Technology Tehran, Iran
2014 -2018	Doctoral Candidate Florida International University Miami, Florida

PUBLICATIONS AND PRESENTATIONS

Shafieifar, Mohamadreza, Mahsa Farzad, and Atorod Azizinamini. "A comparison of existing analytical methods to predict the flexural capacity of Ultra High Performance Concrete (UHPC) beams." *Construction and Building Materials* 172 (2018): 10-18.

Shafieifar, Mohamadreza, Mahsa Farzad, and Atorod Azizinamini. "Experimental and numerical study on mechanical properties of Ultra High Performance Concrete (UHPC)." *Construction and Building Materials* 156 (2017): 402-411.

Shafieifar, Mohamadreza, Mahsa Farzad, and Atorod Azizinamini. "New Connection Detail to Connect Precast Column to Cap Beam Using UHPC in ABC Applications". *Journal of the Transportation Research Board*, 2018.

Shafieifar, Mohamadreza, and Vahid Khonsari. "A Numerical Investigation on Behavior of Column Base Plates with Different Configurations." *Civil Engineering Journal*, 4, no. 6 (2018): 1223-1239.

Garber, D., Gull, J., Sheifiefar, M., & Rezaei, N. (2016). Compilation of Accelerated Bridge Construction (ABC) Bridges (No. ABC-UTC-ProjectDatabase-v1).

Mahsa Farzad, Shafieifar, Mohamadreza, and Atorod Azizinamini. "Experimental and numerical study on an innovative sandwich system utilizing UPFRC in bridge applications." *Engineering Structures*, 180 (2019): 349-356.

Shafieifar, Mohamadreza, Atorod Azizinamini. "Alternative ABC Connections Utilizing UHPC". April Monthly ABC Webinar, 2018.

Shafieifar, Mohamadreza, Mahsa Farzad, and Atorod Azizinamini. "New Connection Detail to Connect Precast Column to Cap Beam Using UHPC in ABC Applications". *TRB Washington D.C* 2018.

Mahsa Farzad, Shafieifar, Mohamadreza, and Atorod Azizinamini. "Accelerated Retrofitting of Bridge Elements Subjected to Predominantly Axial Load Using UHPC Shell". *TRB Washington D.C* 2018.

Shafieifar, Mohamadreza, Mahsa Farzad, and Atorod Azizinamini. "Alternative ABC Connection Using UHPC". 2017 UTC Spotlight Conference, Washington, D.C., 2017.

Shafieifar, Mohamadreza, Mahsa Farzad, and Atorod Azizinamini. "Alternative ABC Connection Using UHPC". Western Bridge Engineers 2017, Oregon, 2017.

Shafieifar, Mohamadreza, Mahsa Farzad, and Atorod Azizinamini. "Alternative ABC Connection Utilizing UHPC". TRB 2017, Washington, D.C., 2017.

Farzad, Mahsa, Alireza Mohammadi, Mohamadreza Shafieifar, Huy Pham, and Atorod Azizinamini. "Development of Innovative Bridge Systems Utilizing Steel-Concrete-Steel Sandwich System". TRB 2017, Washington, D.C., 2017.

Azedeh Jaberi, Morgan Dickinson, Mohamadreza Shafieifar, "Design of Bridges for service life using ABC", 2015 FIU highlight report, Miami, 2015.

Shafieifar, Mohamadreza and Atorod Azizinamini. "Innovative ABC solutions using UHPC". 2015 National Accelerated Bridge Construction Conference, Miami, 2015.

Shafieifar, Mohamadreza and S. Vahid. Khonsari, "Studying the Behaviour of Base Plates with High Degree of Rigidity" –15th World Conference on Earthquake Engineering 2012 (15th WCEE).